Optimal Planning and Impact Analysis of Electric Vehicle Fast Charging Stations in Distribution Systems

Ph.D. Thesis

AKANKSHA SHUKLA

ID No. 2015REE9015

DEPARTMENT OF ELECTRICAL ENGINEERING

MALAVIYA NATIONAL INSTITUTE OF TECHNOLOGY JAIPUR

November 2019

Optimal Planning and Impact Analysis of Electric Vehicle Fast Charging Stations in Distribution Systems

Submitted in

fulfillment of the requirements for the degree of

Doctor of Philosophy

by

Akanksha Shukla

ID: 2015REE9015

Under the Supervision of

Dr. Kusum Verma

Prof. Rajesh Kumar

DEPARTMENT OF ELECTRICAL ENGINEERING

MALAVIYA NATIONAL INSTITUTE OF TECHNOLOGY JAIPUR

November 2019

Declaration

I, **Akanksha Shukla** declare that this thesis titled, ***"Optimal Planning and Impact Analysis of Electric Vehicle Fast Charging Stations in Distribution Systems"*** and work presented in it, is my own. I confirm that:

- This work was done wholly or mainly while in candidature for a research degree at this university.
- Where any part of this thesis has previously been submitted for a degree or any other qualification at this university or any other institution, this has been clearly stated.
- Where I have consulted the published work of others, this is always clearly attributed.
- Where I have quoted from the work of others, the source is always given. With the exception of such quotations, this thesis is entirely my own work.
- I have acknowledged all main sources of help.
- Where the thesis is based on work done by myself, jointly with others, I have made clear exactly what was done by others and what I have contributed myself.

Date:

Akanksha Shukla

(2015REE9015)

Certificate

This is to certify that the thesis entitled **"Optimal Planning and Impact Analysis of Electric Vehicle Fast Charging Stations in Distribution Systems"** being submitted by **Akanksha Shukla (ID: 2015REE9015)** is a bonafide research work carried out under my supervision and guidance in fulfillment of the requirement for the award of the degree of **Doctor of Philosophy** in the Department of Electrical Engineering, Malaviya National Institute of Technology, Jaipur, India. The matter embodied in this thesis is original and has not been submitted to any other University or Institute for the award of any other degree.

Place:
Date:

Dr. Kusum Verma
Associate Professor

Dr. Rajesh Kumar
Professor

Department of Electrical Engineering
MNIT Jaipur

This thesis is dedicated to

My parents & my sister Anshuma

Acknowledgement

This thesis is the result of challenging journey of four years of my doctoral studies during which many people have been instrumental in the completion of the study. It is a great pleasure to convey my gratitude to all those who contributed in many ways.

First and foremost, I would like to give my sincere gratitude to my supervisors, ***Dr. Kusum Verma*** (Associate Professor, Department of Electrical Engineering, MNIT Jaipur) and ***Dr. Rajesh Kumar*** (Professor, Department of Electrical Engineering, MNIT Jaipur) for their patient guidance, enthusiastic encouragement and useful critiques of this research work. ***Dr. Kusum Verma*** introduced me to the culture of research during my master's program. She has taught me, both consciously and unconsciously how to be creative and systematic while conceptualizing the research. I am thankful to ***Dr. Rajesh Kumar*** for providing me critique environment to question my own work and venture into new ideas. They have given me freedom to pursue my research while ascertaining that I stay on course and do not deviate from the core of my research. I am highly indebted to them for their supervision and valuable suggestions for successful completion of my PhD work. It was a great opportunity to complete my doctoral study under their guidance.

My sincere thanks to each member of the Departmental Research Evaluation Committee (DREC), ***Prof. Manoj Fozdar*** and ***Prof. Rajive Tiwari*** for their insightful comments and suggestions throughout the course of my doctoral work. I have been greatly benefitted from the constructive feedbacks of DREC members.

My sincere thanks to ***Prof. Udaykumar R Yaragatti***, Director, MNIT Jaipur, ***Prof. Rajesh Kumar***, HOD, Department of Electrical Engineering, MNIT Jaipur and ***Prof. Harpal Tiwari***, DPGC Convener, Department of Electrical Engineering, MNIT Jaipur for providing the required infrastructural facilities. I am also thankful to all the faculty members and staff of the Electrical Engineering Department, MNIT Jaipur for promptly offering their support and advice whenever needed.

I would also like to thank my Raman lab colleagues, ***Dr. Shashank Vyas***, ***Dr. Chandra Prakash***, ***Dr. Omji Shukla***, ***Dr. Shalini Pal***, ***Dr. Venu Sangwan***, ***Dr. Sujil A.***, ***Mr. Rahul Singhal***, ***Ms. Vishu Gupta***, ***Mr. Ankit Vijayvargiya*** and ***Mr. Mitulkumar Gamit*** for their help and encouragement which enabled me to complete my work.

My time at MNIT Jaipur was made enjoyable despite the hardships PhD offers due to the constant support of my friends who became a part of my life. I feel profound pleasure to

thank my friends, ***Dr. Nikita Saxena*** and ***Mrs. Reenu Singh*** and my roommate, ***Dr. Vibha Uttam*** for believing and supporting me during this time. I would also like to thank my friends at MNIT Jaipur, ***Dr. Abhilash Kumar Gupta***, ***Dr. Venu Sangwan***, ***Ms. Vishu Gupta*** and ***Dr. Pradeep Singh***. Special thanks to ***Dr. Venu Sangwan*** for always encouraging me to work hard and providing moral support. I owe my deepest gratitude to ***Dr. Abhilash Kumar Gupta*** for proofreading, listening, offering me advice and supporting me through this entire process.

My acknowledgement would be incomplete without thanking the biggest source of my strength, my family. For my father, ***Mr. Vijay Kumar Shukla*** who raised me to be a perfectionist, my mother, ***Mrs. Sudha Shukla*** who taught me to be a hard worker, my coolest uncle and aunt, ***Mr. Shrawan Kumar Shukla*** and ***Mrs. Sneh Shukla*** for providing hearty laugh, support and being my second parent. Special mentions to my siblings, ***Mannu***, ***Harshit*** and ***Manthan*** for stupid jokes, late night talks, movies and constant motivation. My brother in law, ***Mr. Loveneet Nigam*** for timely advices and my life coach, my sister, ***Anshuma***.

Thank you for everything. Also, I would like to take this opportunity to convey my thanks to all those individuals who have directly or indirectly provided me with invaluable assistance for completion of this PhD.

Above all, I am thankful to the Almighty God for showing me the right path and showering his blessings towards me in all walks of my life. Thank you everyone.

(Akanksha Shukla)

Abstract

All over the world, the problem of environmental pollution and energy crisis is increasing rapidly. Transportation and fuel based electric utilities are the major sources of Green House Gas (GHG) emissions. To reduce GHG emissions and energy crisis, employing Electric Vehicles (EVs) with integration of renewable sources are the promising solutions. The current growth of EVs is slow due to the issues such as slow charging time, range anxiety, lack of charging infrastructure, higher cost and capacity fading of the EV battery. The range anxiety and lack of charging infrastructure can be dealt by building convenient charging infrastructures. While charging time, cost and capacity fading can be managed by the advancement in battery and charger technology. In the past few years, more attention has been paid towards the optimal planning of Fast Charging Stations (FCS) as they are needed for urgent charging during long distance trips and emergency conditions. The planning of FCS requires knowledge of demand and characteristic of fast charging EV load. These additional fast charging EV load will affect the performance of distribution system and their adverse effect can be mitigated by integrating the renewable generation in the system. But, the intermittency associated with the renewable generation like wind energy may not supply the EV fast charging load demand completely or may further degrade the performance of distribution system. Hence, it becomes necessary to analyse the impact of fast charging of EVs for assisting the distribution planners in making the decisions in case of any system violations. Therefore, this thesis attempts to address the major issues of load modelling, planning and impact analysis of FCS with renewable on the performance of distribution system. A detailed literature survey pertaining to these areas has been carried out and on the basis of that research objectives are framed.

For identifying the characteristic and demand of fast charging EV load, a mathematical model is developed stating the relation between power consumed by the fast charger, supply voltage and State of Charge (SOC) of fast charging EV load and validated by simulating a fast charger. The power vs voltage characteristic obtained from the simulated EV fast charger is further used to determine the accurate voltage-dependent load model for power flow analysis. EV fast charging demand has spatial-temporal characteristics, therefore, stochastic FCS charging demand is developed using queuing theory incorporating uncertain factors. The impact of different voltage-dependent load models and stochastic EV charging demand is investigated on modified IEEE 123-bus distribution system. Results reveal that the exponential load model is the better representation of EV fast charging load and EV charging demand depends on location and time of charging. Also, different load models affects the energy demand, energy losses and voltage profile of the system. Therefore,

load models play an important role in assessing the true energy demand and energy losses incurred due to fast charging of EVs.

The planning of FCS is technically challenging as the operation of FCS effects the operation of distribution and transportation system and driving behaviour of EV users. In this thesis, a synergistic planning strategy is proposed which takes into account distribution system and transport network's operational constraints and heterogeneous driving ranges based on the initial SOC of the EV while considering FCS load as exponential load model. Multi-objective synergistic planning model attempts to reduce the negative impact of FCS on the performance of distribution system, improve utilization of FCS and provide better service quality to the EV owners considering range anxiety issue. Multi-Objective Grey Wolf Optimizer (MOGWO) algorithm is used to obtain the non-dominated solutions and fuzzy satisfaction-based decision making method is employed to reach final planning scheme. The effectiveness of the proposed model is investigated on the IEEE 123-bus distribution system coupled with 25-node transportation network. The influence of different objectives, service radius and waiting time on the planning of FCS is studied to verify the effectiveness of the proposed planning model. The study shows that the proposed planning model is able to provide rational siting and sizing of FCS. This method also suggest the way to select proper service radius and waiting time.

The increased penetration of FCS may overload the distribution system components and can cause low voltage problems. The rapidly increasing wind integration in the distribution system may lessen the negative impacts of FCS but it may also cause reverse power flow and voltage rise problem. Therefore, it is important to study the impact of FCS and wind generation to assist the distribution planner in decision making in case of any system violations. In this thesis, wind generator power output is modelled incorporating the uncertainties associated with the wind speed using Weibull distribution function. Different performance indices characterizing the impact of FCS and wind generator on load profile, congestion of conductor, voltage deviation and unbalance and system losses are proposed. The impact assessment of FCS and wind is investigated on modified IEEE 123-bus distribution system. The simulation results show that variation in load profile, congestion of conductors, voltage deviation and unbalance and power system losses not only depends on the penetration of EVs and number of wind generators but also on the topology of the distribution system and the time of the analysis during the day. It is also found that wind will act only as partial solution and for maintaining power balance, the support from the main grid may be required for satisfying the FCS load demand.

Contents

List of Tables

List of Figures

List of Abbreviations

AECP	Aggregated EV Charging Profile
CC-CV	Constant Current Constant Voltage
CCL	Constant Current Load
CDF	Cumulative Distribution Function
CIL	Constant Impedance Load
CPL	Constant Power Load
DF	Diversity Factor
EV	Electric Vehicle
FCS	Fast Charging Stations
G2V	Grid-to-Vehicle
GHG	Green House Gas
ICE	Internal Combustion Engine
MAE	Mean Absolute Error
MCS	Monte Carlo Simulation
MDD	Maximum Diversified Demand
MINLP	Mixed Integer Nonlinear Programming
MOEA/D	Multi-Objective Evolutionary Algorithm/Decomposition
MOGWO	Multi-objective Grey Wolf Optimizer
MOPSO	Multi-Objective Particle Swarm Optimization
NILP	Nonlinear Integer Programming
NSGA-II	Non-dominated Sorted Genetic Algorithm
PAR	Peak to Average Ratio
PDF	Probability Distribution Function
PEV	Plug-in Electric Vehicle
PHEV	Plug-in Hybrid Electric Vehicle
PWM	Pulse Width Modulation
OD	Origin and Destination
SOC	State of Charge
SPEA	Strength Pareto Evolutionary Algorithm
TTS	Transportation Tomorrow Survey
V2G	Vehicle-to-Grid

List of Symbols

Chapter 3

k	Index of phase (1,2,3)
L	Inductance of input filter
R	Total resistance of active rectifier switches and input filter
C_{dc}	DC-link capacitor
E_k	Phase voltage
S_k	Switching function
$I_{dc},\ V_{dc}$	Output dc current and voltage of AC/DC rectifier
$V_d,\ V_q$	Direct and quadrature axis voltage of AC-DC rectifier
$i_d,\ i_q$	Direct and quadrature axis current of AC-DC rectifier
w	Frequency of grid
$S_d,\ S_q$	Switching functions in dq reference frame
$P,\ Q$	Active and reactive power drawn by the EV fast charger
V_s	Voltage across diode in DC-DC buck converter
V_b	Voltage across battery terminals
R_{dc}	Resistance of the output filter
L_{dc}	Inductance of the output filter
I_L	Output current of DC-DC buck converter
I_b	Battery charging current
C_o	Capacitor connected parallel to the battery
V_o	Battery constant voltage in V
r_b	Internal resistance of battery in Ω
K	Polarization constant in V/Ah
Q	Rated battery capacity in Ah
$A,\ B$	Exponential zone amplitude and time constant of battery in V and Ah^{-1}
SOC	State of charge of the battery
SOC_{ini}	Initial SOC of the EV
P_o	Active power consumed at the rated voltage
$a_p,\ n_p,\ b_p$	Parameters of exponential load model
$Z_p,\ I_p,\ P_p$	Parameters of ZIP load model
$A_i,\ P_i$	Actual and predicted value for i^{th} operating condition
e_i	Difference between the A_i and P_i
N_{EV}	Number of EVs
N_{houses}	Number of residential houses
α	Average number of vehicle per house
p	Penetration of EVs
n_{house}	Number of houses connected to each spot load
S_{house}^{max}	Maximum individual demand of each house

f_{OD}	Probabilities assigned to each OD pair
$w_O,\ w_D$	Weight assigned to origin and destination
d_{OD}	shortest route distance between O and D
$f_{OD,t}$	Probabilities assigned to each OD pair during time t
$f_{total,t}$	Average number of EVs that travel through the transportation network in time t
$N_T,\ N_D$	Set of transportation and distribution nodes
$T_{\lambda_t^k}$	Inter-arrival time of EVs for k^{th} FCS in time t
T_μ	Mean service time of EVs
p_t^k	Occupation rate of the k^{th} FCS per charging slot at t^{th} hour
N_c^k	Maximum number of EVs that can be charged simultaneously at k^{th} FCS
$P_t^k(n)$	Probability of n EVs charging simultaneously at k^{th} FCS
f_t^k	EV flow served by k^{th} FCS in time t
ξ_{OD}^k	Binary variable representing status of EV flow is served on OD path
^{k}	Binary variable representing status of location of k^{th} FCS on path OD
$E_{d_\mu},\ E_d$	Mean daily recharge energy and daily recharge energy
d_μ	Mean daily driving distance
ϵ	Energy consumption of EV per mile
C_{bat}	Battery capacity
C_{rate}	Charging rate of EVs
$d_m,\ d_{m_{max}}$	Daily driving distance and maximum range of EV in miles
Z	Standard normal variate
$\mu_m,\ \sigma_m$	Mean and variance of lognormal distribution
ΔSOC	Change in SOC
$SOC_{min},\ SOC_{max}$	Minimum and maximum SOC limit
q	Number of piecewise linear functions representing power curve
$f_z(x)$	z^{th} linear function of power curve of battery
$u_z,\ l_z$	Upper and lower limit of $f_z(x)$
$avgP_{SOC_{ini}}$	Average charging power of EVs with SOC_{ini}
$P_{FCS_{k,t}}$	Total charging power of k^{th} FCS in time t
$E[P_{FCS_t^k}]$	Expected power charging demand of k^{th} FCS in time t
$V_{i,t},\ V_{j,t}$	Voltage magnitude of bus i and j
$\theta_{j,t}$	Phase angle difference between bus i and j
$P_{G_{i,t}},\ P_{D0_{i,t}}$	Active power generation of generator and active load demand at bus i

Chapter 4

SOC_d	SOC of the battery when EV needs to recharge
d_{max}	Maximum travel range of EV

η	Loss factor
d_{SC}	Available travel range when EV needs to recharge
$\mu_{d_{sc}}, \sigma_{d_{sc}}$	mean and standard deviation of normally distributed d_{SC}
d_{SR}	Service radius of FCS
W_{ph}^{k}	Average waiting time at kth FCS during peak hour
W^{max}	Maximum permissible waiting time (minutes)
$T_{\lambda_{ph}^{k}}$	Inter-arrival time of EVs during peak hour
C_{min}^{k}	Minimum number of identical charging slots of k^{th} FCS
$P_{G_{i,t}}$, $Q_{G_{i,t}}$	Active and reactive power generation at bus i in time t
$P_{D_{i,t}}$, $Q_{D_{i,t}}$	Active and reactive power demand at bus i in time t
G_{ij}, B_{ij}	Conductance and susceptance of branch ij
$I_{ij,t}$	Current in branch ij in time t
V_i^{min}, V_i^{max}	voltage limits of bus i
I_{ij}^{max}	Rated current of branch ij
N_B,N_L	Set of buses and lines of distribution system
d_{FCS}	Distance between two adjacent FCS
μ_{F_i}	Fuzzy membership indicator for ith objective function

Chapter 5

P_{wind}	Power extracted from wind
v	Average wind velocity in time t
$f_t(v)$	PDF of wind speed data in t^{th} hour
$l_t,\ c_t$	Weibull shape and scale parameters respectively at t^{th} hour
$P\left(S_m^t\right)$	Probability of wind speed being in state m at t^{th} hour
$v_{m1},\ v_{m2}$	Wind speed limits
C_p	Power index coefficient
v_{am}	Average wind speed of state m
$v_{ci},\ v_r,\ v_{co}$	Cut–in, rated and cut–off speed of wind turbine
P_m^w	Output power of wind corresponding to each state m
$CI_{avg},\ CI_{max}$	Average and maximum congestion indices
$VDI_{avg},\ VDI_{max}$	Average and maximum voltage deviation indices
$VU_{L-N}^{avg},\ VU_{L-N}^{max}$	Average and maximum voltage unbalance
$V_{t,\phi-N}$	Phase to neutral voltage at time t
$PL,\ PL_{max}$	Average and maximum active loss indices
$QL,\ QL_{max}$	Average and maximum reactive loss indices
$losses_t,\ losses_t^0$	Complex power losses with and without FCS and wind generator
$\Re(.),\ \Im(.)$	Real and imaginary parts of complex term
EPG_t^W	Excess active wind power generation
RP_t	Reverse power flow in time t

Chapter 1

Introduction

1.1 Background

Transportation sector is one of the substantial contributors of Green House Gas (GHG) emission as shown in Fig. 1.1 and oil consumption globally [1]. Highly efficient electrified transportation is a promising solution to combat energy crisis, dependency on imported oils and environmental change when coupled with low carbon electricity generation. Road electric mobility can help in reducing significant carbon emission and anticipated energy demand due to the higher efficiency compared to the Internal Combustion Engine (ICE) Vehicles. Therefore, governments, automobile industries and energy corporation around the world are making great efforts to successfully deploy Electric Vehicles (EVs). In India, government is taking initiatives to adopt new pathways to provide efficient, clean and cost-effective mobility services that can reduce dependence on oil imports and impact on environment and human health. It is reported in the guidance note of smart utility led by NITI Aayog [2] that India can save 64% of anticipated passenger road-based mobility-related energy demand and 37% of carbon emissions in 2030 by pursuing shared, electric, and connected mobility future.

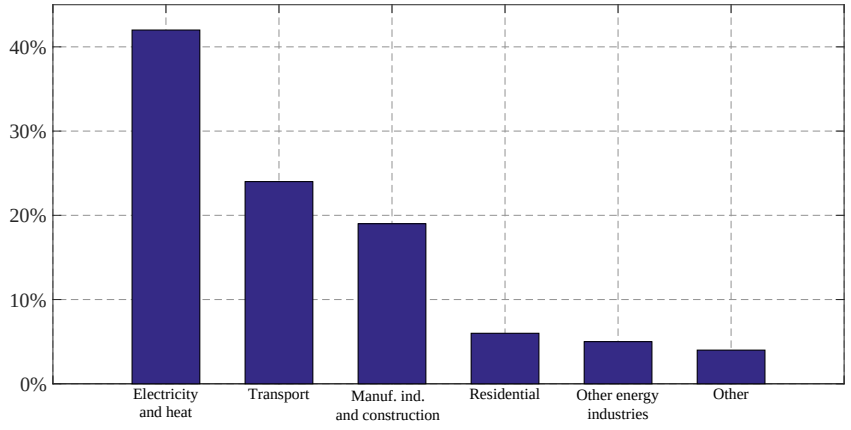

FIGURE 1.1: Various sector wise emission of GHG

The Electric Vehicle initiative estimated EV penetration in 2017 to be more than 3 million worldwide, an expansion of over 50% from 2016 [3]. India also plans to attain the ambitious goal of 6–7 millions by 2020. This increase in growth is due to the advantages associated with it like lower operating cost and less emissions along with the social

benefits. However, the growth of EVs will bring both benefits and challenges for the power grid. The EVs provide certain benefits in the form of ancillary services like energy arbitrage, voltage regulation, frequency regulation and backup power due to charging and discharging capabilities known as grid-to-vehicle (G2V) and vehicle-to-grid (V2G) respectively [4]. However, large growth of EVs will also pose challenges to the power grid like increased losses in the distribution system [5–11], voltage deviations [7, 8, 10, 12–14], poor power quality [15–17], problem of instability [18] and overloading of cables and transformers [8–11]. The benefits provided by the EVs outweighs the challenges but there are several issues hindering the large scale adoption of EVs.

1.2 Challenges Associated with EV Adoption

The adoption of EV is increasing over the years but the rate of growth is still small compared to the total vehicle population in the world. This is due to several issues like slow charging times, range anxiety, lack of charging infrastructure, higher cost of vehicles and degradation of battery life.

- **Slow Charging Times**

EVs can take minutes to many hours depending on the battery capacity, vehicle type and charging infrastructure compared to the ICE vehicles which require only few minutes to refuel their gasoline reservoir. The time taken by the battery to charge through residential charging needs approximately 7 hours. Currently, the level of charging available are Level I, II and III [19] where level I and II are AC slow charging and level III is DC fast charging. Most of the EVs in the market come with Level I cordset where one side consists of standard SAE J1772 plug and the other is a standard household plug. These charging outlets are available at home, offices and commercial places. But Level I charging requires large charging time. The Level II charging requires installation of special chargers and potential upgrades. The time required by Level II charging is still in hours. Lastly, Level III charging is the fastest taking less than 30 minutes. However, they require installation in public areas and upgradation of power grid equipments may also be needed.

- **Range Anxiety**

Range anxiety is when the EV user is worried about the depletion of complete battery energy before it reaches destination or the charging station. Majority of EVs have lithium ion chemistry-based batteries which provide shorter driving range in one charge compared to their equivalent ICE vehicles. The EVs at present can be divided into two subgroups: Plug-in Hybrid Electric Vehicle (PHEV) and Plug-in Electric Vehicle (PEV) [3]. The PHEVS has the combination of electric battery and combustion engine for the mobility.

This means that PHEVs can run on both electricity and gasoline. Range anxiety issue is not evident in PHEVs as they can refuel at any time. While PEVs are pure battery EVs and run only on electricity. Usually the battery capacity of PEVs is larger compared to the PHEVs and PEVs suffer from range anxiety issue. Table 1.1 shows efficiency data of common PHEV and PEVs [3]. The possible solution for the range anxiety is to improve battery technology and/or by installing adequate charging infrastructure. The adequate installation of charging infrastructure is must for the large scale deployment of EVs.

TABLE 1.1: All Electric and Total Range of common PHEVs and PEVs

Model	**Type**	**All Electric Range (miles)**	**All Gasoline Range (miles)**	**Total (miles)**
Nissan Leaf	EV	75	–	75
BMW i3	EV	81	–	81
Tesla Model S	EV	265	–	265
Toyota Prius	PHEV	11	600	611
Chevrolet Volt	PHEV	38	344	382

- **Lack of Public Charging Infrastructure**

The infrastructure of ICE vehicles are well developed in most of the countries, however, the same cannot be said about the EVs. For example, There are 156,000 gasoline station in US as compared to the 42029 EV charging stations as of 2016 [20]. The slow growth of EVs does not attract investors to justify the investment in public infrastructure and charging stations may still employ Level I and II charging equipments which does not benefit EV users due to large waiting time. Thus, innovative approaches are needed to deploy the public charging infrastructure so that waiting time can be reduced.

- **Higher Cost**

Most EVs like Tesla motors, Nissan Leaf and other use lithium-ion chemistry-based batteries. The cost of lithium-ion battery technology is continuously decreasing from $500 per kilowatt-hour (kWh) as of 2010 to $300 per kWh in 2015 causing the retail price of EVs to also come down. The Nissan Leaf housing 24 kWh battery costed $29,000 which is still significantly higher than their ICE counterparts [20]. The price per kWh battery is rapidly decreasing with time and this is a positive sign for the advent of EVs.

- **Capacity Fading of Battery**

Battery capacity fades with each charging cycle shortening the driving ranges. Replacement of batteries are required once it reaches its end-of-life. The decrement in driving range is smartly dealt by oversizing the battery and only showing the driving range. The bandwith

for charging battery is kept small during the starting and increased till it reaches its full capacity range in order to keep the driving range constant over the time. Replacement of battery is required once it reaches its end-of-life. Life cycle of battery can be improved with the advancement in battery technology.

1.3 Motivation

To realize an EV paradigm shift, issues pertaining to EV adoption needs to be dealt. As stated in the earlier section, slow charging time, range anxiety, lack of public charging infrastructure, higher cost and capacity fading hinders the growth of EVs. The range anxiety and lack of charging infrastructure can be dealt by building convenient charging infrastructures. While charging time, cost and capacity fading can be managed by the advancement in battery and charger technology. Fast charging infrastructures are needed for long distance trips and during emergency condition. Therefore, it is expected that Fast Charging Stations (FCS) will increase in the near future. Thus, proper investigation on the planning of FCS is needed. The planning of FCS is technically challenging since the operation of FCS will effect the operation of distribution and transportation system as well as the driving behaviour of EV users. The planning of FCS needs to be done with the consideration of charging demand distribution, traffic flow distribution, topology of distribution grid and road networks. To provide proper guidance for the planning of EV charging stations, forecasting of the EV charging demand is needed. Further, EV load characteristics are different from the conventional loads. Therefore, behavioural characterization for power flow analysis is also important to accurately realize the operational parameters of distribution system. The FCS will add extra load to the power grid and may adversely affect its operation. Therefore, analysis of impact of FCS on power grid is also needed to provide information to the distribution engineers so that they can take decision in case of any system violations. Also, the integration of low carbon electricity generation like wind and solar can be both beneficial or detrimental for the power grid. Thus, impact assessment of both FCS and renewable sources is essential on the distribution system. Therefore, this research work attempts to address the major issues of load modelling, planning and impact analysis of FCS with renewables on the performance of distribution system.

1.4 Thesis Organization

The thesis is divided into six chapters. In this chapter, a brief introduction of the proposed research work is presented.

Chapter 2 presents a comprehensive literature survey of significant works in the areas of behavioural characterization of EVs for load flow analysis, stochastic modelling of EV charging demand, planning of FCS and impact analysis of FCS on distribution system with FCS and wind generation as inferred from textbooks, technical reports and research publications. On the basis of literature survey, the research objectives framed are also presented.

In Chapter 3, mathematical model characterizing the behaviour of FCS and method for parameter estimation of closely representing standard load models for power flow analysis is proposed. Also, stochastic-based method for development of EV load profile for the assessment of impact of different load models on distribution system is proposed. Simulation and results are presented and discussed in detail.

In Chapter 4, a multi-objective synergistic planning model of FCS is proposed for distribution system coupled with transportation network. The effect of different planning objectives, waiting time and service radius are also investigated. The implementation and illustration of the proposed method is carried out on standard test system.

In Chapter 5, impact analysis of FCS and wind generation on the performance of distribution system is investigated. For this, the different performance indices are proposed and output power of wind is modelled. Simulations are carried out on standard test system and discussed in detail.

In chapter 6, conclusions of the research work are presented with a brief description of the future scope of this research work.

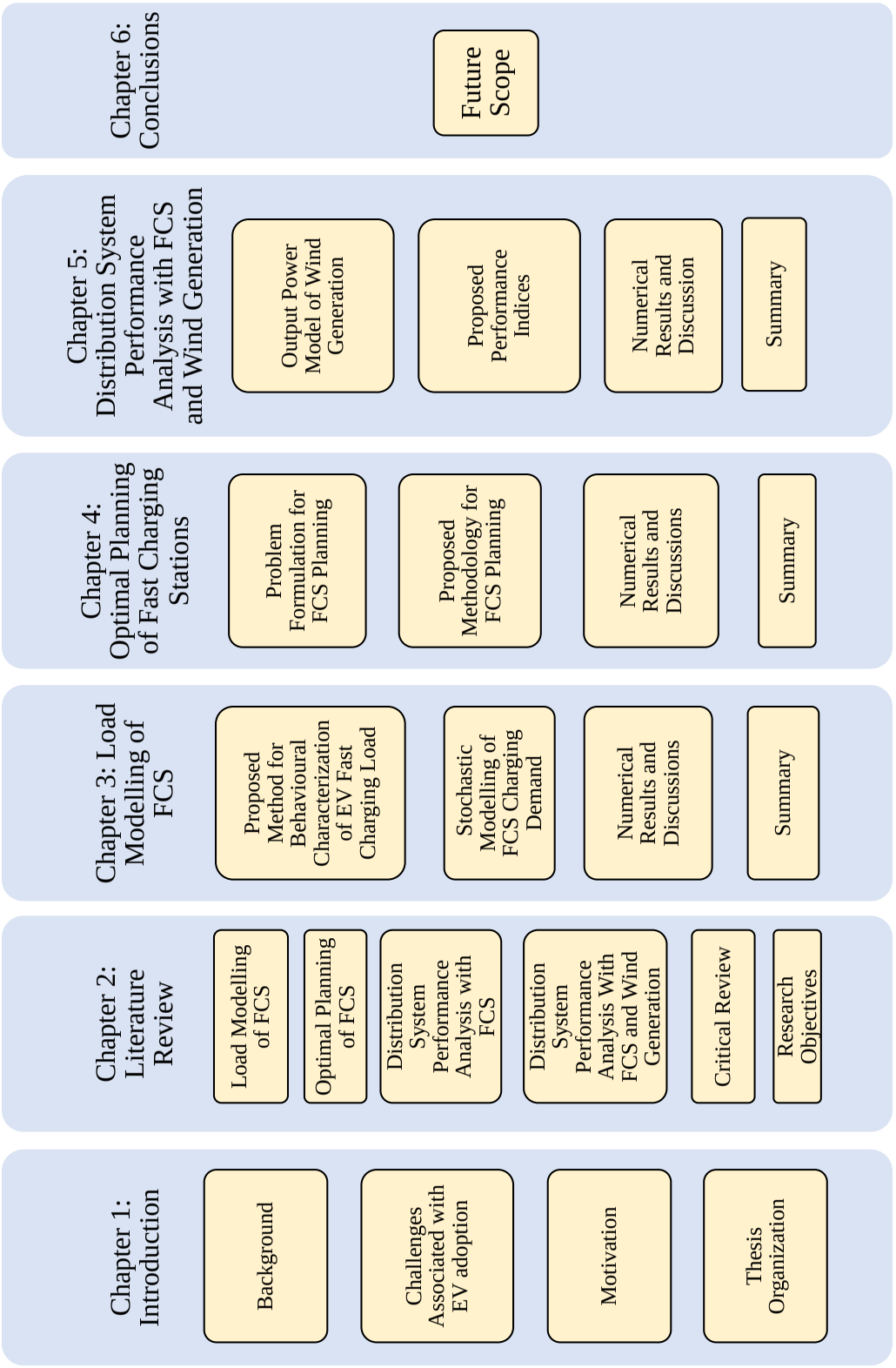
Chapter 1: Introduction
Background
Challenges Associated with EV adoption
Motivation
Thesis Organization
Chapter 2: Literature Review
Load Modelling of FCS
Optimal Planning of FCS
Distribution System Performance Analysis with FCS
Distribution System Performance Analysis With FCS and Wind Generation
Critical Review
Research Objectives
Chapter 3: Load Modelling of FCS
Proposed Method for Behavioural Characterization of EV Fast Charging Load
Stochastic Modelling of FCS Charging Demand
Numerical Results and Discussions
Summary
Chapter 4: Optimal Planning of Fast Charging Stations
Problem Formulation for FCS Planning
Proposed Methodology for FCS Planning
Numerical Results and Discussions
Summary
Chapter 5: Distribution System Performance Analysis with FCS and Wind Generation
Output Power Model of Wind Generation
Proposed Performance Indices
Numerical Results and Discussion
Summary
Chapter 6: Conclusions
Future Scope

Chapter 2

Literature Survey

The adoption of Electric Vehicles (EVs) is increasing over the years. However, the current global market share of EVs is still 3% [3]. This is due to the range anxiety, slow charging times and lack of proper charging infrastructure. These challenges can be dealt by building convenient fast charging infrastructures. The fast charging infrastructure or Fast Charging Stations (FCS) couples both the distribution system and transportation networks. For the planning of FCS, it is important to study the characteristics and estimate the demand of fast charging load. The installation of FCS will impose an extra load on the distribution systems affecting their performance. The adverse effect of fast charging load can be mitigated by integrating the local renewable generation in the system and charging with renewable will further reduce the greenhouse gas emissions. But, the intermittent nature of renewable generation like wind energy may not support the extra load during some time of the day. Therefore, it becomes necessary to analyse the impact of fast charging of EVs for assisting the distribution planners in making the decisions in case of any system violations. The accuracy of the impact analysis will depend on the load modelling of FCS.

Researchers and engineers have previously contributed to the understanding of the problem to promote the successful deployment of EVs by identifying and providing solutions to challenges associated with the placement of FCS in the distribution system. This section provides exhaustive literature survey of the methodologies of load modelling and charging demand of FCS, optimal siting and sizing of charging stations, characterization of the impacts on the grid and interaction between EVs and the renewable energy resources.

2.1 Load Modelling of FCS

To analyse the effect of EV fast charging on the distribution system performance and planning of FCS in the system, it is necessary to identify their load profile. Load can be defined as the total power (active and/or reactive) consumed by the device connected to the power system [21]. FCS load will not only depend on the distribution system parameters like system voltage and frequency but also on the uncertain factors like number of EVs charging simultaneously, initial State of Charge (SOC), charging characteristics, the amount of energy required and the charging level. Based on these factors, load modelling of FCS is categorized as behavioural characterization of FCS and estimation of charging demand of FCS considering uncertain parameters.

2.1.1 Behavioural Characterization of EV Fast Charging Load

Behaviour characterization of load is the identification of the relationship between the power consumed by the load and the voltage and/or frequency [21] for power flow analysis. The two types of the load mentioned in the literature are static and dynamic load [21–23]. The static load models are important for the power flow analysis. It is described by algebraic functions of voltage and frequency. The per unit variation in frequency is much less compared to the per unit variation in voltage. Therefore, voltage dependent load models like Constant Impedance Load (CIL), Constant Current Load (CCL), Constant Power Load (CPL), exponential load and polynomial (ZIP) load model are generally reported in the literature [24].

Different kinds of load model representing slow and fast charging EV load behaviour are mentioned in the literature. In [25], EV load is modelled for small signal stability analysis as CPL model with constant current charging technique and as CIL model by varying the charging current such that charger's input impedance remains constant. It is suggested that the penetration of EVs can be increased when the EVs are charged as CIL model. Ref. [26–28] developed charging demand as PQ buses considering exponential functions over time due to the chemical process involved in charging/ discharging. CPL model is considered for investigating the impacts of slow charging EVs on distribution system in [29–31]. In [18, 32–34], analytical relationship is derived to identify the relationship between variation in power consumed by the FCS with respect to the supply voltage. It is suggested by the authors that FCS load model consists of negative exponential load and constant power load model. FCS load is modelled in [32,33] for the planning of FCS in the distribution system and [18,34] developed voltage-dependent load model to investigate its impact on voltage stability of the system. Polynomial ZIP load model for slow charging EVs are also reported in the literature [35–37]. In [35], multi-state time variant model is developed to describe the energy consumed by the end-use load. This model describes the voltage and physical attributes dependency. Multi-stage ZIP load model is developed in [36, 37] by considering different stages based on the battery charging characteristics. Ref. [38] developed ZIP load model for different EVs at different voltage levels.

2.1.2 Charging Demand of FCS Considering Uncertain Parameters

EV charging load demand will depend on the number of EVs in the system, charging location, charging time, initial SOC, charging mode, charging duration, EV type and battery capacity. These parameters are uncertain in nature and hence, estimating charging demand becomes a complex problem. Several studies [9, 16, 17, 39–55] conducted in the past have suggested that the mobility surveys describing driving patterns can be utilized

to obtain the uncertain parameters for developing the stochastic models of EV charging demand. Based on the literature, the EV charging demand can be categorized into two levels as: i) EVs charging demand in a system, ii) Demand of charging station.

2.1.2.1 EVs Charging Demand in a System

Charging demand with spatial and temporal characteristics is estimated for all the EVs in the system. These characteristics are due to the driving behaviours of EV owners as the location of charging, charging start and end time are user dependent variables and adds randomness to the problem. The EV charging model can be developed by understanding the travel patterns, required energy by the EVs and aggregated power consumption at the charging locations. The travel patterns are obtained from transportation surveys [56, 57] to model the driving behaviour of users which provides the information about trip origin, trip distance and additional information about purpose of the trips. Two methods are mentioned in the studies to analyse the travel patterns. First method is deterministic-based method which directly utilizes travel survey data [39–41]. Direct use of survey looses uncertainty of the driving patterns and produce deterministic models of charging demand. The second is stochastic-based method which develops Probability Distribution Functions (PDFs) of the variables describing the EV travel behaviour to capture the uncertainty associated with them. This method also relies on travel survey data.

The variables of the stochastic based methods include arrival and departure time at the charging area and distance travelled in between the charging duration. However, trip purpose for modelling the charging demand is also considered [42]. Monte Carlo Simulation (MCS) [9,16,17,42–50] is used in most of the studies which uses inversion method of random number generation to sample the Cumulative Distribution Functions (CDFs) obtained from corresponding PDFs to develop the EV charging demand. Some studies [51–53] have used the travel patterns to estimate the expectation and standard deviation of the EV travel behaviour variables to further determine the expectation of the charging demand. The developed stochastic models become more accurate when the correlation between random variables is accounted. The joint distribution function of correlated variables is estimated by copula functions [54]. The study mostly assumes that the users charge theirs EVs only when arriving home while ignoring the public charging behaviour. Recent studies have shifted to study the spatial-temporal characteristics of EV charging demand [16, 41, 50].

Once the trip distance is obtained, the PDF of SOC is generated at the starting time of charging to estimate the energy requirement of EVs. A linear relationship between the travelled distance and SOC is usually considered [9, 16, 17, 39, 40, 42, 44–46, 48, 51, 52].

Further, the aggregated power is determined by estimating the number of EVs charging simultaneously in the system, charging level and duration of the charging to develop the charging demand profile. It is also extracted from the travel survey data.

2.1.2.2 Demand of Charging Station

Queuing theory is extensively used to model the demand of charging station where charging facility is considered as the queue and the EVs are modelled as the customers in the queue. Two types of queuing model are discussed in the literature that is EVs charging at charging station and at residential community. The former is modelled as $M/M/c$ [43, 47, 55] and the latter as $M/M/c/K/N_{max}$ [43] queuing model. The queuing model has inter-arrival and service time. The inter-arrival time is usually modelled as Poisson process and service time is modelled as exponential distribution. The inter-arrival time is derived from the travel survey data and may be homogeneous [43] or non-homogeneous [47, 55] in nature. The battery charging behaviour is also considered in [55] while modelling the service time. The queuing model helps in estimating the number of EVs charging simultaneously and then the charging power can be determined based on the energy required by individual EVs.

2.2 Optimal Planning of FCS

Charging infrastructure as an energy provider to EVs plays an important role in the adoption of EVs. Charging infrastructures is divided into four levels based on their charging power [19] as given in Table 2.1. The classifications of different charging levels is based upon the level at which the equipment can dispense power. The levels of charging provides range of voltage and current rating of charging stations and the maximum power output, the charging station can provide. It also mentions charging time depending on the capacity of the battery. The DC level 1 and 2 are also known as level III charging infrastructure. It is further categorized based on the purpose of charging. That is destination (slow) charging and urgent (fast) charging. AC level I and II comes under slow charging while level III comes under fast charging. The charging stations which uses level III charging are known as Fast Charging Station (FCS). It can provide power up to 96 kW and charging current up to 200A. The model of EV charger for both slow and FCS are same. An EV charger circuit is composed of AC-DC rectifier followed by a DC-DC converter for insulation of the battery from the AC supply. The difference between slow and fast charging stations are:

TABLE 2.1: Charging levels of the SAE standard J1772

Level	**Input Voltage & Current**	**Maximum Power (kW)**	**Battery Size (kWh)**	**Charging time (h)**	**Typical use**
AC Level 1	120VAC-15A 120VAC-20A	1.44 1.92	24	10-13	Home or Office
AC Level 2	240VAC-40A 240VAC-80A	7.7 25.6	24	1-3	Private or Public Outlets
DC Level 1	200VDC-80A 500VDC-80A	13.3 38.4	24	0.5-1.44	Public or Commercial
DC Level 2	200VDC-200A 500VDC-200A	33.3 96	24	0.2-0.58	Public or Commercial

- In level 1 and 2, the conversion of the utility AC power to the DC power required for battery charging occurs in the vehicle's on-board charger.
- In DC Fast Charging, the conversion from AC to DC power typically occurs off-board, so that DC power is delivered directly to the vehicle.

The urgent charging is needed when the long trip distance exceeds the driving range of the EVs [58]. The destination charging serves as the major recharging way and urgent charging will provide complimentary way to recharge the EVs since the daily driving mileage of most of the customers falls below the driving range of the EVs. However, it is necessary to develop fast charging infrastructures to provide urgent charging to the customers with long distance trips and consequently more attention has been paid towards the optimal planning of Fast Charging Stations (FCS) in the past few years. Planning of charging facilities requires determining the location and size of the FCS in the planning region where sizing of FCS means estimating the number of chargers. It also deals with number of FCS to be located. There are certain challenges associated with the planning of FCS [59, 60]:

- The current electric infrastructure may not handle the surge in demand during the peak hours for those charging stations.
- FCS may overload feeder elements based on the penetration level of EVs and vehicle usage schedules.
- They may increase transformer and network losses, voltage deviations, harmonic distortion and peak demand.

- Range anxiety due to shorter range of EVs and delay time by charging queue may cause inconvenience to EV consumers.

Therefore, these challenges needs to be considered in planning of FCS. Other factors such as transportation network's operational parameters and costumer convenience also controls the FCS planning. The study [61] suggested that the planner must consider the charging demand distribution, traffic flow distribution, regional distribution grid, road network requirements, service radius of FCS and the future development trend of EVs while planning charging infrastructure. FCS location and sizes not only affect the driving behaviour of EV owners but also impacts the power and transportation network operations. Therefore, the location and sizing of FCS should consider the driver's convenience, while simultaneously satisfying distribution and transportation network's operational constraints. Based on this, the planning of FCS can be categorized into three approaches:

2.2.1 FCS Planning from Distribution System's Perspectives

The time and location of charging is uncertain due to the EV mobility, hence, the fast charging of EVs is likely to adversely affect the distribution system performance such as increased power losses, voltage variations and overloading of the system components when large number of EVs charge simultaneously at the same location. The FCS charging demand can significantly modify the loading profile of the distribution system. Therefore, it becomes necessary to plan the FCS such that the negative impact of FCS on the distribution system performance can be reduced. The existing literature has aimed to optimally plan the FCS to satisfy the distribution system operating constraints while minimizing the power losses, variation in voltages and the investment and operation cost of FCS. Power loss depends on the loads in the system and the distance of loads from the substations. The studies [62, 63] have developed the optimization problem with the objective to minimize system power losses while [63] planned level-II charging stations with cooperation approach so that the charging stations are able to support each other. Multi-objective optimization is also proposed in the literature with the aim to minimize the power losses and voltage deviations [64–67]. In addition to these objectives, [66] added charging cost reduction and [67] CO_2 emissions in the optimization problem. Ref. [66] determined the optimal siting and sizing of FCS and renewable energy sources and [67] studied the planning of charging station with vehicle to grid capability in the distribution system. The power loss is also formulated as cost function with the inclusion of development, operation, maintenance and travelling cost in [68–70]. Further [69] identified the candidate location with two-step screening method based on the environmental factors and service radius of charging stations to deal with range anxiety issues of EV customer and then the sizing of

charging station is determined by solving the optimization function. In [71], a framework based on the life cycle cost for the optimal planning of battery charging/swapping stations in distribution systems is developed.

2.2.2 FCS Planning from Transportation Network's Perspectives

The methods used in the planning of gasoline stations have been adopted and redeveloped for the FCS planning. From the transportation perspectives, methodologies presented in the studies can be divided into three categories: (i) node demand-based method (ii) real traffic simulation-based method (iii) traffic flow-based method. In node demand-based method, charging demand is associated with each demand node and the facilities are located such that maximum node demand gets covered [72–77]. The planning area is divided based on the service radius of each charging facility with the help of Voronoi diagram [72, 74]. The charging infrastructure are assumed to be located at the center of this area and the total EVs lying at a distance within the service radius are the charging demand of that unit area. This model assumes the charging demand as static and fixed at each node. This method ignores constraints related to the traffic network congestion. The real traffic simulation-based planning methods [78–80] use simulation to estimate PEV charging demands. The simulations utilize the GPS data of a concerned vehicle time, speed, position and working conditions. Then the vehicle and transportation network information are coupled to estimate the spatial-temporal distribution of the potential EV charging demand. To consider EV mobility, traffic flow-based method is reported in the literature [60, 81–87]. This method is based on the assumption that user will charge their EVs during the travel. Therefore, the traffic flow is used to estimate the charging demands of EVs. The charging infrastructure planning will depend on the distribution of traffic flows. It is determined by estimating the number of EVs travelling between each origin and destination (OD) pairs. Traffic flows between each OD pair can be obtained from navigation systems [85], generated based on household traffic survey, or can be artificially generated by traffic simulator models [60]. The charging infrastructure is planned in this manner such that maximum traffic flow is captured by the stations. The simple model does not consider the driving range of EVs and may result in range anxiety issues. Further, constraint of driving range is added to the problem by determining the service radius of the charging stations [60, 84–87].

2.2.3 FCS Planning from Multidisciplinary Perspectives

There are few studies that have considered both transportation network and distribution system for the planning of FCS [88–102]. The objective of these studies is to integrate

FCS such that the negative effect of FCS charging demand on the distribution system performance can be reduced while simultaneously maximizing the service quality to satisfy the EV owners. The developed problems are generally constrained with the transportation and distribution system operation parameters. The objectives of the developed planning problems slightly differ from each other. Some studies have minimized the power losses and voltage deviation while simultaneously maximizing the captured EV flow [89–91]. EV energy loss due to the distance travelled to the charging stations is also included in [91,92]. In [90, 94–96], authors have minimized the investment cost associated with the FCS that includes upgradation cost of existing electrical network to support the extra FCS charging demand. In [98], agent-based modelling is proposed to identify the locations of charging stations while ensuring maximum utilization of the charging infrastructure. There are few studies which utilized fuzzy approach for multi criteria decision making to optimally select the locations of charging stations from sustainability perspective [99–102]. The evaluation index system for the optimal site selection is developed based on the literatures, feasibility reports and expert opinions. It includes environmental, economic, social and technological criteria. The technological criteria consists of different distribution system and traffic parameters while the social criteria tries to satisfy the EV owners based on the quality of the charging service.

2.3 Distribution System Performance Analysis with FCS

The proper planning of FCS will favour the large deployment of EVs in the system and the fast charging load will demand additional power from the distribution system. This may result in negative impacts on the system such as increased system losses, voltage drops, phase unbalance, overloading of equipment like distribution lines and transformer, increased power demand and stability issues. The uncertainty associated with the charging location, energy requirement, charging level, charging patterns, charging profiles and driving patterns further complicates the impact assessment of EVs on the distribution system [9,103]. Various studies have been carried out earlier for analysing its impact. The existing literature based on the studies is broadly classified as:

2.3.1 Impact on Load Profile

Various studies have been conducted to examine the effect of EV charging on the load profile of the system. The increase in peak demand due to large deployment of EVs are widely investigated in the literature and power grids all around the world are considered for the study. Ref. [104] studied the load profile of German grid in 2030 due to EVs charging and found that the slow charging of EVs will slightly increase the peak demand

for uncontrolled charging of one million EVs. However, the peak load will be approximately two times if all the conventional vehicles in Germany are replaced by the EVs. Similar study is carried out in [105] for United States and it indicates that the uncontrolled charging will result in increased load in the morning and in the late afternoon as it is the time of arrival at work and home respectively. Western Australian grid can serve 200,000 EVs during the peak demand hour [106]. Similarly peak load increases by 5% in Estonian grid for 30% penetration level of EVs when they are allowed to charge according to their convenience [107] and increase in load demand due to EV charging will affect the reliability of the Korean power grid [108]. The peak load increases by 28% and by 42% of the total load in [40] and [10] respectively. Ref. [109] investigated the load profile for dumb charging that is the EVs can charge anytime and anywhere. This results in shift in peak demand loading and the peak demand increases by 74%. All the investigation carried out are for the level-I (slow) charging. Author in [41] examined the effect of dc level-I charging on the load profile of the system and compared with the ac level-I and found that the peak demand is significantly affected by the level of the charging. To sum up, the large penetration of EV in the system will significantly increase the peak demand of the distribution system [11–13, 110–112]. Further, the EV owners tend to charge their vehicles once they arrive home or at office which increases the peak demand as well as the overall demand of the system. This increased demand may affect the distribution system operation and its performance.

2.3.2 Impact on Components of System

Large power drawn by the EVs for charging may overload the existing system components like distribution cables or lines as these components may not be designed to handle the extra load demand due to the EV charging. Several studies are carried out to investigate the impacts of EV charging on the the distribution cables or lines [5–11]. In [5], a real distribution system in Canada is examined to investigate the impact of uncontrolled charging on cable loading during peak demand and found that current system can handle penetration rate of 25% and 15% for normal and fast charging respectively. The cable in British distribution network [6] reaches its maximum ratings for medium and high EV penetration levels. Ref. [7] suggested reinforcement for 20 kV medium voltage distribution system as the fast charging of EV overloads the cable. Further, strong Finnish distribution network has negligible effect of EV charging on the overloading of cables [8]. In [9–11], it is shown that EV charging congests the distribution lines for higher penetration of EVs. From the literature it can be inferred that the impact of EV charging on the system

components of distribution system depends on the network considered and the penetration rates and charging level of EVs.

2.3.3 Impact on Voltage Profile and Phase Unbalance

EV charging will cause voltage drop and voltage deviation from the reference voltage due to the increased load demand which may result in violation of safe voltage limits [6–10,12–17, 36,46,53,113]. In addition to this, the phase unbalance may occur which can increase the current in the neutral further contributing to the voltage drop and have negative effects on electrical and electronic end user appliances [10, 14–17, 114, 115]. In [13, 113], travel survey data is utilized to assess the impact of EV charging on the node voltage profiles of the system and it is found that the system voltage limits are violated. Probabilistic approach is considered in [6, 9, 12, 46, 53] to address the uncertainties associated with the EV charging demands using Monte Carlo simulations. The study is conducted for the slow charging EVs resulting in voltage deviation from the reference values and violating the voltage limits during the peak hour. EV penetration rate of 60% [12] causes voltage limit violation in several nodes of the network. However, studies in [7,8] suggested that the EV charging does not have significant impact on the system voltage profile and the voltage deviations are within the acceptable limits. In [36], the impact of different load models of EV charging load on the voltage profile of the system is analysed and established that the load model significantly affects the terminal voltages. Some studies have also analysed the EV charging impact on the phase unbalance along with examining the voltage profile of the system. Literature has mostly used probabilistic based-methods and revealed that the residential EV charging causes unbalancing in the system [14] while slight unbalancing is reported in [114, 115] and it remains within the acceptable limits over different testing conditions. The maximum unbalancing increases with the increase in EV penetration as reported in [16]. Dynamic simulations [15] are also executed to investigate the EV charging impacts on phase unbalancing and shows that the phase unbalancing is of 5% for 7.7% of time per week causing incompliance with set standards.

2.3.4 Impact on System Losses

The increased penetration of EVs will require more power transmission causing more power losses in feeder of distribution system thus reducing the efficiency of the system. To measure the power loss, probabilistic approach is reported in the literature [6, 9, 12, 46, 113] to consider the uncertainties associated with the EV driving patterns. However, few studies have also used the deterministic approach [11, 13, 116, 117] to account for the losses and investigated it for the future years [40]. Deterministic approaches have used

the transportation survey data for the analysis. In [116], a Danish network is considered with all the three level of charging incorporated for the analysis. The losses increases by 40% for 50% EV penetration rate. The losses during off-peak hours are found to be maximum in [117] where it assumes that EV charges overnight resulting in simultaneous charging of EVs. Further the impact of fast charging is also investigated and it accounts for more losses as compared to the slow charging EVs. Similar findings are reported in [12, 13, 113]. [9, 46] modelled stochastic EV fast charging load and analysed its impact on the system losses. The losses increases from 900 kWh to 1100 kWh when number of EVs increases from 0 to 500. Further, [36] investigated the impact of different load models on the losses of the system and the result shows that the load model has significant effect on the losses and may provide misrepresentation if the EV load model for the analysis is not accurate. The comprehensive survey reveals that the power losses depends on the distribution system topology, load models of EV charging, charging level, charging time, charging mode, penetration rate of EVs and the driving behaviour of the EV owners.

2.4 Distribution System Performance Analysis with FCS and Wind Generation

The CO_2 emissions related to transportationy will not reduce significantly if the electricity used to charge the EVs is generated from fossil fuel based conventional power plants. Integration of renewable generation can help in reducing these greenhouse gas emissions and the negative effects of the EV fast charging on the distribution system. However, renewable generation such as solar and wind are intermittent in nature and depends on weather condition [118]. Many studies have proposed EVs interacting with the renewable in smart grid environment [119–121]. The smart grid enables two-way communication between the power grid and the end users. The effective utilization of communication through intelligent charging techniques will allow the power grid to embrace the large-scale deployment of EVs and integration of renewables [122]. Nonetheless, the intelligent charging technology is not mature and it is expected that convenient charging will take place mostly. Therefore, it becomes important to investigate the distribution system performance in presence of both renewables and fast charging EVs rather than studying each independently. Very few studies have been reported in the literature that studies the synergy between the EVs and renewables and performance of distribution system [48, 123–129]. Ref. [123] shows that there will be reduction in excess power with electrification of transportation, however, the uncontrolled charging increases the imbalance between wind power production and power consumption. Voltage stability and security analysis of

U.K. distribution network model is investigated in [124] with different penetration of wind and EVs and found that voltage limits are violated even with high penetration of winds generation. Voltage limit violation probability is also reported in [125] for 40% penetration of EVs and wind. Impact of uncontrolled slow charging of EVs in distribution system embedded with roof top solar photovoltaic [126] and wind generation [48] on distribution system performance is investigated. It suggest that the impact of EV charging can be mitigated by introducing the renewable in the system, however, they act as partial solution due to their intermittent nature. In [127], it is suggested that around 49% of EVs can charge through local renewable and daily peak export power is also present since local renewable is not sufficient to supply the EV charging demand. In [128, 129], it is reported that PV support did not assist in increasing the lowest voltage occurring during the night due to the EV charging.

2.5 Critical Review

It is clear from the literature survey that the load modelling of EV charging is important to investigate its impact on the distribution system. Load modelling will depend on the type of study to be carried out; for load flow analysis, static load model needs to be developed which can indicate the effect of supply voltage on the power consumption and time domain simulation requires dynamic load models. Most of the literature has considered CPL model for the analysis, that is variation of power consumption with feeder voltage is ignored, but analytical studies have clearly demonstrated that CPL model does not represent the true nature of the EV charging load. The effect of battery characteristics should also be considered as the power consumption varies with respect to the SOC of the battery. Most of the studies have modelled the slow charging EV load. However, to analyse the impact of FCS on distribution system, the static modelling of FCS load becomes important. Since, the EV charging load is not fixed and will vary throughout the day, hence, FCS charging load profile should be developed which also includes the effects of voltage variation and battery charging characteristics. The FCS load will depend on a number of uncertain factors like number of EVs charging simultaneous at FCS, energy required by the EVs, driving behaviour and the location of charging. The general pattern with these uncertain variables needs to be established such that it estimates the FCS charging load profile. The FCS load have both spatial and temporal characteristics. Thus, the charging demand of FCS will also depend on the location of FCS in the planning region. FCS couples both the transportation and distribution network, therefore, traffic flow in the transportation network will also effect the FCS charging demand. Hence, the FCS charging demand profile needs to be modelled with spatial-temporal characteristics,

uncertainty of the driving behaviour, the effect of battery characteristics and the feeder voltage.

From the literature of planning of FCS, it can be inferred that the location and sizing of FCS will affect the operation of both distribution system and the transportation network as well as the convenience of the EV customer. It is important for planning of FCS to be performed such as: (i) to reduce the negative impact of FCS on the distribution system by proper siting and sizing of FCS (ii) to maximize the utilization of FCS (iii) to provide better service quality to the EV customers. The studies have either considered only the distribution system or the transportation network parameters. There are few studies which have considered both the system's constraints in developing the planning model of FCS. The battery capacity also plays an important role in the planning so as to ensure that the EVs can reach to its nearest charging station within its battery capacity. Further, the spatial-temporal charging demand is necessary to estimate the number, location and sizes of FCS. This demand is considered as static in nature which is not true due to the EV mobility. Real traffic simulation-based studies are also reported in the literature which accounts the mobility of the EVs but the collection of this data is costly. Another way to consider the mobility is the traffic flow based method which represents the EVs as a flow in the transportation network. This method also focusses on the maximum utilization of the FCS. The service quality will depend on the charging service time which will depend on the energy require by the EV to recharge and the waiting time. The waiting time can greatly affect the service quality. Therefore, the service quality and the distribution system parameters will become the deciding factor for the sizing of FCS. Further, all the studies have considered the CPL model to estimate the distribution system's performance parameters. It has already been stated that the CPL model is not the true representation of FCS charging demand. Therefore, the correct load model should be accounted while planning the FCS. The literature has partially addressed the aforementioned factors for the planning of FCS. Therefore, further investigations are needed to plan the FCS considering the EV mobility, the topologies of distribution system and the traffic network, the economics and security issues of power systems and customer satisfaction with the correct load model of FCS charging demand.

The installation of FCS imposes an additional load demand on the grid resulting in degradation of operating parameters of distribution system. The few consequences of fast charging EV load reported in the literature are change in load profile of the grid, increased peak demand, increased system losses, overloading of the system components, voltage deviation and phase imbalances. Investigation of system performances in terms of

mentioned parameters is mostly done for the slow charging EVs and they are assumed to be charged at home on their arrival and very few literature mentions the impact of fast charging EVs. Deterministic and probabilistic approaches are considered to determine the system performance parameters of the distribution systems. It is inferred that the probabilistic approaches incorporating uncertainties associated with the driving patterns are important to explore the performance of the system. The phase unbalancing is mostly investigated for the slow charging EVs and not for the fast charging stations. It is also observed that the system losses, voltage deviations and overloading of system component depends on the topology of the considered distribution system, location of charging and charging level. Further, most of the literature have considered CPL model in power flow for the analysis but it is stated earlier that the CPL model is not a better representation of EV fast charging load. Also, there is a dearth of literature analysing all the aforementioned parameters together for the FCS load. The investigations are generally carried out for one or two parameters.

The literature survey reveals that integration of the EVs will add an extra demand to the power grid, thus, resulting in negative impacts like increased demand, losses and voltage dips in the network. While, integration of renewable such as solar or wind may result in reverse power flow and voltage rise at various nodes of the network. Further the renewable may cause demand supply mismatch as they tend to be variable in electricity generation with no correlation to the changes in demand. Most of the literature has studied their impacts individually and very few papers have attempted to analyse the simultaneous effect of EV fast charging and renewable integration on the performance of the distribution system. It is reported that even the high penetration of renewable may not mitigate the negative effects of EV fast charging on the system completely. Moreover, wind is the fastest growing clean source of energy and can be installed at urban areas and large cities. Therefore, it is expected that wind will be used in conjunction with the FCS in the future. Hence, it is necessary to analyse the synergy of FCS and wind generation and their impact on the distribution system performance rather than studying each independently.

2.6 Research Objectives

On the basis of the literature survey and the critical review, following research objectives have been formulated in this thesis work:

1. To carry out a comprehensive literature survey on load modelling and planning of FCS in distribution system.

2. To develop EV fast charging load model by characterizing its voltage dependent behaviour.
3. To develop stochastic load demand profile of FCS considering the uncertainties associated with the EVs.
4. To propose a suitable synergistic strategy for planning of FCS with transportation network.
5. To investigate the performance of distribution system in presence of FCS embedded with wind generation and transportation network.

In this chapter, an exhaustive literature survey of load modelling, planning of FCS and performance analysis of distribution system in presence of FCS and wind generation has been carried out. The critical analysis of literature survey has been performed related to these aspects and on that basis research objectives have been framed for the present research work.

Chapter 3

Load Modelling of Fast Charging Station

3.1 Introduction

In recent years, various problems such as rapid depletion of fossil reserves, volatility in fuel prices, environmental and health issues related to the vehicular emissions led to the fast growth of Electric Vehicles (EVs) [130]. The EV charging technologies are classified into ac and dc and further according to the level (I–III) [19]. Slow charging levels I and II are used in home or office and level III is the commercial fast charger. There is a need for level III charging in emergency conditions, long trips and to meet the anxiety of the EV owners. Fast charging of simultaneous EVs will have a significant effect on the distribution system. Therefore, it is necessary to study the characteristics of the load model for the power flow analysis and estimate the stochastic demand of fast charging EVs to investigate its impact on the distribution system. The increased penetration of fast charging EV load will impose an additional large load demand. Also, EV load characteristics are different from the conventional loads. It depends on uncertain parameters such as location, time, driving pattern, initial State of Charge (SOC), charging level, number and type of EVs, battery capacity and charging characteristics.

Defining the load model for power flow analysis requires identification of the relationship between the active and/or reactive power consumed by the load and system voltage and/or frequency [22]. As the per unit variation of power with per unit variation of frequency is negligible compared to the per unit variation of power with per unit variation of voltage. Therefore, the investigation of mathematical relationship between the power consumed and the voltage becomes important. Various load models like Constant Impedance Load (CIL), Constant Current Load (CCL), Constant Power Load (CPL), exponential and polynomial (ZIP) load model are reported in the literature [24]. Different load models representing slow and fast charging EV loads are used to carry out different investigations like small signal stability analysis [25], voltage stability analysis [18, 32–34] and it is found that the load models affects the analysis of the studies. The studies have modelled slow charging EV load and considered CPL model. However, it is stated in [18] that CPL model does not represent the true behaviour of EV charging load. Further, the effect of battery characteristics on the load model is not properly explored. Therefore, identification of accurate static load model is needed to analyse the impact of FCS on the distribution system.

The load model is not sufficient enough to analyse the impacts of EV charging load on the distribution system as the charging demand has spatial-temporal characteristics and depends on uncertain parameters like charging level, time, SOC and the number of EVs charging simultaneously. Several studies [9,16,17,39–55] conducted in the past suggest that the mobility surveys are the good source to identify the driving patterns. These driving patterns can be utilized to estimate the EV charging demand. The literature reports the development of overall charging demand of the system [9, 16, 17, 39–53] and the demand at the charging station [43, 47, 55]. Most of the literature developed overall charging demand and few attempted to develop demand of charging station. Therefore, in this thesis, the voltage-dependent charging profile of FCS is developed which has spatial-temporal characteristics and uncertainty associated with driving behaviour is also incorporated.

The objective of this chapter is to develop a suitable mathematical model to establish the relationship between power consumed by the fast charger, supply voltage and the battery SOC. The developed mathematical model is validated by simulating a fast charger. Then, the accurate voltage-dependent load model for power flow analysis is explored using the power voltage characteristics obtained from the simulated fast charger. Estimation of parameters of voltage-dependent model is achieved through measurement approach by formulating a constrained least square optimization problem. Further, the effectiveness of the load model is assessed in terms of performance measurement parameter. The accurate load model is then used to develop the EV fast charging demand profile also known as Aggregated EV Charging Profile (AECP). The AECP requires development of queuing model of each installed FCS which consists of spatial-temporal characteristics. Then the effectiveness of the developed AECP for different load models is analysed on IEEE 123-bus distribution system. The standard system needs modification in its secondary side so as to include the residential houses, distribution transformer and FCS. Then the developed voltage-dependent FCS charging demand profile is integrated within a distribution system to study the impact of EV charging behaviour and feeder voltage dependency on distribution system.

3.2 Proposed Method for Behavioural Characterization of EV Fast Charging Load

Behavioural characteristics of the load can be categorized depending on how the power consumed by the load changes by varying different operating conditions like voltage and/or frequency. Identification of voltage dependent characteristics is important for the static studies like power flow analysis. This requires determining the mathematical relationship

between the voltage and power consumption and then finding the most suitable model from the well established load model for power flow analysis.

3.2.1 Derivation of Mathematical Model of EV Fast Charging Load

EV fast charging load is a power electronically controlled load which consists of a three phase charging unit and a EV battery as shown in Fig. 3.1. Currently, most of the chargers used are unidirectional chargers [131, 132] with conventional charging method of Constant Current Constant Voltage (CC-CV) charging. The well established EV fast charger consists of two converters: i) AC-DC front end converter ii) DC-DC buck converter at the battery end. The front end converter performs AC to DC rectification with power factor correction feature while keeping the the DC link voltage constant. The DC-DC buck converter is equipped with different Pulse Width Modulation (PWM) techniques to maintain the voltage and current requirements for different State of Charge (SOC) conditions. This subsection considers three stages in EV battery charging that is AC-DC rectifier, DC-DC buck converter and the battery to model the EV fast charging load.

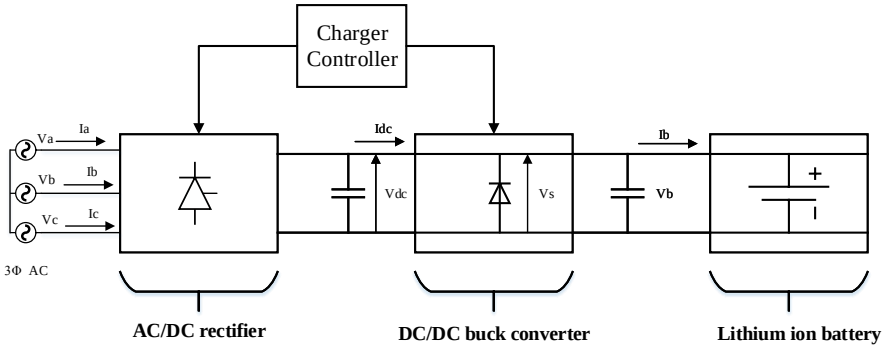

FIGURE 3.1: Schematic diagram of DC fast charger

3.2.1.1 AC-DC Rectifier Modelling

AC-DC rectifier as shown in Fig. 3.2 can maintain the DC-link voltage constant inspite of any voltage variations within the designed limits and can perform unity power factor correction [132].

Analytical relationship between supply voltage and constant DC-link voltage is determined in this section. The governing equation [32, 133] for the front end rectifier from Fig. 3.2 can be derived as:

For Phase 1:

$$L\frac{di_1}{dt} + R_L i_1 = V_{AD} = E_1 - (V_{DN} + V_{NO}) \tag{3.1}$$

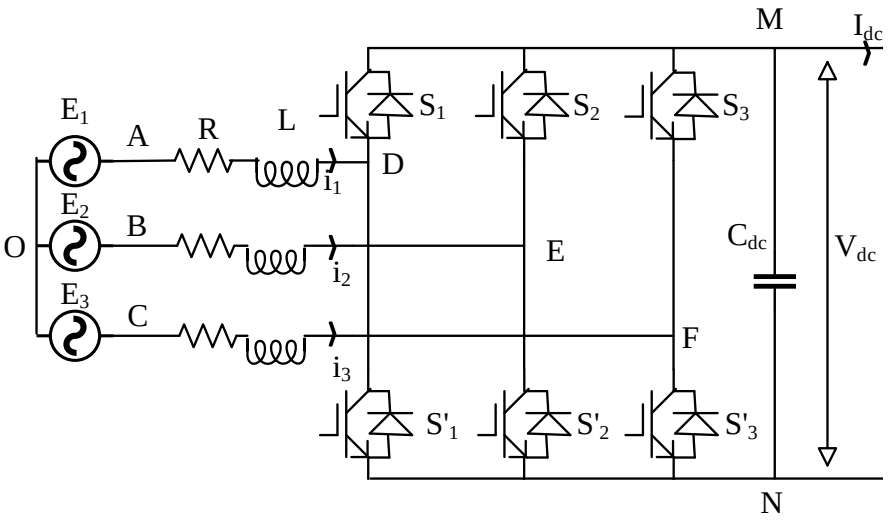

FIGURE 3.2: Front-end controlled AC-DC rectifier

when switch S_1 is in ON and and S_1' is OFF, the switching function is $S_1 = 1$ and $S_1' = 0$ and $V_{DN} = i_1 R_s + V_{dc}$

where, R_s is the equivalent resistance of switching device.

When switch S_1 is in OFF and and S_1' is ON, the switching function is $S_1 = 0$ and $S_1' = 1$ and $V_{DN} = i_1 R_s$ Then, equation (3.1) becomes,

$$L\frac{di_1}{dt} + R_L i_1 = E_1 - \left[(i_1 R_s + V_{dc})S_1 + i_1 R_s S_1' + V_{NO}\right] \tag{3.2}$$

$$S_1 + S_1' = 1 \tag{3.3}$$

Then, equation (3.2) becomes,

$$L\frac{di_1}{dt} = -R_L i_1 - [i_1 R_s + V_{dc} S_1 + V_{NO}] + E_1 \tag{3.4}$$

$$L\frac{di_1}{dt} = -Ri_1 - [V_{dc} S_1 + V_{NO}] + E_1 \tag{3.5}$$

where, $R = R_L + R_s$ is total series resistance in one phase. Similarly, for phase 2 and 3,

$$L\frac{di_2}{dt} = -Ri_2 - [V_{dc} S_2 + V_{NO}] + E_2 \tag{3.6}$$

$$L\frac{di_3}{dt} = -Ri_3 - [V_{dc} S_3 + V_{NO}] + E_3 \tag{3.7}$$

For a three phase system without a neutral line, $i_1 + i_2 + i_3 = 0$ and if ac supply is balanced, then, $E_1 + E_2 + E_3 = 0$

Adding equation (3.5),(3.6) and (3.7), we get,

$$V_{NO} = -\frac{V_{dc}}{3}\sum_{k=1}^{3} S_k \tag{3.8}$$

Then, governing equations for AC-DC rectifier are:

$$L\frac{di_k}{dt} + Ri_k = E_k - V_{dc}(S_k - \frac{1}{3}\sum_{k=1}^{3} S_k) \tag{3.9}$$

$$I_{dc} = \sum_{k=1}^{3} S_k i_k - C_{dc}\frac{dV_{dc}}{dt} \tag{3.10}$$

where,

k	index of phase (1,2,3)
L	inductance of input filter
i_k	line current
R	total resistance of active rectifier switches and parasitic resistance of the input filter
E_k	phase voltage
C_{dc}	DC-link capacitor
S_k	switching function
I_{dc}	output dc current of AC/DC rectifier
V_{dc}	output dc voltage of AC/DC rectifier

Equation (3.9) and (3.10) is further written in the stationary dq reference frame using Clark's and Park transformation.

$$V_d = L\frac{di_d}{dt} + Ri_d - L\omega i_q + S_d V_{dc} \tag{3.11a}$$

$$V_q = L\frac{di_q}{dt} + Ri_q + L\omega i_d + S_q V_{dc} \tag{3.11b}$$

$$I_{dc} = \frac{3}{2}(S_d i_d + S_q i_q) - C_{dc}\frac{dV_{dc}}{dt} \tag{3.11c}$$

where, ω is grid frequency, i_d, i_q, V_d *and* V_q represents direct axis and quadrature axis current and voltage and S_d, S_q are switching functions in dq reference frame. In steady state, equation (3.11a), (3.11b) and (3.11c) becomes:

$$V_d = Ri_d - L\omega i_q + S_d V_{dc} \tag{3.12a}$$

$$V_q = Ri_q + L\omega i_d + S_q V_{dc} \tag{3.12b}$$

$$I_{dc} = \frac{3}{2}(S_d i_d + S_q i_q) \tag{3.12c}$$

The active and reactive power in dq reference frame is given by:

$$P = \frac{3}{2}(V_d i_d + V_q i_q) \tag{3.13a}$$

$$Q = \frac{3}{2}(V_d i_q - V_q i_d) \tag{3.13b}$$

where, P and Q are the total active and reactive power drawn by EV fast charger which also includes power losses in parasitic resistance of input filter, resistance of active rectifier switches, resistance of output filter and internal resistance of battery. In the steady state $i_q = 0$, as the reference current with which it is compared is made zero to gain unity power factor and $V_q = 0$ as it is assumed that the dq frame is rotating with ω speed with d axis aligned along the supply voltage. Equation (3.13a) with the help of equation (3.12a) and (3.12c) becomes

$$P = \frac{2RI_{dc}^2}{3S_d^2} + V_{dc}I_{dc} \tag{3.14}$$

3.2.1.2 DC-DC Buck Converter Modelling

The objective of DC-DC buck converter is to maintain constant current to flow into the battery during CC charging. When voltage of the battery reaches certain threshold limit, then DC-DC buck converter maintains constant voltage across the battery terminals. The DC-DC buck converter is shown in Fig. 3.3. Further, it maintains the charging ripple current within the safe limits.

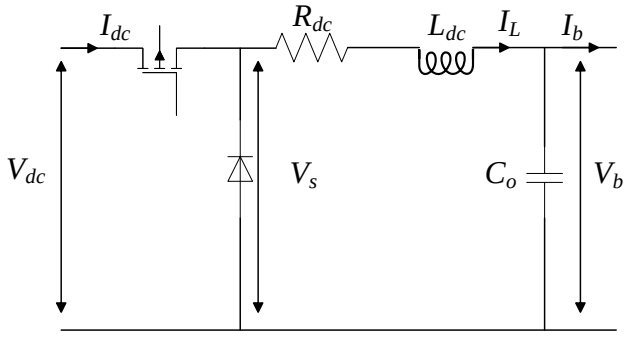

FIGURE 3.3: DC-DC buck converter at the battery end

Referring to Fig. 3.3, relationship between battery voltage V_b and voltage V_s across diode is written as:

$$V_s = I_L R_{dc} + L_{dc}\frac{dI_L}{dt} + V_b \tag{3.15}$$

$$I_L = I_b + C_o\frac{dV_b}{dt} \tag{3.16}$$

where, I_L is the output current of DC-DC buck converter, R_{dc} is resistance of the output filter and L_{dc} is the inductance of the output filter. Here it is assumed that the battery of EVs coming to the charging station will not be completely depleted and it will be charged to a certain SOC by constant current for fast charging till the battery voltage reaches threshold limit.

3.2.1.3 Battery Modelling

Lithium ion battery is mostly used in the EV due to its advantage over other battery chemistry like high energy density, low self discharge, low maintenance and high charging and discharging capabilities [134]. Dynamic model [134] of battery is considered here to state the relationship between SOC and battery terminal voltage given by equation (3.17).

$$V_b = V_o - r_b.I_b - K\frac{Q}{Q - \int I_b dt}.\int I_b dt + Aexp^{-B.\int I_b dt} \tag{3.17}$$

where V_o is battery constant voltage (V), r_b is internal resistance of battery (Ω), K is polarization constant (V/Ah), Q is rated battery capacity (Ah), $\int I_b dt$ is extracted battery charge (Ah), A is exponential zone amplitude (V), B is exponential zone time constant (Ah^{-1}), I_b is battery charging current (A) and V_b is battery voltage (V) . Theoretically $\int I_b dt = 0$ when battery is fully charged. Therefore, equation (3.17) can be written as:

$$V_b = V_o - r_b.I_b - K\frac{Q(Q - \int I_b dt)}{\int I_b dt} + Aexp^{-B.(Q-\int I_b dt)} \tag{3.18}$$

For constant current charging, $I_b = constant$, therefore equation (3.16) with the help of equation (3.18) can be written as:

$$I_L = I_b + C_o\left[\frac{KQ^2 I_b}{(\int I_b dt)^2} + ABI_b exp^{-B.(Q-\int I_b dt)}\right] \tag{3.19}$$

thus, equation (3.15) can now be written as:

$$V_s = V_o - I_b(r_b - R_{dc}) - \frac{KQ}{\int I_b dt}\Bigg[(Q - \int I_b dt) - C_o R_{dc} I_b \frac{Q}{\int I_b dt} + 2L_{dc}C_o I_b^2 \frac{Q}{(Q - \int I_b dt)^2}\Bigg] + A(1 + C_o B I_b R_{dc} + L_{dc} C_o I_b^2 B^2) exp^{-B.(Q - \int I_b dt)} \quad (3.20)$$

Equation (3.19) and (3.20) can be written in terms of SOC of the battery as

$$I_L = I_b + C_o\Bigg[\frac{KI_b}{SOC^2} + ABI_b exp^{-BQ.(1-\frac{1}{SOC})}\Bigg] \quad (3.21)$$

$$V_s = V_o - I_b(r_b - R_{dc}) - \frac{K}{SOC}\Bigg[Q(1 - SOC) - C_o R_{dc} I_b \frac{1}{SOC} + 2L_{dc}C_o I_b^2 \frac{1}{Q.SOC^2}\Bigg] + A(1 + C_o B I_b R_{dc} + L_{dc} C_o I_b^2 B^2) exp^{-B.Q(1-SOC)} \quad (3.22)$$

where SOC of the battery is given by equation (3.23). The value of SOC_{ini} is considered 0 and values of SOC lies between 0 and 1.

$$SOC = SOC_{ini} + \frac{\int_0^t I_b dt}{Q} \quad (3.23)$$

SOC_{ini} is considered 0 to reduce mathematical calculations. The equation (3.21) and (3.22) can be approximated as equation (3.24) and (3.25) respectively as exponential part and the terms containing C_o does not have significant effect on the values of I_L and V_s when range of SOC is bounded of the nominal capacities in order to protect the batteries [135] and due to small value of C_o.

$$I_L = I_b \quad (3.24)$$

$$V_s = V_o - I_b(r_b - R_{dc}) - \frac{K}{SOC}\Bigg[Q(1 - SOC)\Bigg] \quad (3.25)$$

Assuming continuous conduction mode operation and lossless switching of the buck converter, the steady state duty ratio of buck converter f can be expressed as:

$$f = I_{dc}/I_L \quad (3.26a)$$

$$V_s = fV_{dc} \quad (3.26b)$$

Combining equation (3.26a), (3.26b) and (3.14) and assuming $S_d = V_d/V_{dc}$ equation (3.27) can be obtained

$$P = \frac{2RV_s^2 I_L^2}{3V_d^2} + V_s I_L \tag{3.27}$$

On observing equations (3.25) and (3.27), it can be said that the power consumption of the EV charging load comprises of two components:

(i) Power losses in parasitic resistance of input filter that depends on ac side voltage and *SOC* of the EV battery.

(ii) Power losses in output filter of DC-DC buck converter, internal resistance of the battery and the power consumed by the battery during charging that depends on *SOC* of the EV battery.

Therefore, power consumed by the fast charger will depend on *SOC* of the EV battery and ac side supply voltage. It is evident from the first part of equation (3.27) that power consumed by the fast charger has inverse square relationship with supply voltage. This follows standard exponential load behaviour.

3.2.2 Parameter Estimation of EV Fast Charging Load

The impact of EV fast charging can be investigated by performing power flow analysis. It requires to define the type of load model from the well established load models [22, 23]. Most studies have considered conventional load models such as CPL and CCL. However, the mathematical model derived in Section 3.2.1 clearly shows that the EV fast charging load consists of negative voltage-dependent exponential and constant power component. There are two voltage-dependent load models existing in the literature that closely resemble the derived analytical relationship. They are exponential and ZIP load model [22] given as

$$\frac{P}{P_o} = a_p\Big(\frac{V}{V_o}\Big)^{n_p} + b_p \tag{3.28}$$

where P_o is the active power consumed at the rated voltage V_o. a_p, n_p, b_p are the unknown parameters of the exponential load model for the active power. From equation (3.28), it is observed that exponential load model has nonlinear relationship between active power and voltage. It also has constant power term that is independent of the voltage.

$$\frac{P}{P_o} = \underbrace{Z_p\Big(\frac{V}{V_o}\Big)^2}_{CIL} + \underbrace{I_p\Big(\frac{V}{V_o}\Big)}_{CCL} + \underbrace{P_p}_{CPL} \tag{3.29}$$

where Z_p, I_p, P_p are the unknown coefficients of ZIP load model for active power. P_o is the active power at the rated voltage V_o. Polynomial ZIP load model is the combination of

CIL, CCL and CPL model. On observing the above two load models and comparing it with equation (3.27), it can be said that the exponential load model is the better representation of EV fast charging load. To validate the accuracy in the load representation, parameters of both exponential and ZIP load model are estimated using the measurement-based approach. It is mathematically an identification problem where the variations of power consumed with variation of voltage are identified. The identified load model for the given voltage will produce the estimated load. The difference between the estimated load and the measured load should be minimum under same operating conditions. Therefore, this becomes a minimization problem given as

$$Min \quad \sum_{i=1}^{n} e_i^2 \tag{3.30}$$

where, e_i is the difference between the measured value and the estimated value for i^{th} operating condition and n represents total operating conditions. For the estimation of parameters of exponential load model, the objective function is written as

$$Min \quad \sum_{i=1}^{n} \left[\left(a_p \Big(\frac{V_i}{V_o} \Big)^{np} + b_p \right) - \frac{P(V_i)}{P_o} \right]^2 \tag{3.31}$$

$$Subject\ to: \quad a_p + b_p = 1$$

Further, the parameters of ZIP load model are also estimated to analyse the effectiveness of the proposed exponential load model given by equation (3.32).

$$Min \quad \sum_{i=1}^{n} \left[\left(Z_p \Big(\frac{V_i}{V_o} \Big)^2 + I_p \Big(\frac{V_i}{V_o} \Big) + P_p \right) - \frac{P(V_i)}{V_o} \right]^2 \tag{3.32}$$

$$Subject\ to: \quad Z_p + I_p + P_p = 1$$

where, V_i and $P(V_i)$ are the i^{th} pair of measured values. The performance of each load model is assessed in terms of Mean Absolute Error (MAE) given by equation (3.33).

$$MAE = \frac{1}{m} \sum_{i=1}^{m} \left| \frac{A_i - P_i}{A_i} \right| \times 100\% \tag{3.33}$$

where A_i is the actual power consumption, P_i is the predicted value of power consumption by voltage dependent load models and m represents the number of values to be predicted.

It denotes the deviation of predicted value from the actual value. The value closer to zero indicates that the predicted value is close to the actual value.

3.3 Stochastic Modelling of FCS Charging Demand

Previous section determined the accurate load model of EV fast charging for power flow analysis. However, the complete impact of FCS can be analysed by having the information about the charging demand that occurs throughout the day. Therefore, there is a need to develop Aggregated EV Charging Profile (AECP) of each FCS in the distribution system. AECP will depend on many factors like number of EVs in the system, charging level, initial SOC of EVs, daily energy requirement, spatial-temporal distribution of vehicles, driving behaviour and battery capacity. The aforementioned parameters are uncertain, therefore, in this section, 24-hour AECP for each FCS is developed which has spatial-temporal characteristics and uncertainties associated with EV charging are also incorporated. To develop the AECP, the first step is to estimate the number of EVs in the system. The number of EVs (N_{EV}) depends on the number of residential houses (N_{houses}), average number of vehicle per house (α) and penetration (p) of EVs with respect to the total vehicles in the planning area.

$$N_{EV} = N_{houses} \times p \times \alpha \tag{3.34}$$

The number of houses is estimated by replacing the spot loads of the distribution system with the residential houses and distribution transformer based on the peak loading of the spot loads. It is assumed that the distribution transformer sees Maximum Diversified Demand (MDD) calculated by the equation (3.35).

$$MDD = \frac{n_{house} \times S_{house}^{max}}{DF} \tag{3.35}$$

where n_{house} is the number of houses connected to each spot load, S_{house}^{max} is the maximum individual demand of each house and DF is the Diversity Factor. The values of DF is chosen from DF table given in [136] such that MDD is close to the corresponding peak value of the spot loads. Therefore, N_{houses} is total number of peak spot load replaced times the n_{house}. Based on the number of EVs in the system, the spatial-temporal distribution of vehicles is determined.

3.3.1 Spatial-Temporal Distribution of Vehicles

Spatial-temporal distribution model works on systematic integration of distribution system and transportation network as FCS couples both the networks. It provides the information about the location and time that EV starts charging. Origin-Destination (OD) analysis is used to model the spatial behaviour of EV mobility and transportation surveys are utilized to determine the temporal characteristic of the EVs. In an urban area, the daily travel pattern generally follows a regular pattern. An OD matrix $A_{N_T \times N_T}$ is introduced in this study with probabilities (f_{OD}) assigned to each OD pair to represent the amount of traffic it attracts. This value is generated using gravity spatial interaction method [137] which suggest that the ability to attract the traffic flows between the OD pair will depend on the weight assigned to the origin and the destination node and the distance between the OD pairs as given in equation (3.36).

$$f_{OD} = \begin{Bmatrix} 1.5 * \frac{w_O w_D}{d_{OD}} & if & O \neq D \\ 0 & if & O = D \end{Bmatrix} \tag{3.36}$$

where, w_O and w_D are the weight assigned to origin and destination node respectively and d_{OD} is the shortest route between OD pair. Then, the traffic flow between the OD pair during the day at any time t is determined in equation (3.37) using the average traffic that travel through the transportation network in time t. The information about the average traffic is obtained from the distribution of vehicles during the day given in transportation surveys.

$$f_{OD,t} = f_{total,t} \times \frac{f_{OD}}{\sum\limits_{O \in N_T} \sum\limits_{D \in N_T} f_{OD}}, \; t \in [1, 24] \tag{3.37}$$

where $f_{total,t}$ is the average number of EVs that travel through the transportation network in time t and N_T are set of transportation nodes. The generated EV mobility data for each OD pair is further used to estimate the number of EVs charging simultaneously at each FCS using queuing theory.

3.3.2 FCS Queuing Model

The charging of EV can be considered to be a service provided by FCS in a queue. Therefore, queuing theory [138] is employed here to model the arrival and service of EV charging at FCS and estimate the charging demand of each FCS. $M_1/M_2/N_c$ queuing model is considered to serve the EV owners as shown in Fig. 3.4. M_1 denotes a system with exponentially distributed inter arrival times with mean T_λ ($T_\lambda > 0$). T_λ varies hourly and modelled as non-homogeneous Poisson process. M_2 denotes exponentially distributed service time with mean T_μ ($T_\mu > 0$). The service time will depend on the SOC of the EV

battery at the start of the charging. N_c denotes the maximum number of EVs that can be charged simultaneously.

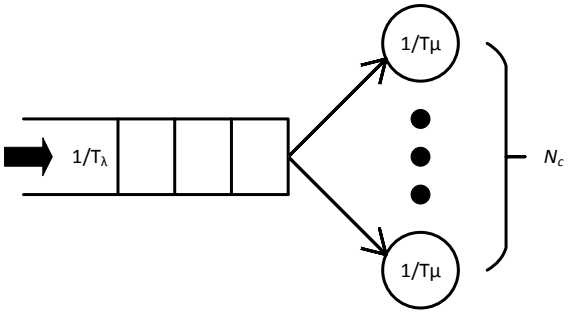

FIGURE 3.4: $M_1/M_2/N_c$ queuing model

The exponential distribution is employed here because the arrival and charging of EVs are assumed to be independent of each other, i.e., both their arrival and charging are the Poisson process. The number of customers waiting at the EV charging station is assumed to be infinite for simplicity. The probability of number of EVs being charged at k^{th} FCS in time t denoted as $P_t^k(n)$ and follows a discrete distribution as

$$P_t^k(n) = \begin{Bmatrix} \left(\sum_{j=0}^{N_c^k-1} \frac{\left(N_c^k p_t^k\right)^j}{j!} + \frac{\left(N_c^k p_t^k\right)^{N_c^k}}{N_c^k!} \cdot \frac{1}{1-p_t^k} \right)^{-1} & n = 0 \\ \frac{\left(N_c^k p_t^k\right)^n}{n!} . P_t^k(0) & n = 1, 2, ...N_c^k \end{Bmatrix} \tag{3.38}$$

where, p_t^k is the occupation rate of the k^{th} FCS per charging slot at t^{th} hour defined as follows

$$p_t^k = \frac{T_\mu}{N_c^k T_{\lambda_t^k}} \tag{3.39}$$

The occupation rate (p_t^k) of the k^{th} FCS should be less than one so that system is stable. The inter-arrival time ($T_{\lambda_t^k}$) for k^{th} FCS is obtained by estimating the EV flow served by k^{th} FCS in time t given by:

$$T_{\lambda_t^k} = 1/f_t^k \tag{3.40}$$

where

$$f_t^k = \sum_{O \in N_T} \sum_{D \in N_T} f_{OD,t} \xi_{OD}^k \psi^k \tag{3.41}$$

where ξ_{OD}^k is 1 if k^{th} FCS is able to serve the EV flow on path OD and 0 otherwise. ψ^k is 1 if k^{th} FCS is located on path OD and 0 otherwise. The mean service time T_μ will depend on the daily recharge energy (E_{d_μ}) need of EVs which further depends on the daily driving

distance given in equation (3.42). The mean daily driving distance (d_μ) is obtained from the transportation travel survey data.

$$E_{d_\mu} = \epsilon \times d_\mu \tag{3.42}$$

The change in SOC (ΔSOC) and $T\mu$ is calculated as

$$\Delta SOC_\mu = E_{d_\mu}/C_{bat} \tag{3.43}$$

$$T\mu = \Delta SOC_\mu/C_{rate} \tag{3.44}$$

where, ϵ is energy consumption per mile, C_{bat} is the battery capacity and C_{rate} is rate at which EV is charged. It is derived in the Section 3.2.1, that power consumed by the EVs charging at FCS depends on the current SOC of the battery. Consequently, average power required by EVs can be determined by estimating the initial SOC which is uncertain. The initial SOC and the average charging power is determined in the next section.

3.3.3 Proposed Method for Estimation of Initial SOC and Charging Power of EVs

The initial SOC of the battery before the charging start depends on how much discharged the EV was. It can be estimated by knowing the daily recharge energy as

$$E_d = \begin{Bmatrix} \epsilon \times d_m & if \quad d_m < d_{m_{max}} \\ (SOC_{max} - SOC_{min}) \times C_{bat} & if \quad d_m \geq d_{m_{max}} \end{Bmatrix} \tag{3.45}$$

d_m and $d_{m_{max}}$ is the daily driving distance and maximum range of EV in miles. The daily driving distance according to the driving pattern statistics follows a lognormal distribution given by

$$d_m = e^{(\mu_m + \sigma_m . Z)} \tag{3.46}$$

where Z is a standard normal variate, μ_m and σ_m are the mean and variance of lognormal distribution respectively given by

$$\begin{Bmatrix} \mu_m = ln\left(\frac{\mu_{d_m}}{\sqrt{1+\frac{\sigma^2_{d_m}}{\mu^2_{d_m}}}}\right) \\ \sigma_m = \sqrt{ln\left(1+\frac{\sigma^2_{d_m}}{\mu^2_{d_m}}\right)} \end{Bmatrix} \tag{3.47}$$

Based on the daily recharge energy, the change in SOC and initial SOC is determined as

$$\Delta SOC = E_d / C_{bat} \tag{3.48}$$

$$SOC_{ini} = SOC_{max} - \Delta SOC \tag{3.49}$$

Based on the initial SOC given in equation (3.49), the average charging power is determined. It has been previously mentioned that the charging power required by EVs vary with SOC of the battery and the supply voltage. The power curve of EV battery with respect to SOC for rated voltage is used to determine the average charging power. The power curve is piecewise linearized for 5% SOC intervals to retain nonlinearity. Then, average charging power is given as

$$avgP_{SOC_{ini}} = \frac{1}{q} \sum_{z=1}^{q} \left(\frac{1}{u_z - l_z} \int_{l_z}^{u_z} f_z(x) dx \right) \tag{3.50}$$

$$l_z = SOC_{ini} + \frac{(z-1)}{q} * (SOC_{max} - SOC_{ini}) \tag{3.51}$$

$$u_z = SOC_{ini} + \frac{z}{q} * (SOC_{max} - SOC_{ini}) \tag{3.52}$$

where q is the number of piecewise linear functions representing power curve and u_z, l_z are the upper and lower limit of z^{th} linear function $f_z(x)$ of power curve of battery. Once the average charging power is known, the total charging power for N_o number of EVs being charged simultaneously at k^{th} FCS at time t is given as follows:

$$P_{FCS_{k,t}} = \sum_{j=1}^{N_o} avgP^j_{SOC_{ini}} \tag{3.53}$$

Hence total expected EV charging demand at time t for all possible values of N_o (where $N_o \in 1 \; to \; N_c$) is given by:

$$E[P_{FCS^k_t}] = \sum_{N_o}^{N_c} P^k_t(N_o) * P_{FCS^k_t} \tag{3.54}$$

The expected power charging demand obtained from equation (3.54) is used to examine the impact of fast charging EV load on distribution system performance. Further, active power balance equation in power flow analysis is modified to incorporate the voltage-dependent

characteristic of FCS load given by equation (3.55).

$$P_{G_{i,t}} = P_{D0_{i,t}} + \psi^k E[P_{FCS_t^k}]\left[a_p\left(\frac{V_{i,t}}{V_o}\right)^{n_p} + b_p\right] + V_{i,t}\sum_{j=1}^{N_B} V_{j,t}\left(G_{ij}\cos\left(\theta_{ij,t}\right) + B_{ij}\sin\left(\theta_{ij,t}\right)\right) \quad (3.55)$$

where $V_{i,t}, V_{j,t}$ are the voltage magnitude of bus i and j, $\theta_{j,t}$ is the phase angle difference between bus i and j, $P_{G_{i,t}}$ is active power generation of generator at bus i, $P_{D0_{i,t}}$ is active load at bus i and ψ^k is 1 if FCS is located at bus i of distribution system and 0 otherwise.

3.4 Numerical Results and Discussions

The effectiveness of the proposed methodology is investigated on IEEE 123-bus distribution system [139]. It operates at a nominal voltage of 4.16 kV. The system has 85 spot loads and 118 distribution lines. It has both underground and overhead lines, characterized by unbalance loading with constant power, impedance and current loads, four voltage regulators, shunt capacitor banks, and multiple switches. The detailed system data with single line diagram is given in the Appendix A. The simulations are performed using MATLAB 2015b [140] and OpenDSS software [141] with Intel Core i5, 2.50 GHz, 4GB RAM computer.

3.4.1 Validation of Derived Mathematical Load Model of FCS

In this section, the derived mathematical model representing the relationship between voltage and power consumption is verified. A 30 kW DC fast charger is simulated in MATLAB Simulink which consists of AC-DC rectifier and DC-DC buck converter. 24 kWh lithion ion battery with battery parameters similar to 24 kWh Nissan leaf is incorporated. The turn on resistances of IGBT switches in AC/DC rectifier are set to 0.2 $m\Omega$, resistance and inductance of input filter are kept as $0.1m\Omega$ and $0.1mH$ respectively. The resistance and inductance of output filter are set to 1 $m\Omega$ and $10mH$ respectively. The battery is fast charged at $1C$ charging rate and input voltage is varied from 0.8 to 1.2 p.u. for 10% to 95% of battery SOC at a step of 5% SOC.

The objective of AC-DC rectifier is to maintain constant DC-link voltage of 500 V and achieve unity power factor as shown in Fig. 3.5 and Fig. 3.6 respectively. It is observed in Fig. 3.5 that a constant DC-link voltage of 500 V is maintained. This shows that the simulated rectifier is able to regulate the DC-link voltage to the desired value. However, there is a surge in voltage during the start of charging which dies down soon and small

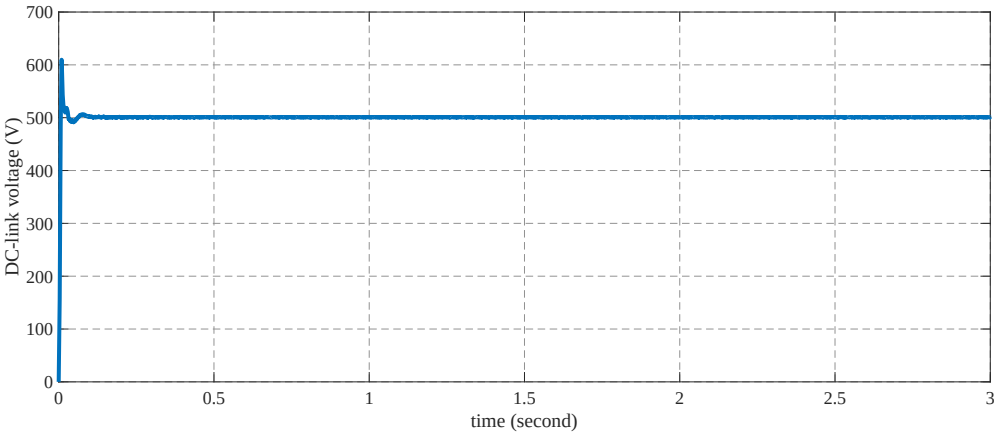

FIGURE 3.5: DC-link voltage of fast charger

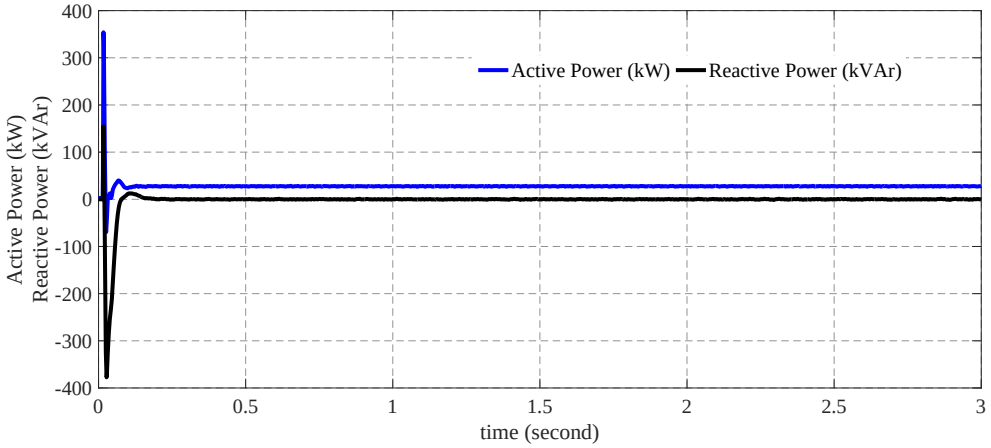

FIGURE 3.6: Active and reactive power drawn by the fast charger

amount of ripples in voltage waveform are also present due to the switching actions of power electronic devices. Since the ripples are small, they do not effect rectifier performance. Further, Fig. 3.6 shows the active and reactive power drawn by the fast charger and it can be seen that reactive power drawn is nearly zero. Thus, it can be inferred from Fig. 3.6 that AC-DC rectifier also achieves the unity power factor.

The second stage in the fast charger is DC-DC buck converter which regulates the charging current and voltage according to the requirement of CC-CV charging. During fast charging, battery is charged with constant current till certain SOC. It is not fully charged which requires constant voltage once battery reaches certain voltage threshold. The charging current at the output side of the converter is shown in Fig. 3.7 which remains constant. However, ripples are present in the charging current and there is a surge during start of charging due to the switching action of power electronic devices of the two converters.

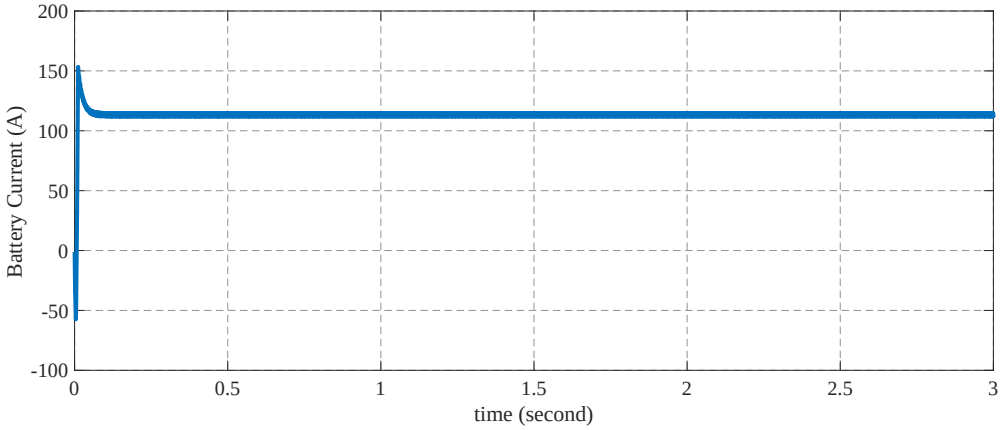

FIGURE 3.7: Regulated current for CC-CV charging

Again, the ripple current is small and does not effect the performance of the converters. Dynamic voltage across battery terminals is shown in Fig. 3.8 which shows that battery voltage increases with time. Fig. 3.9 shows the battery SOC with respect to time and it is observed that SOC has linear relationship with time. This validates equation (3.23) that signifies that SOC increases linearly with time when charging current is constant. The above results demonstrate that the simulated fast charger works satisfactorily. Therefore, measured load using simulated fast charger for different values of voltage and SOC is further used to determine the parameters of exponential and ZIP load model.

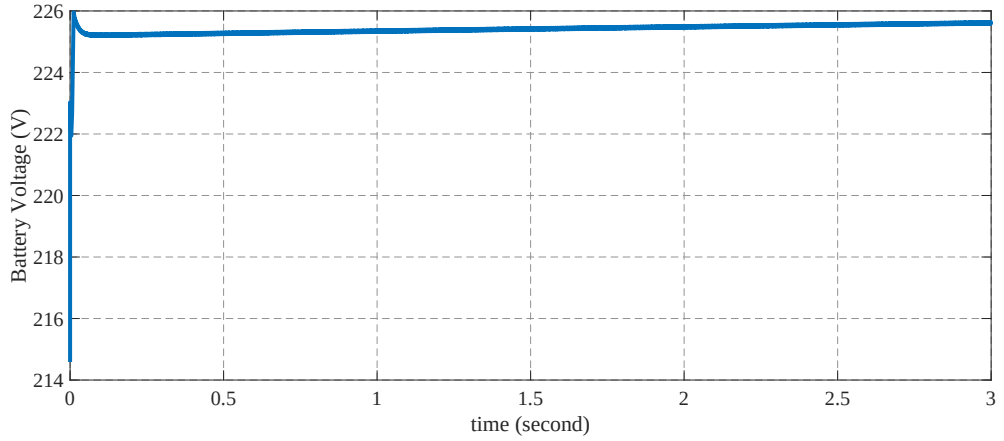

FIGURE 3.8: Voltage across EV battery terminals for fast charging

Simulated fast charger is used to obtain the power curve with respect to SOC of the battery at rated voltage as shown in Fig. 3.10. It is observed that the active drawn by the fast charger increases nonlinearly with SOC and the rate of change of active power drawn by the charger decreases with increase in SOC. The power consumption of EV battery during fast charging with variation in supply voltage for different SOC is shown in Fig.

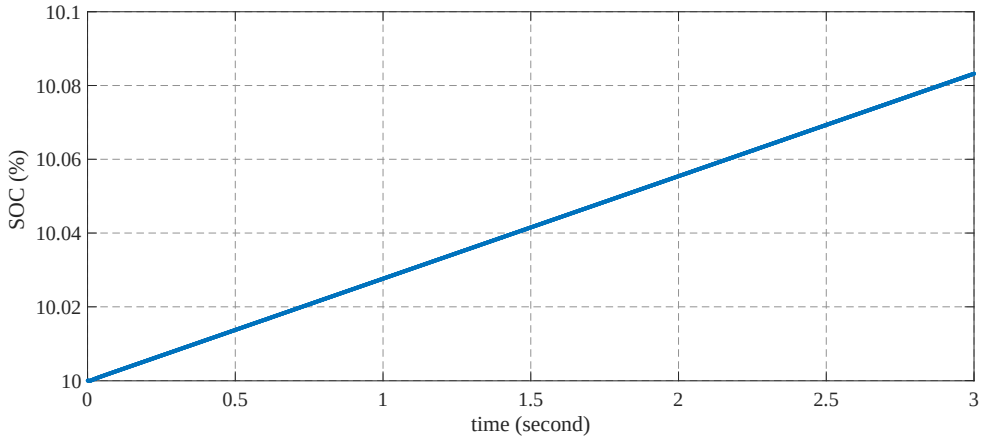

FIGURE 3.9: SOC of the battery for fast charging

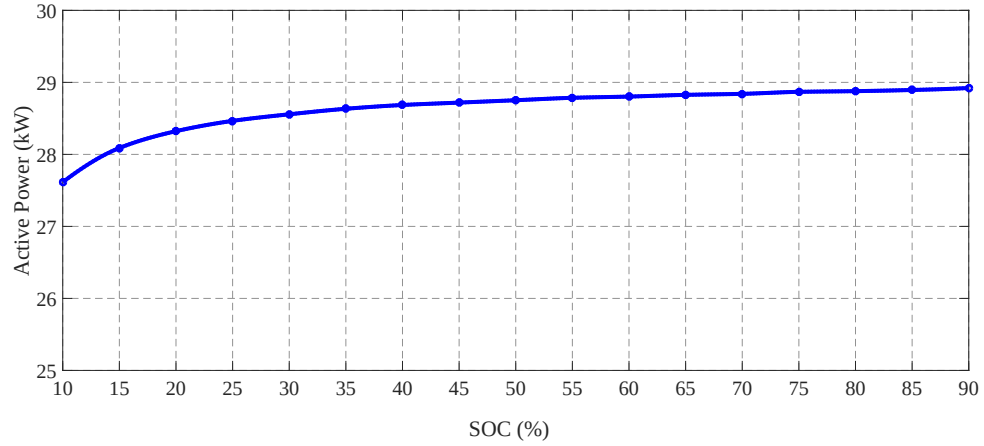

FIGURE 3.10: Power curve of fast charging EV for rated voltage

3.11. From the figure, it can be seen that the power consumption decreases with the increase in supply voltage, thus verifying the mathematical model derived in Section 3.2.1 which states that power drawn by the fast charger has inverse relationship with supply voltage and also depends on the SOC of the battery. The power voltage curve obtained from the dynamic simulation of the fast charger is used in the next section to estimate the parameters of the active power load model for different values of SOC. However, the parameters of load model for reactive power are not estimated as reactive power is negligible compared to the active power drawn by the fast charger.

3.4.2 Parameters Estimation and Performance of FCS Load Model

Parameter estimation of exponential load model is carried out in this section. For the comparison of accuracy of exponential load model, parameters of polynomial ZIP load model and power consumed by the fast charger based on the derived mathematical model

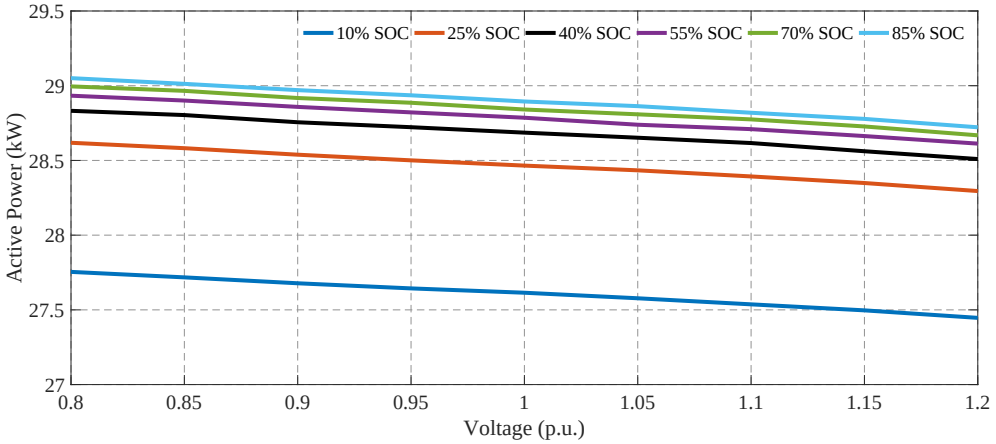

FIGURE 3.11: Voltage-dependent active power for different SOC

are also estimated. For active power determination based on the derived mathematical load model, certain parameters like battery constant voltage, internal resistance of battery, polarization constant, exponential zone amplitude and time constants are required. The parameters of dynamic model of battery can be determined with the help of discharge characteristics of battery at nominal discharge current. The discharge characteristics is shown in Fig. 3.12 and the parameters obtained are assumed to be the same for charging.

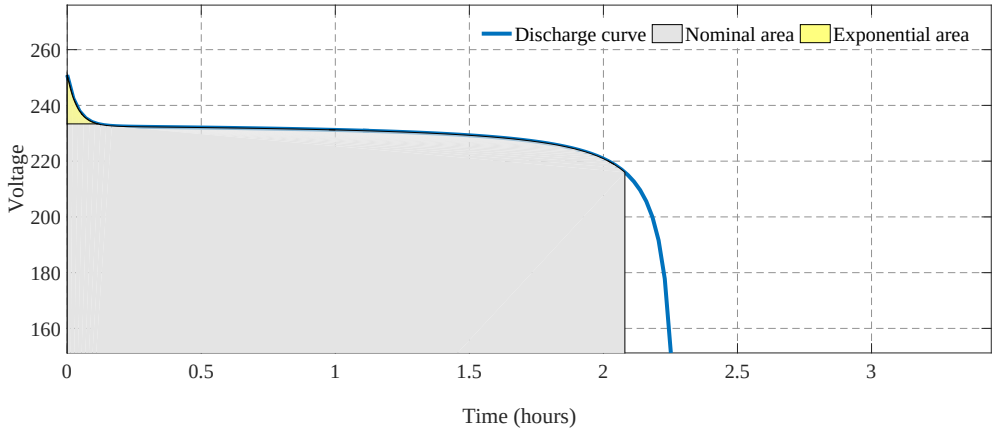

FIGURE 3.12: Nominal current discharge characteristic of EV battery

Discharge curve is divided into three sections that is exponential area, nominal area and total discharge of battery. In the first section, voltage drops exponentially from the full discharge as the battery begins to discharge. Second section is the linear area where the battery is typically operated and in third section, the voltage discharges rapidly. The parameters of equivalent circuit of battery obtained from discharge characteristics is given in Table 3.1.

TABLE 3.1: Parameters of Equivalent Circuit of Battery

Parameter	**Values**
V_0 (V)	234.01
r_b (Ω)	0.019047
K (V/Ah)	0.010752
A (V)	18.3501
B (Ah^{-1})	0.53847
Nominal Current (A)	49.3038

TABLE 3.2: Parameter Values of Exponential Load Model

SOC	a_p	n_p	b_p
10	0.0249	-1.8523	0.9751
15	0.0250	-1.8567	0.9750
20	0.0251	-1.8588	0.9749
25	0.0255	-1.8383	0.9745
30	0.0254	-1.8219	0.9744
35	0.0247	-1.8337	0.9753
40	0.0248	-1.8663	0.9752
45	0.0248	-1.9210	0.9752
50	0.0246	-1.9392	0.9754
55	0.0247	-1.8898	0.9753
60	0.0254	-1.8429	0.9746
65	0.0249	-1.8848	0.9751
70	0.0252	-1.8729	0.9748
75	0.0244	-1.9061	0.9756
80	0.0259	-1.7597	0.9741
85	0.0262	-1.7429	0.9738
90	0.0261	-1.7265	0.9739
95	0.0263	-1.7010	0.9737

Determination of accurate exponential load model requires estimation of three parameters that is a_p, n_p and b_p where a_p and b_p represents the measure of exponential and constant power characteristic present in the load model and n_p defines nonlinear relationship between voltage and power drawn by the charger. These parameters are estimated by minimizing a constrained least square problem. It is a simple nonlinear regression problem and solved

by curve fitting. Table 3.2 shows the values of the parameters of exponential load model. The conclusions drawn from the Table 3.2 can be summarized as:

1. It can be seen from Table 3.2 that the values of n_p are negative for different SOC values. This suggest that power drawn by the fast charger will decrease with increase in supply voltage.
2. The value of b_p for different operating SOC is closer to one signifying that the behavioural characteristic of fast charger load model is closer to the CPL model.
3. The obtained parameter values vary slightly for different operating SOC reflecting that SOC has little effect on the voltage-dependent load model of EV fast charger.

Table 3.3: Parameter Values of ZIP Load Model

SOC	Z_p	I_p	P_p
10	-0.02182	0.032005	0.989815
15	-0.02186	0.032083	0.989774
20	-0.02187	0.032118	0.989756
25	-0.02189	0.032140	0.989754
30	-0.02191	0.032174	0.989732
35	-0.02190	0.032170	0.989730
40	-0.02191	0.032185	0.989723
45	-0.02191	0.032187	0.989723
50	-0.02191	0.032195	0.989719
55	-0.02191	0.032196	0.989717
60	-0.02192	0.032198	0.989716
65	-0.02192	0.032204	0.989714
70	-0.02191	0.032198	0.989710
75	-0.02192	0.032201	0.989710
80	-0.02190	0.032200	0.989700
85	-0.02192	0.032209	0.989710
90	-0.02192	0.032216	0.989706
95	-0.02194	0.032239	0.989695

Determination of accurate ZIP load model requires estimation of three parameters that is Z_p, I_p and P_p where Z_p, I_p and P_p represents the measure of Constant Impedance Load (CIL), Constant Current Load (CCL) and Constant Power Load (CPL) component of EV fast charging load. The parameter Z_p and I_p reflects the voltage-dependent behaviour of power drawn by the fast charger. These parameters are estimated by minimizing a constrained least square problem. Table 3.3 shows the values of the parameters of

polynomial ZIP load model. The conclusions drawn from the Table 3.3 can be summarized as:

1. It can be seen from Table 3.3 that the values of Z_p are negative for different SOC values. This suggest that power drawn by the fast charger will decrease with increase in supply voltage.
2. The value of P_p for different operating SOC is closer to one signifying that the behavioural characteristic of fast charger load model is closer to the CPL model.
3. The obtained parameter values (Z_p, I_p and P_p) vary slightly for different operating SOC reflecting that SOC has little effect on the voltage-dependent load model of EV fast charger.

From Table 3.2 and Table 3.3, similar conclusions are drawn. However, the better voltage-dependent load model between the two needs to be further investigated. This is achieved by determining the Mean Absolute Error (MAE), which reflects deviation of estimated load model from the actual value, given in Table 3.4. MAE value closer to zero represents that the estimated load model is close to the actual value. The conclusion drawn from Table 3.4 can be summarized as:

1. It is observed from Table 3.4 that MAE values are least for exponential load model and most for CPL model. Thus, suggesting that exponential load model represents true behaviour of power drawn from the fast charger amongst all the load models. The performance of CPL model in terms of MAE is worst amongst all the load models.
2. It is also observed that MAE values of analytical model are less compared to the CPL model. However, it is more than the exponential and ZIP load model. This is due to the assumptions like ignorance of voltage drop across inductor of input filter and exponential part of the battery while deriving the mathematical model of EV fast charging load. Thus, resulting in analytical model to loose some voltage-dependent property of EV fast charging load.

It is concluded that exponential load model is the most accurate load model for describing the relationship between power consumed by the fast charger and the supply voltage. Further, the power drawn also depends on SOC of the battery. But the slight variation of parameters values for different SOC shows that SOC has little effect on the load models. This is investigated by obtaining power voltage relationship characteristics of exponential load model for different values of SOC as shown in Fig. 3.13.

It is found that there is negligible effect of SOC on power voltage relationship of the charger. Therefore, a single set of parameters of exponential and ZIP load model should be sufficient enough to represent the EV fast charging load for different level of $SOCs$.

TABLE 3.4: MAE Values for Different Load Models

SOC	**Exponential**	**ZIP**	**CPL**	**Analytical**
10	0.0749	0.1529	0.2707	0.2694
15	0.0696	0.1530	0.2706	0.2694
20	0.0584	0.1536	0.2714	0.2701
25	0.0682	0.1537	0.2715	0.2702
30	0.0525	0.1503	0.2672	0.2659
35	0.0666	0.1530	0.2706	0.2693
40	0.0670	0.1519	0.2693	0.2680
45	0.0522	0.1534	0.2708	0.2695
50	0.0523	0.1525	0.2701	0.2688
55	0.0660	0.1528	0.2705	0.2692
60	0.0509	0.1543	0.2717	0.2704
65	0.0551	0.1534	0.2709	0.2696
70	0.0519	0.1564	0.2736	0.2723
75	0.0744	0.1525	0.2701	0.2688
80	0.0536	0.1529	0.2703	0.2690
85	0.0521	0.1529	0.2704	0.2691
90	0.0611	0.1526	0.2703	0.2690
95	0.0604	0.1506	0.2685	0.2672

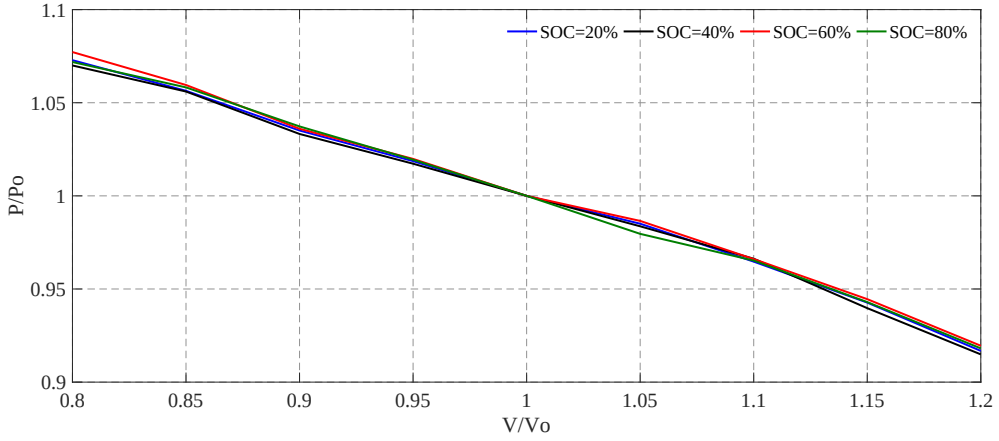

FIGURE 3.13: Power voltage relationship for the voltage-dependent expoential load model

The choice of single set of parameter that will work best for different values of SOC needs investigation. This is achieved by minimizing the summation of MAE values obtained for each single set of parameters given in Table 3.2 for different values of SOC given by

equation (3.56).

$$Minimize: \quad F_{MAE} = \frac{1}{N_{param}} \sum_{j=1}^{N_{param}} \frac{MAE_{i,j} - MAE_{i,i}}{MAE_{i,i}}, \ i\epsilon[1, N_{SOC}] \tag{3.56}$$

where, N_{param} and N_{SOC} are the total number of set of estimated parameters and different SOC values respectively. The MAE values for each set of exponential parameters for different SOC values are listed in Table 3.5. Total 18 sets corresponding to each SOC level are obtained. From the table, it is observed that Set 18 gives minimum value of objective function given in equation (3.56) where the parameters of set 18 corresponding to a_p, n_p and b_p are [0.0263, -1.701, 0.9737]. This set of parameters are used for exponential load model for different values of SOC.

This is validated and shown in Fig. 3.14. It shows that the actual and predicted values of power consumption by EV during fast charging for exponential load model, ZIP load model and CPL model for different values of SOC. From the figure it is found that single set of parameters of exponential load model are sufficient to predict the actual active power drawn by the charger.

Table 3.5: MAE Values for Different Exponential Load Models

SOC	**Set 1**	**Set 2**	**Set 3**	**Set 4**	**Set 5**	**Set 6**	**Set 7**	**Set 8**	**Set 9**
10	0.0749	0.0755	0.0759	0.0765	0.0753	0.0748	0.0751	0.0775	0.0774
15	0.0691	0.0696	0.0700	0.0705	0.0693	0.0690	0.0693	0.0715	0.0715
20	0.0579	0.0581	0.0584	0.0586	0.0578	0.0577	0.0581	0.0597	0.0598
25	0.0574	0.0577	0.0579	0.0581	0.0573	0.0572	0.0576	0.0592	0.0593
30	0.0527	0.0529	0.0531	0.0532	0.0525	0.0525	0.0529	0.0543	0.0544
35	0.0667	0.0672	0.0676	0.0681	0.0670	0.0666	0.0669	0.0691	0.0691
40	0.0668	0.0672	0.0675	0.0679	0.0668	0.0666	0.0670	0.0690	0.0690
45	0.0511	0.0510	0.0511	0.0510	0.0505	0.0508	0.0513	0.0522	0.0524
50	0.0505	0.0507	0.0509	0.0513	0.0503	0.0503	0.0507	0.0524	0.0523
55	0.0652	0.0657	0.0661	0.0665	0.0654	0.0651	0.0654	0.0676	0.0676
60	0.0509	0.0510	0.0510	0.0509	0.0505	0.0507	0.0512	0.0521	0.0523
65	0.0546	0.0546	0.0548	0.0549	0.0542	0.0542	0.0548	0.0561	0.0562
70	0.0518	0.0517	0.0516	0.0514	0.0510	0.0514	0.0520	0.0526	0.0528
75	0.0740	0.0745	0.0749	0.0754	0.0743	0.0739	0.0742	0.0765	0.0764
80	0.0548	0.0550	0.0551	0.0551	0.0545	0.0545	0.0550	0.0563	0.0565
85	0.0529	0.0531	0.0534	0.0538	0.0528	0.0527	0.0532	0.0548	0.0548
90	0.0626	0.0630	0.0633	0.0637	0.0627	0.0625	0.0628	0.0648	0.0647
95	0.0624	0.0628	0.0632	0.0636	0.0626	0.0623	0.0626	0.0647	0.0647
F_{MAE}	-0.0008	0.0036	0.0076	0.0116	-0.0028	-0.0042	0.0028	0.0305	0.0314

SOC	**Set 10**	**Set 11**	**Set 12**	**Set 13**	**Set 14**	**Set 15**	**Set 16**	**Set 17**	**Set 18**
10	0.0757	0.0762	0.0762	0.0769	0.0753	0.0745	0.0747	0.0737	0.0730
15	0.0699	0.0702	0.0703	0.0709	0.0695	0.0685	0.0687	0.0678	0.0671
20	0.0585	0.0584	0.0587	0.0590	0.0585	0.0569	0.0569	0.0562	0.0557
25	0.0581	0.0579	0.0583	0.0586	0.0580	0.0564	0.0565	0.0558	0.0553
30	0.0533	0.0531	0.0534	0.0537	0.0534	0.0516	0.0517	0.0510	0.0506
35	0.0675	0.0678	0.0679	0.0685	0.0671	0.0661	0.0664	0.0654	0.0648
40	0.0675	0.0677	0.0678	0.0683	0.0674	0.0660	0.0661	0.0653	0.0647
45	0.0516	0.0510	0.0515	0.0515	0.0520	0.0496	0.0495	0.0491	0.0488
50	0.0511	0.0511	0.0512	0.0517	0.0513	0.0495	0.0497	0.0488	0.0484
55	0.0660	0.0663	0.0664	0.0669	0.0657	0.0646	0.0647	0.0638	0.0632
60	0.0515	0.0509	0.0514	0.0514	0.0519	0.0495	0.0494	0.0490	0.0487
65	0.0551	0.0548	0.0551	0.0554	0.0555	0.0532	0.0533	0.0526	0.0522
70	0.0522	0.0514	0.0520	0.0519	0.0527	0.0501	0.0498	0.0496	0.0493
75	0.0748	0.0752	0.0752	0.0759	0.0744	0.0735	0.0737	0.0727	0.0720
80	0.0554	0.0551	0.0555	0.0556	0.0555	0.0536	0.0535	0.0530	0.0525
85	0.0535	0.0536	0.0537	0.0542	0.0538	0.0520	0.0521	0.0513	0.0508
90	0.0633	0.0635	0.0636	0.0641	0.0632	0.0618	0.0619	0.0611	0.0606
95	0.0631	0.0634	0.0635	0.0640	0.0628	0.0617	0.0619	0.0610	0.0604
F_{MAE}	0.0101	0.0090	0.0132	0.0192	0.0106	-0.0177	-0.0165	-0.0287	-0.0371

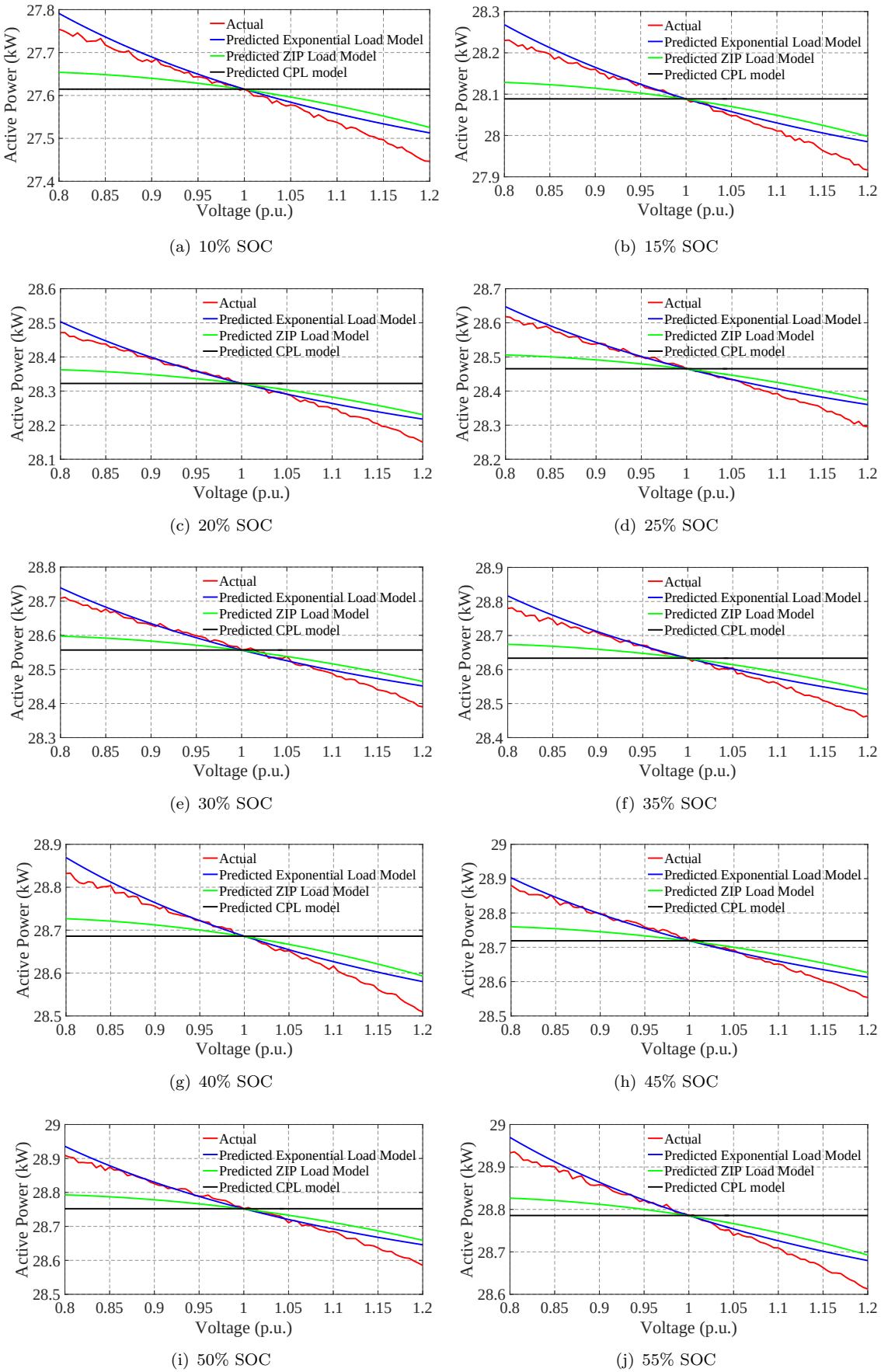

(a) 10% SOC (b) 15% SOC

(c) 20% SOC (d) 25% SOC

(e) 30% SOC (f) 35% SOC

(g) 40% SOC (h) 45% SOC

(i) 50% SOC (j) 55% SOC

FIGURE 3.14: Actual and predicted values of power consumption for exponential, ZIP and CPL model

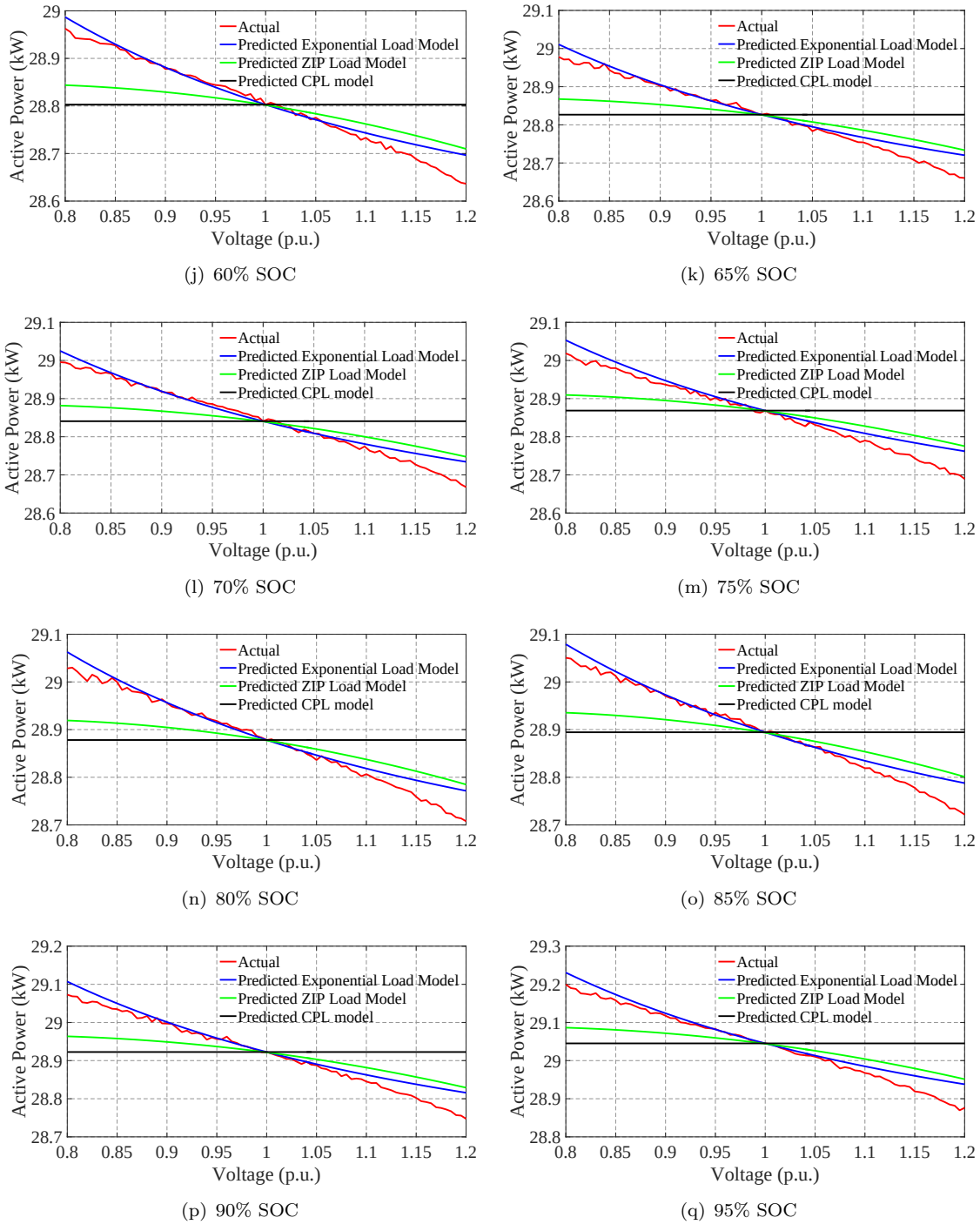

(j) 60% SOC (k) 65% SOC

(l) 70% SOC (m) 75% SOC

(n) 80% SOC (o) 85% SOC

(p) 90% SOC (q) 95% SOC

FIGURE 3.14: Actual and predicted values of power consumption for exponential, ZIP and CPL model

3.4.3 Stochastic Charging Demand and Impact of Load Models on System Performance

To analyse the impact of load models on the distribution system performance, 24-hour AECP needs to be developed. It requires to modify the original IEEE 123-bus distribution system to account for the number of residential houses which assist in determining the number of EVs present in the system. The standard test system is modified by removing the spot loads of the distribution system and replacing them by the equivalent secondary circuit consisting of distribution transformer, service lines, service drops and equivalent residential houses. The number of residential houses replacing the spot load on the primary side of the distribution system is determined by equation (3.35). Further, a 500 *kVA* transformer is connected to each distribution bus where FCS is located. In this thesis, maximum individual demand of each house considered is 12 *kVA*. The power factor of residential houses is kept same as that of original spot loads. The modification made in the spot loads are as follows:

- Spot loads of 44.72 *kVA* are replaced by 10 residential houses supplied by 50 *kVA* transformer.
- Spot loads of 22.36 *kVA* are replaced by 4 residential houses supplied by 25 *kVA* transformer.

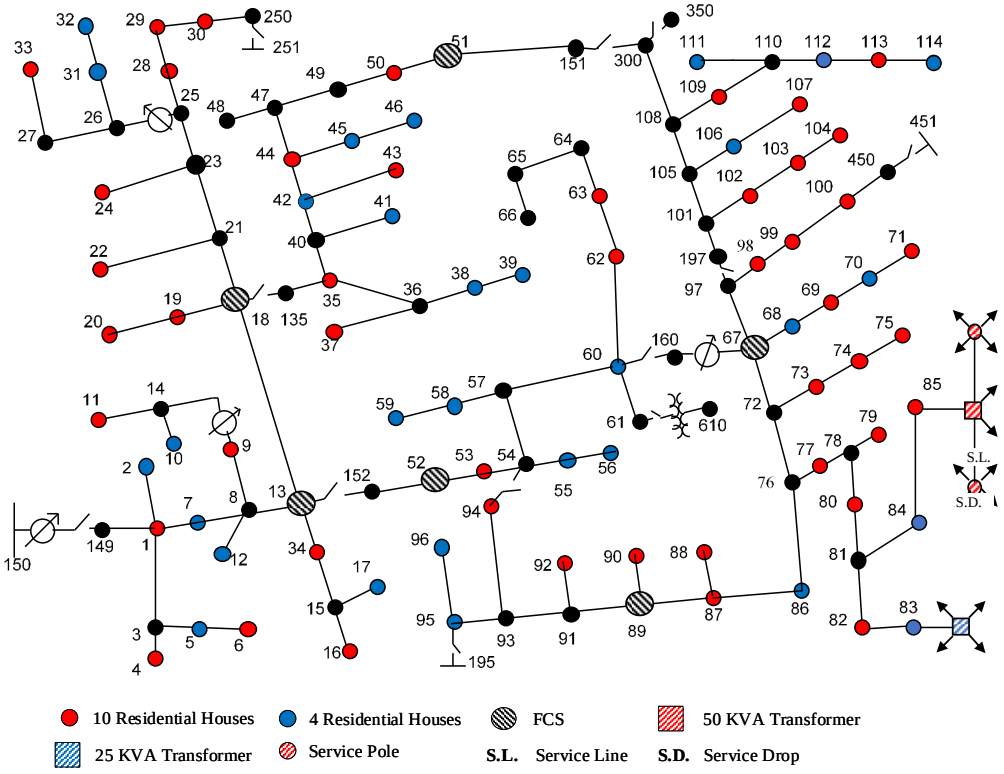

FIGURE 3.15: Modified IEEE 123-bus distribution system

A total of 594 residential houses are obtained. As per NHTS 2009 [56], each residential house has 1.86 vehicles per household. The penetration of EVs is varied from 0 to 100% in step of 20%. It is assumed that six FCS are arbitrarily located at three–phase buses 51(2), 18(10), 67(12), 13(14), 52(19) and 89(23) where the number in parentheses is corresponding node of the transportation network. The modified IEEE 123-bus distribution system is shown in the Fig. 3.15.

The spatial-temporal distribution of EVs depend on probabilities assigned to each *OD* pair as shown in Fig. 3.16(a) and the average number of vehicles that travel during the day in the transportation network. The temporal distribution of vehicles is obtained from the travel survey data of Waterloo Region Transportation Tomorrow Survey (TTS) [57] 2011 which considers 43,165 unique trips as shown in Fig. 3.16(b). It is observed that the average number of vehicles are high during peak hours that is at 8^{th} and 16^{th} hour.

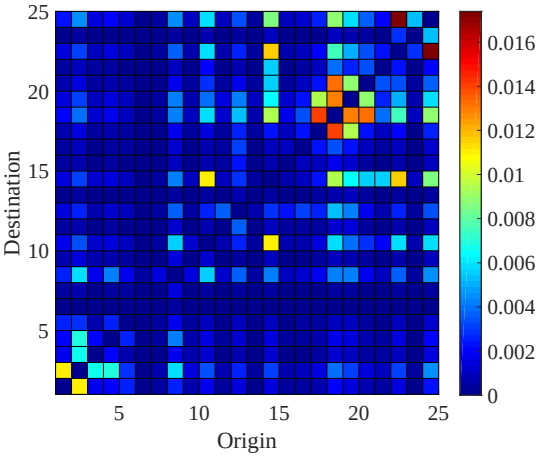

(a) Probability OD matrix

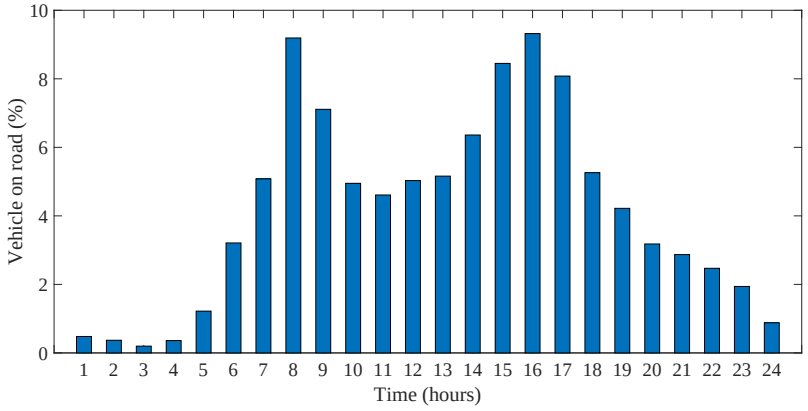

(b) Distribution of vehicles on the road

FIGURE 3.16: Data of spatial-temporal distribution model

The distribution of daily miles driven is derived from the TTS data. Lognormal distribution is fitted on the daily driven miles and the mean of 40 miles and standard deviation of 20 miles is obtained. Based on the mean daily driven distance, mean service time is determined using equation (3.42)–(3.44) which comes out to be 27.2 minutes. Then, the mean service time and EV flow served by each path during the peak hour is used to determine the number of slots of each FCS such that the occupation rate is less than 1 during the peak hour. The number of slots of each FCS is given in Table 3.6.

TABLE 3.6: Location and size of FCS in IEEE 123-bus distribution system

DB-TN	**Charging Slots**
51-2	10
18-10	15
67-12	10
13-14	20
52-19	10
89-23	10

DB-Distribution Bus, TN-Transportation Node

The amount of EV flow that passes through the node of transportation network at which FCS is located is the inter-arrival rate of EVs in the queuing model. The inter-arrival rate, mean service time and the number of identical slots of each FCS governs the Probability Distribution Function (PDF) of EVs charging simultaneously at the FCS. The PDF for each FCS for the peak hour is shown in Fig. 3.17. From the figure, it is observed that the FCS located at distribution bus 51 has maximum probability for 4 EVs charging simultaneously. This implies that there is a high chance of 4 EVs charging simultaneously at this FCS. Similar observation are made for other 5 FCS and it is to be noted that maximum EVs are served by FCS located at bus 13 of the distribution system.

Based on the PDF of each FCS and the SOC_{ini} determined from equation (3.49), expected active power demand for each FCS is calculated for different penetration levels of EVs as shown in Fig. 3.18. Following conclusions are drawn from the Fig. 3.18.

1. Expected charging demand is maximum during the peak hour for every FCS as the temporal distribution of vehicle is maximum during this period. This shows that the temporal distribution of vehicles on the road effect the charging demands occurring at FCS.
2. The maximum 24-hour expected charging demand occurs for the FCS located at bus 13 of the distribution system as the EV flows passing through this node is maximum

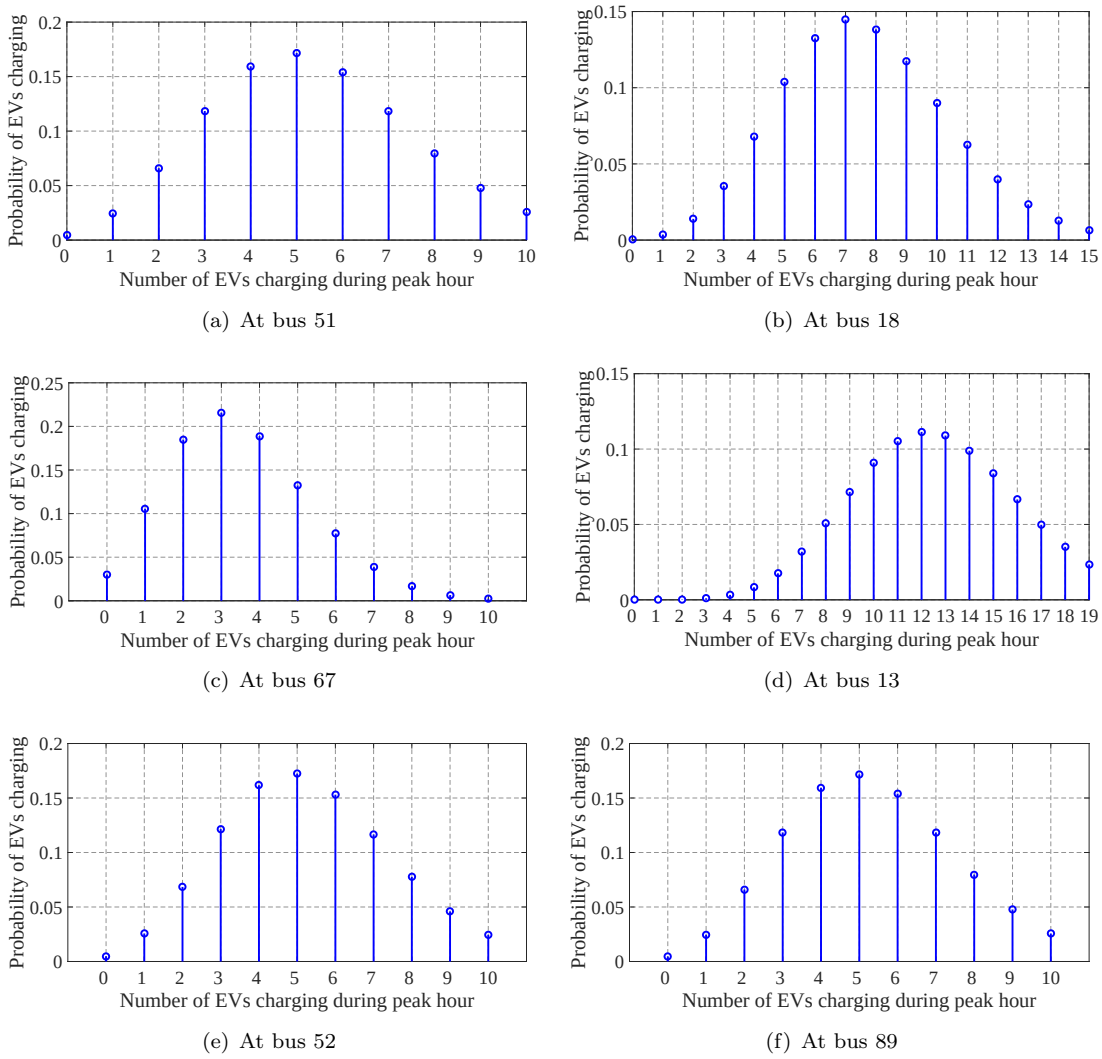

(a) At bus 51

(b) At bus 18

(c) At bus 67

(d) At bus 13

(e) At bus 52

(f) At bus 89

FIGURE 3.17: Probability distribution of EVs charging simultaneously at FCS using queuing analysis

when compared to the other FCS. Therefore, it shows that the developed model is able to capture the spatial characteristics in determination of the charging demand.

3. The variation in expected charging demand for different penetration level of EVs is high when the percentage of vehicles on the road is high. During the low peak period, the variation in expected charging demand is not significant.
4. The average charging demand of EVs based on the initial SOC lies in a small range of 28.4–28.74 kW for the SOC lying in the range of 0.2–0.85. Thus, initial SOC does not have significant effect on charging demand. However, the initial SOC effects the charging time, thus affecting the mean service time of FCS. It governs the PDF of number of EVs charging simultaneously which affects the expected charging demand.

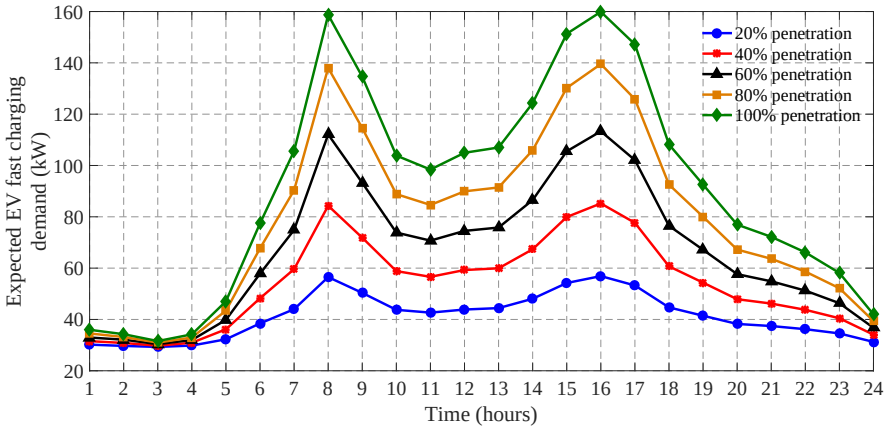

(a) At bus 51

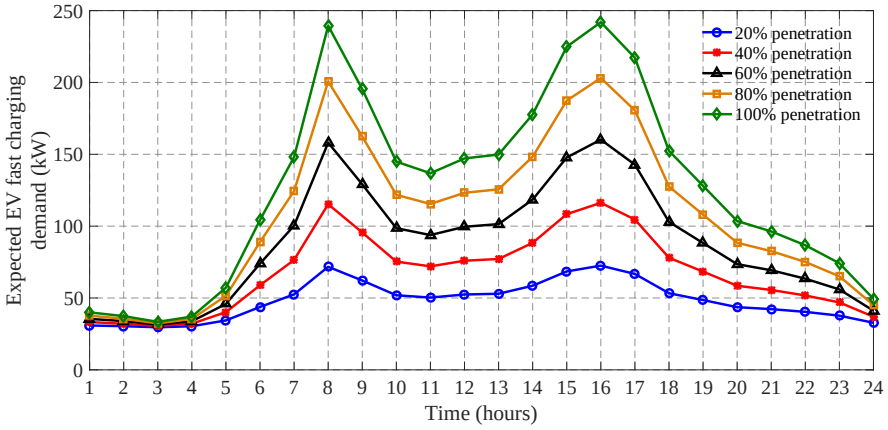

(b) At bus 18

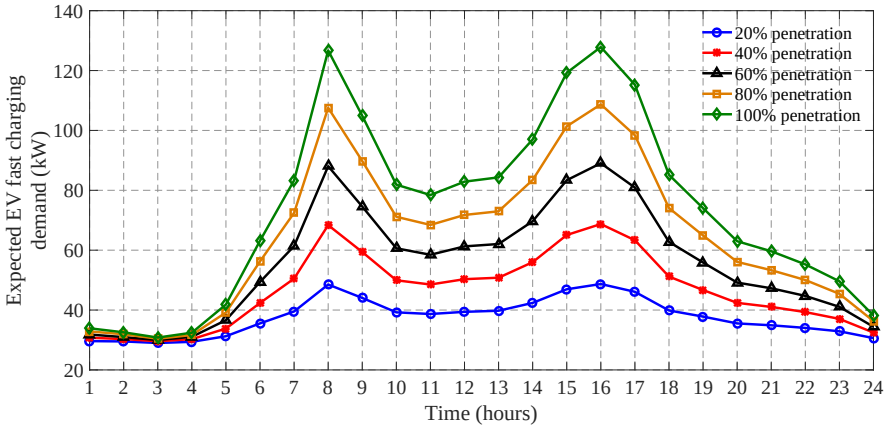

(c) At bus 67

FIGURE 3.18: Expected fast charging demand of EV

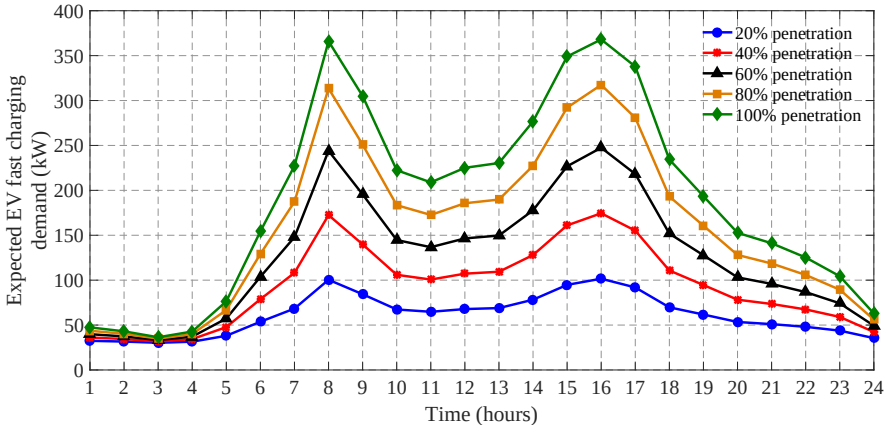

(d) At bus 13

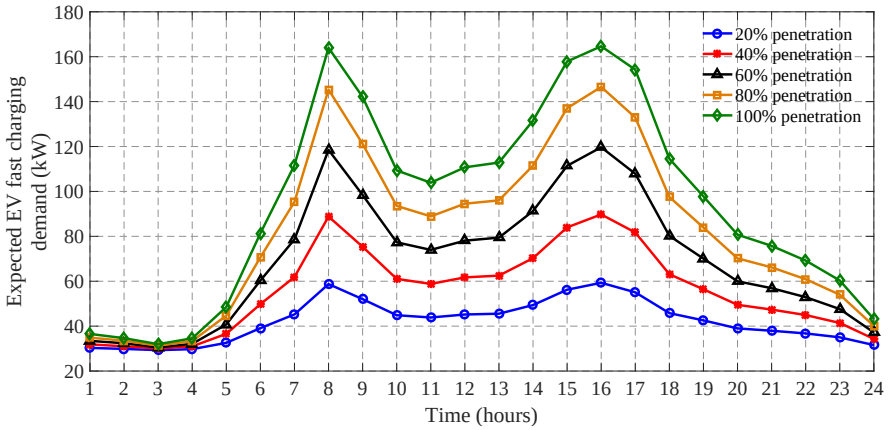

(e) At bus 52

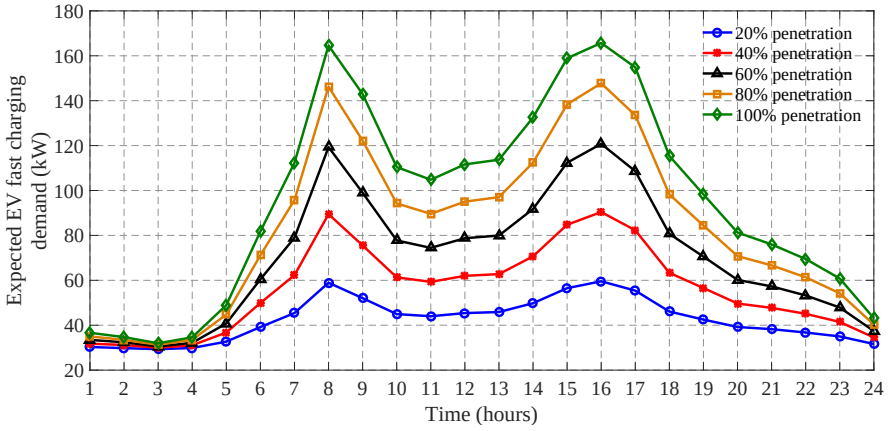

(f) At bus 89

FIGURE 3.18: Expected fast charging demand of EV

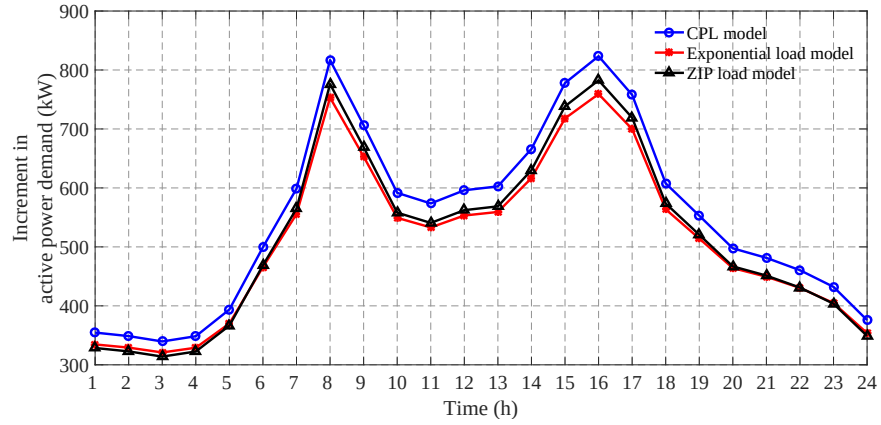

(a) 40% penetration

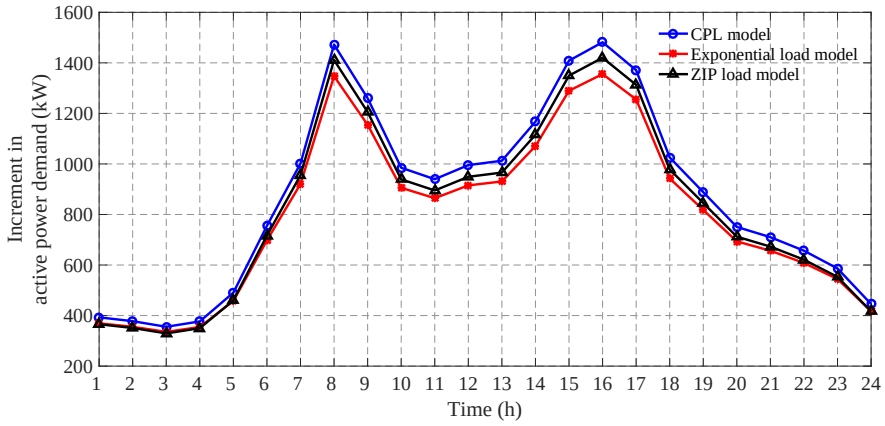

(b) 100% penetration

FIGURE 3.19: Increment in active power demand (kW)

The developed expected charging demand is further used to determine the impact of different load models on the distribution system in terms of increased power demand, system losses, voltage profile and the power factor of distribution system. The graphical results are shown for 40% and 100% penetration of level of EVs. The increment in expected 24-h load demand for different load models due to EV fast charging is shown in Fig. 3.19(a) and Fig. 3.19(b) during the day. From the figures, it is observed that the increment in active power demand is high for CPL model and low for the exponential load model. The difference between the increment in active power demand increases with the increase in penetration level of EVs. The difference between the increment in active power demand for the CPL and exponential model is 64.19 kW and 125.97 kW during the peak hour for 40% and 100% penetration level of EVs respectively. The difference between the increment in active power demand for ZIP and exponential load during peak hour is 23.33 kW and 64.50 kW for 40% and 100% penetration level of EVs respectively. Both exponential load

and ZIP load model results in better performance compared to the CPL model in terms of MAE. Thus, it is concluded that the type of load models significantly affects the system load demand particularly when the EV penetration is high.

This is further examined by determining the expected power loss and voltage profiles during the day as shown in Fig. 3.20, Fig. 3.21 and Fig. 3.22. Fig. 3.20 and Fig. 3.21 show the expected active and reactive power loss during the day. It is observed that both the expected active and reactive power losses increase due to increased expected load demand. The effect of load model on losses are significant during the peak hour of the day. Higher losses occur when EV fast charging load is assumed as CPL model and less for the exponential load model.

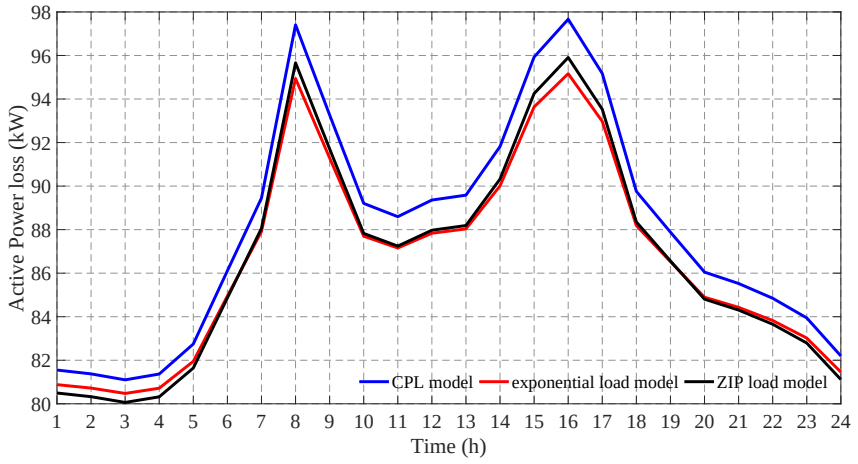

(a) 40% penetration

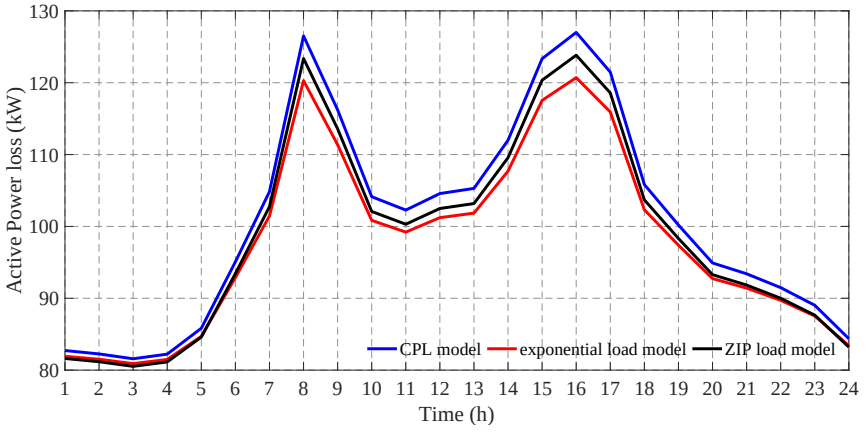

(b) 100% penetration

FIGURE 3.20: Active power loss (kW)

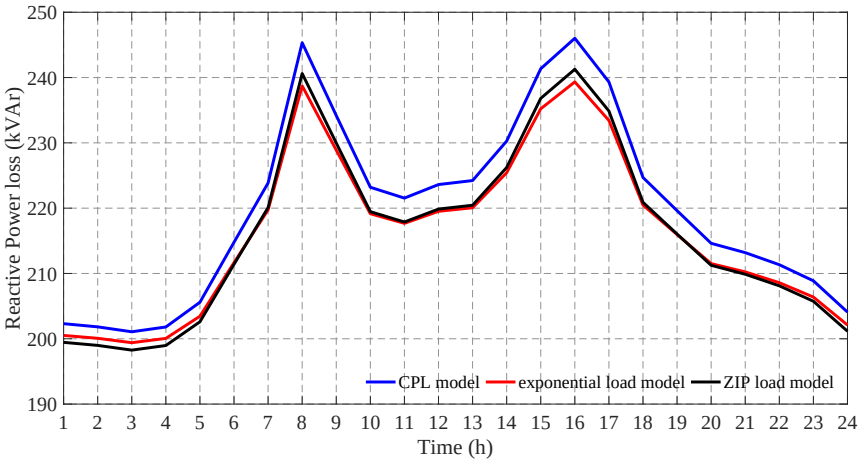

(a) 40% penetration

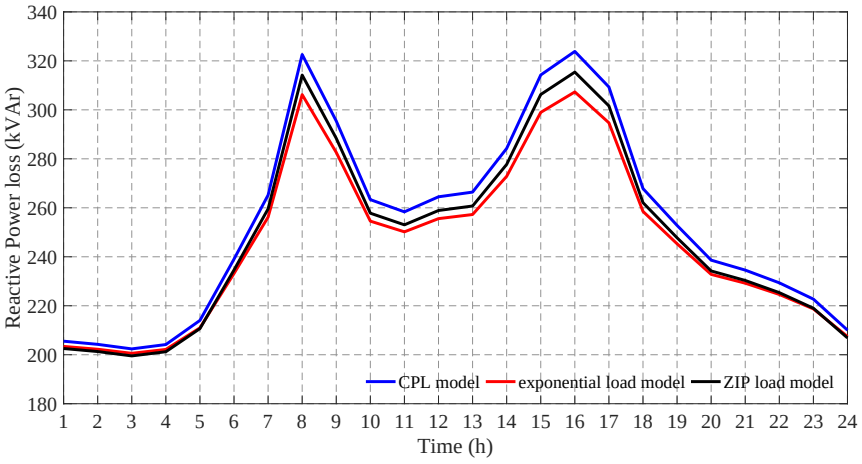

(b) 100% penetration

FIGURE 3.21: Reactive power loss (kVAr)

Fig. 3.22 shows the voltage profile of some buses during the peak hour of the day for 40% and 100% penetration level of EVs. The variation in voltage profile for different load models is hardly observed in Fig. 3.22(a) for 40% EV penetration level. However the variation in voltage profile is visible but not significant for 100% EV penetration level. Further, it is also observed that the voltage corresponding to CPL model is closer to reference voltage 1.0 p.u. as compared to the ZIP and exponential load model. Therefore, it can be expected that the voltage deviation due to the CPL model would be least. On the other hand, no proper conclusion can be drawn regarding voltage deviation for ZIP and exponential load model as the voltages of some buses corresponding to ZIP load model are higher than the exponential load model. This may be due to the presence of voltage regulators and small length of the feeders.

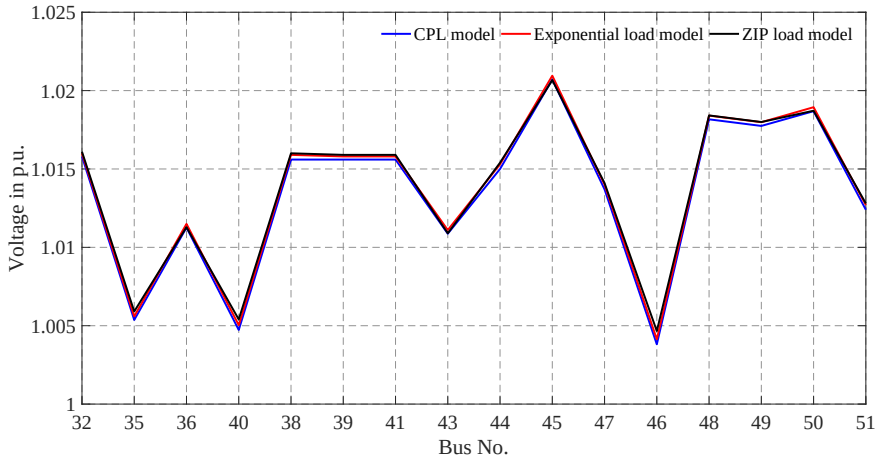

(a) 40% penetration

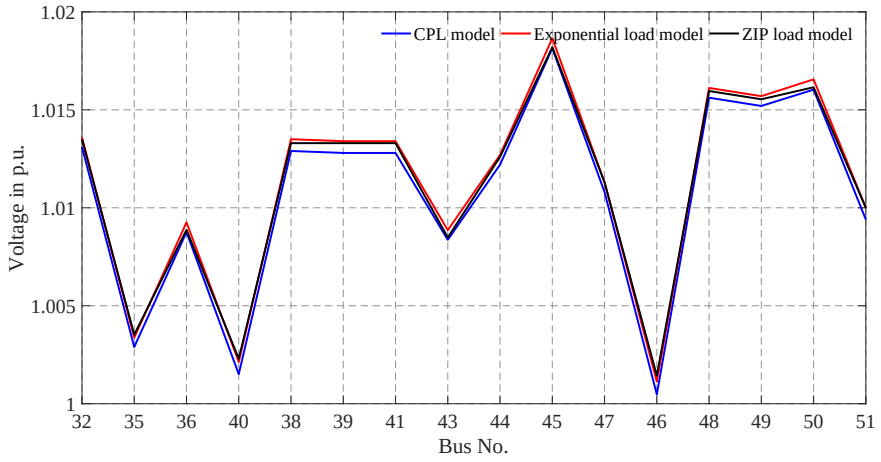

(b) 100% penetration

FIGURE 3.22: Voltage profile of some buses at peak hour

The effect of different load model on power factor of the system is shown in Fig. 3.23. The power factor is improved from 0.933 to 0.952 and 0.960 for 40% and 100% EV penetration level due to the addition of unity power factor fast charging EV load. It is closer to unity for CPL model during peak hours of the day due to the addition of more fast charging EV load as compared to the other load models. This observation shows that the effect of load model on distribution system performance is significant during the high charging demand.

The total active energy demand, reduction in energy demand for different load models and voltage deviation is also studied for different EV penetration levels as given in Table 3.7. The findings from the table are as follows:

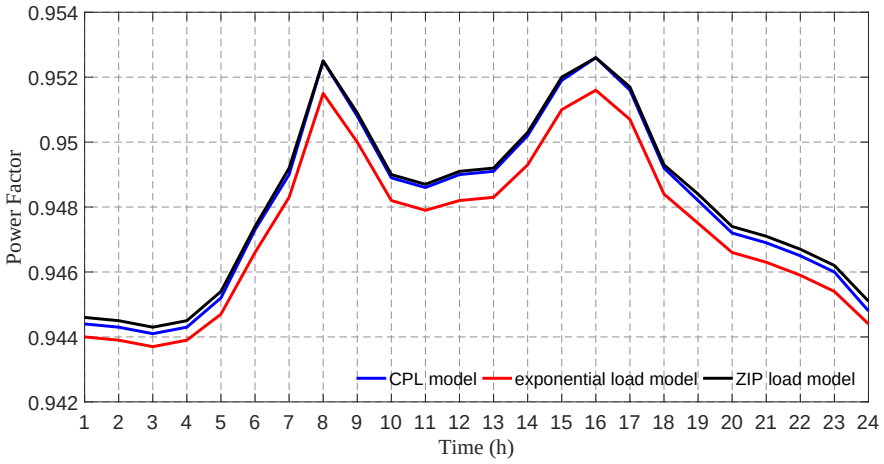

(a) 40% penetration

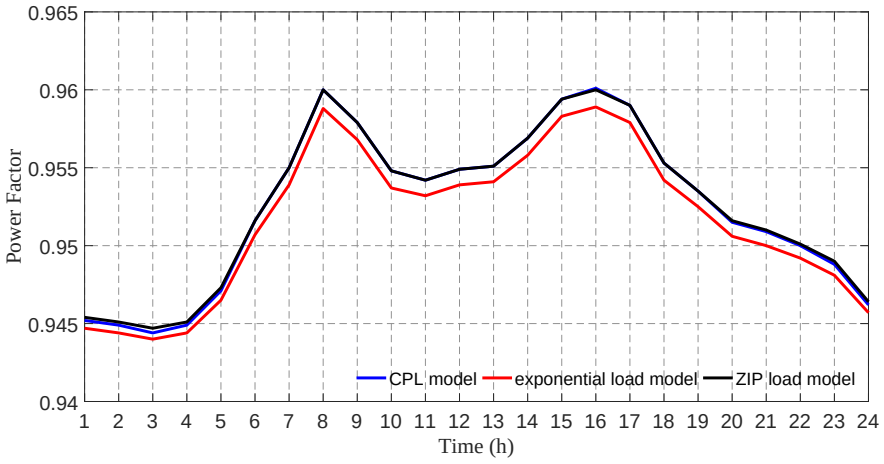

(b) 100% penetration

FIGURE 3.23: Power factor of the distribution system

TABLE 3.7: Energy Demand and Voltage Deviation for Different Load Models

Penetration Level (%)	**Energy Demand**						**Voltage Deviation (%)**		
	Total (MWh)			**Reduction (%)**					
	1	**2**	**3**	**1**	**2**	**3**	**1**	**2**	**3**
20	3851.07	3605.11	3598.80	-	6.38	6.55	2.543	2.556	2.565
40	4819.39	4482.29	4536.67	-	6.99	5.87	2.493	2.512	2.518
60	5785.78	5357.79	5472.71	-	7.39	5.41	2.443	2.466	2.469
80	6736.61	6219.25	6393.71	-	7.68	5.09	2.393	2.422	2.421
100	7631.31	7029.92	7260.36	-	7.88	4.86	2.347	2.379	2.375

1–CPL model, 2–Exponential model, 3–ZIP model

1. The total increment in active energy demand increases with the increase in EV penetration level for CPL, exponential and ZIP load model. The total increment in reactive energy demand is not determined as the EV fast charging load adds active load demand to the system.
2. The reduction in active energy demand for exponential load model compared to the CPL model increases with increase in EV penetration level. However, it decreases with increase in EV penetration level for ZIP load model.
3. The total active energy demand of exponential load model is more than the ZIP load model for 20% EV penetration level. This shows that the voltage of the buses is more for exponential load model as compared to the ZIP load model. Since, the power demand of fast charging EV decreases with increased supply voltage, therefore, energy demand for exponential load model is less than the ZIP load model for 20% EV penetration level.
4. It is also found that the voltage deviation decreases with the increase in EV penetration level. The addition of EV loads increases the voltage drop in the system and thus decreasing the voltage deviation as voltage of the buses gets closer to the reference voltage of 1.0 p.u.

TABLE 3.8: Energy Loss for Different Load Models

Penetration Level (%)	**Active Loss**						**Reactive Loss**					
	Total (MWh)			**Reduction (%)**			**Total (MVArh)**			**Reduction (%)**		
	1	**2**	**3**	**1**	**2**	**3**	**1**	**2**	**3**	**1**	**2**	**3**
20	737.86	729.46	727.64	-	1.14	1.37	1836.48	1813.88	1808.77	-	1.23	1.51
40	770.85	758.72	759.19	-	1.57	1.52	1926.00	1893.46	1894.44	-	1.69	1.64
60	806.56	790.21	793.30	-	2.07	1.64	2022.22	1978.51	1986.38	-	2.16	1.77
80	844.36	823.37	829.35	-	2.49	1.77	2123.43	2067.52	2082.97	-	2.63	1.91
100	882.05	856.29	865.25	-	2.92	1.90	2223.86	2155.53	2178.72	-	3.07	2.03

1–CPL model, 2–Exponential model, 3–ZIP model

The total energy loss and reduction in energy losses are given in Table 3.8. From the table, following observations are made:

1. The total active and reactive energy losses increases with increase in EV penetration level for all the load models. This is expected as the energy demand by the fast charging EVs increases with EV penetration level.
2. The reduction in active energy losses for exponential and ZIP load model compared to the CPL model increases with EV penetration level. However, the reduction in active

energy loss is more for exponential load model than ZIP load model except for 20% EV penetration level. It is likely since the energy demand for ZIP load model is more than the exponential load model for 20% EV penetration level.

3. Similar observations are made for total reactive energy loss and reduction in reactive energy loss. The total reactive energy loss increase with EV penetration level for all the load models. The reduction in reactive energy loss for exponential and ZIP load model compared to the CPL model also increases with the EV penetration level. However, the reduction in reactive energy loss is more for exponential load model than the ZIP load model for all EV penetration level except for 20% as, the active energy demand for 20% EV case is more for ZIP load model. Further, it is observed that change in reduction of reactive energy loss with increase in EV penetration level is less for ZIP load model than the exponential load model. As from Table 3.7, the reduction of energy demand decreases with increase in EV penetration level for ZIP load model.

3.5 Summary

It is important to have information about the EV fast charging load characteristics and demand for accurate analysis of impact of this additional load on the distribution system performance. The EV fast charging load demand depends on the supply voltage, number of EVs and the initial SOC. In this chapter, accurate load model for power flow analysis is identified by deriving the mathematical relationship between the active power consumption, supply voltage and the SOC of the battery during fast charging. Then, the obtained mathematical relationship is validated by simulating 30 kW EV fast charger with power factor correction feature. It can also maintain the required DC link voltage and provide current and voltage according to the CC-CV charging. The power vs voltage characteristic obtained from the simulated EV fast charger is further used to determine the accurate voltage-dependent load model for power flow analysis. As the EV fast charging demand has both spatial-temporal characteristics, therefore, stochastic FCS charging demand is developed using queuing theory incorporating uncertain factors like charging location, level, time and initial SOC. Finally, the impact of different load models are investigated on IEEE 123-bus distribution system to demonstrate the effectiveness of the proposed voltage-dependent load model and stochastic charging demand. Following conclusions are drawn from this chapter:

1. The derived mathematical relationship states that the active power consumption decreases with increase in supply voltage and increases with increase in SOC. The simulated fast charger for verification of derived relationship is able to maintain the

required 500 V DC link voltage and provides unity power factor correction. It is also able to maintain constant current corresponding to the 1C charging rate. The power vs voltage characteristics for different values of SOC obtained from the simulated fast charger shows that the power demand decreases with increase in supply voltage and increases with increase in battery SOC. Thus, verifying the derived mathematical relationship.

2. The parameters of voltage-dependent exponential and ZIP load model for different values of SOC are estimated and it is found that the parameters of these load models vary slightly with the SOC. Based on the MAE values, it is concluded that the exponential load model is the best representation of voltage-dependent behavioural characteristic of EV fast charging load. It also suggest that single set of parameters might be sufficient to represent the load models for different values of SOC. This is confirmed by the power vs voltage characteristics and the most appropriate single set of parameters are selected for both exponential and ZIP load model.

3. The developed stochastic FCS charging demand shows that the demand by the FCS will depend on its location and the time of charging during the day. Thus, having spatial-temporal characteristics. It is also found that the charging demand depends on the penetration level of EVs and initial SOC has little effect on the charging demand. However, the initial SOC governs the charging time, thereby effecting the mean charging time of each FCS. This will further effect the number of EVs charging simultaneously at each FCS and thus, affecting the charging demand of FCS.

4. It is found that the different load models affects the increment in energy demand, energy losses, voltage profile and power factor of the system due to the additional EV fast charging load. It is observed that the exponential load and ZIP load model results in less energy demand than the CPL model as voltages of most of the buses for the considered test system is more that rated 1.0 p.u. The exponential and ZIP load model will not necessarily result in less energy demand than the CPL model but will be governed by the system voltages. The additional load will increase the system losses and it increases with increase in EV penetration level. The power factor of the system also gets improved due to addition of unity power factor load. Further, the voltage deviation of the considered test system improves with the addition of the new load. CPL model has better voltage profile compared to the exponential and ZIP load model as the CPL model results in more voltage drop in the system due to more energy demand compared to the other load models.

Chapter 4

Optimal Planning of Fast Charging Stations

4.1 Introduction

The successful deployment of Electric Vehicles (EVs) is hindered as the time taken to recharge the EV battery is more and driving range is less compared to the Internal Combustion Engine (ICE) Vehicles [41]. The recharging time can be reduced with the advancement in battery and charger technology and driving range limitation can be met by building convenient charging infrastructures. The charging infrastructures is divided into three levels based on their charging power. It is further categorized based on the purpose of charging: destination (slow) and urgent (fast) charging. The destination charging serves as the major and common way of recharging. The urgent charging can provide an additional way to recharge the EVs when the long trip distance exceeds the driving range of the EVs [58] as the daily driving mileage of most of the customers falls below the driving range of the EVs. However, it is necessary to develop fast charging infrastructures to provide urgent charging to the customers with long distance trips. Thus, more attention has been paid towards the optimal planning of Fast Charging Stations (FCS) in the past few years. The study [61] suggested that the planner must consider the charging demand distribution, traffic flow distribution, regional distribution grid, road network requirements, service radius of FCS and the future development trend of EVs while planning charging infrastructure.

Planning of FCS will effect the driving behaviour of EV owners and operation of power and transportation networks. Based on this, the literature reports that the planning of FCS is carried out from distribution system, transportation network and multidisciplinary perspectives. From distribution system perspective, studies have attempted to minimize the power losses, voltage deviation and investment and operation cost for the FCS while satisfying the operating constraints of distribution system [62–67]. In addition to these objectives, Ref. [66] added reduction in charging cost and Ref. [67] added reduction in CO_2 emissions in the optimization problem. In [68–70], problem is formulated as cost function consisting of development, maintenance, travelling and power loss cost. From transportation network perspective, FCS is planned such that it is able serve maximum EV demand [72–77]. The methodologies presented in the literature to serve the EV demand are: node demand-based method, real traffic simulation-based method and traffic flow-based demand. From multidisciplinary perspective, studies have considered both

transportation network and distribution system for the planning of FCS [89–97, 101, 102, 142]. The objectives of these studies are to plan FCS such that service quality is maximized while simultaneously minimizing the negative impacts on the performance of distribution system. The developed problems are generally constrained with distribution system and transportation network operational constraints.

It is inferred from the literature that the planning of FCS will effect the convenience of the EV owner and the operation of both distribution system and transportation networks. The planning of FCS should be done such that the negative impact of FCS on the distribution system can be reduced along with better utilization of FCS and service quality to the EV owners. The planning of FCS should also satisfy the distribution system and transportation network constraints. Based on the literature, the traffic flow-based spatial-temporal charging demand should be utilized to estimate the number, location and sizes of FCS to be installed in the system. Further, the battery capacity also plays an important role in the planning of FCS so as to ensure that the EVs can reach to its nearest charging station within its battery capacity. The waiting time is an important parameter affecting the service quality which will further effect the size of installed FCS. The existing literature has considered different influential factors for the planning of FCS such as the serviceability, distribution and transportation network operational constraints, driving behaviour, heterogeneous driving distance and spatial-temporal charging demand. However, the uncertainties associated with the heterogeneous driving ranges have not been properly addressed. This effects the service radius of FCS and the number of FCS to be located in the system. Further, effect of parameter value for service quality needs to be investigated as this also affects the distribution system performance, number of identical slots and utilization of FCS. Most of the studies have considered the FCS charging demand as Constant Power Load (CPL) model to estimate the losses, voltage profile and distribution system operation constraints like thermal limit and voltage limits of the system. However, in Chapter 3, it is determined that the exponential load model mimics the FCS charging demand more than the CPL model. Hence, proper load model should be incorporated to avoid the misrepresentation of distribution system performance parameters. Thus, in this chapter, a synergistic planning strategy is proposed which takes into account distribution system and transport network's operation constraints and heterogeneous driving ranges based on the initial SOC of the EV while considering FCS load as exponential load model. The objectives of this chapter are:

1. Model the uncertainties associated with the driving range based on the initial SOC to estimate service radius of FCS such that the EVs can drive to the nearest station with the available battery SOC.

2. Using the developed spatial-temporal distribution of vehicles in Chapter 3, develop queuing model to estimate the size of each FCS and estimate the 24-hour charging demand of FCS.
3. Formulate multi-objective Mixed Integer Nonlinear Programming ($MINLP$) planning problem which optimizes the energy losses, voltage deviation and the served traffic flow.
4. To determine the non-dominated solutions of the multi-objective problem using metaheuristic Multi-objective Grey Wolf Optimizer ($MOGWO$) algorithm and utilize fuzzy satisfaction decision making approach to obtain desirable solution.
5. To carry out sensitivity analysis to determine the effect of different objectives, service radius and waiting time on the planning of FCS.

4.2 Problem Formulation for FCS Planning

The planning of FCS requires identification of location and sizes in the planning area. As the FCS couples both power grid and transportation network, therefore, a methodology is developed for the planning of FCS in distribution system coupled with transportation network in this chapter. The location and sizes of FCS will affect the operation of distribution system, transportation network and the customer convenience. Hence, the important aspects to consider while planning the FCS is to reduce negative impact of FCS on distribution system by appropriate siting and sizing, increase the utilization of FCS and provide better service quality. Further, the range anxiety of EV customer is also an important parameter to be considered in the planning problem. The range anxiety can be dealt by determining suitable service radius of FCS. The sizing of FCS will affect the service quality. Therefore, the service radius of FCS is estimated and sizing problem of FCS is proposed to provide better service quality.

4.2.1 Estimation of Service Radius of FCS

The convenience and range anxiety of EV owners will affect the location of the FCS in the planning region. To address this issue, the service radius is introduced to ensure that EVs can reach its nearest FCS for the recharging with remaining SOC_{min} in order to protect the batteries and increase its life cycle. Service radius is the actual transportation distance between the location of EVs and the nearest FCS. It is assumed that the change in SOC varies linearly with the actual travel distance as given in equation (3.48). The travel range available when the EVs need to recharge is mathematically given as

$$d_{sc} = \eta \times (SOC_d - SOC_{min}) \times d_{max} \tag{4.1}$$

where, SOC_d is the state of charge of battery when EV needs to recharge and d_{max} is the maximum travel range of EV. The loss factor η is introduced in the d_{sc} determination to account for the variation in maximum driving range. The driving range of EV depends not only on the battery capacity but also on the external factors like velocity, acceleration, deceleration and weather conditions. The value of η is assumed to be uniformally distributed between the range [0.5-1]. Further SOC_d is assumed to be normally distributed with mean 0.4 and standard deviation 0.001 to incorporate the heterogeneous driving range characteristics. The obtained d_{sc} is normally fitted according to the central limit theorem in probability theory given as

$$P\left(d_{sc}, \mu_{d_{sc}}, \sigma_{d_{sc}}\right) = \frac{1}{\sigma_{d_{sc}}\sqrt{2\pi}} \exp^{-\frac{\left(d_{sc}-\mu_{d_{sc}}\right)^2}{2\sigma^2_{d_{sc}}}} \tag{4.2}$$

where, $\mu_{d_{sc}}$ and $\sigma_{d_{sc}}$ are the mean and standard deviation of the travel range (d_{sc}) when EV needs to recharge obtained from (4.2). The service radius based on the d_{sc} with confidence level $(1-\alpha)$ is given by

$$d_{SR} = \mu_{d_{sc}} - z_{\alpha/2} \times \sigma_{d_{sc}} \tag{4.3}$$

The coefficient $z_{\alpha/2}$ is obtained from the lookup table of the standard normal distribution function corresponding to the confidence level of $(1-\alpha)$. It signifies that $(1-\alpha) * 100\%$ of the EVs can travel to its nearest FCS with the available SOC_d.

4.2.2 Sizing of FCS

The deployment of EVs can be significantly increased by providing good charging service quality. The service quality depends on the time that EV has to spend at the FCS facility. The service time has two components, charging time and waiting time. The charging time depends on the SOC_d and final requested SOC by the EV owner and the charging rate at which the battery is charged. Thus, the charging time is customer dependent and the charging rate is technology dependent. The charging time do not affect the service quality but the reduction in waiting time can greatly improve the service quality. Therefore, in this chapter, the sizing of FCS is done with an aim to reduce number of identical charging slots in each FCS constrained with the waiting time during peak time interval. The waiting time is determined using queuing theory as the FCS can be considered as server which provides service to the EVs waiting in a queue. $M_1/M_2/N_c^k$ queuing model [138] is employed to optimize the size of FCS. M_1 denotes the arrival rate which is different during the day and is modelled as non-homogeneous Poisson process since the arrival of EVs at FCS is independent of each other. The inter-arrival time of EVs is represented by the exponential

distribution with the mean of T_{λ_k}. It is obtained from the spatial-temporal distribution of EVs given in Section 3.3.1. It is calculated by estimating the EV flow served by the k^{th} FCS in time t as given by equation (3.40) and (3.41). M_2 denotes the service time following the exponential distribution with mean T_μ and N_C^k is the identical charging spots in k^{th} FCS. The number of customers waiting in the queue is assumed infinite for the simplicity. The mean service time T_μ will depend on the daily recharge energy (E_d) need of EVs which further depends on the daily driving distance depicted in equation (3.42). The mean daily driving distance (d_μ) is obtained from the travel survey data of Waterloo region [57]. Then based on the d_μ, the mean service time (T_μ) is already determined in equation (3.44). The sizing problem is formulated as Nonlinear Integer Programming ($NLIP$) problem given as:

$$Minimize \;\; N_c^k \tag{4.4}$$

Subject to:

$$W_{ph}^k <= W^{max} \tag{4.5}$$

where, W_{ph}^k is the waiting time at k^{th} FCS in peak hour and W^{max} is the maximum permissible waiting time. The waiting time of this queuing model is determined according to the *Little's Law* [138] in the queuing theory given as

$$W_{ph}^k = \frac{\left(N_c^k \rho_{ph}^k\right)^{N_c^k} \rho_{ph}^k T_{\lambda_{ph}^k}}{N_c^k! \left(1-\rho_{ph}^k\right)^2} P_0^k \tag{4.6}$$

$$P_0^k = \left[\sum_{n=0}^{N_c^k-1} \frac{\left(N_c^k \rho_{ph}^k\right)^n}{n!} + \frac{\left(N_c^k \rho_{ph}^k\right)^{N_c^k}}{N_c^k! \left(1-\rho_{ph}^k\right)}\right]^{-1} \tag{4.7}$$

$$P_n^k = \left(N_c^k \rho_{ph}^k \;/\, n!\right) \tag{4.8}$$

$$\rho_{ph}^k = \frac{T_\mu}{N_c^k T_{\lambda_{ph}^k}} \tag{4.9}$$

The probability of no EV being charged is denoted by equation (4.7) and (4.9) denotes the occupation rate per server. It should be noted that the occupation rate $\rho_{ph}^k < 1$ for the queue to be stable. This becomes deciding factor for the minimum number of identical charging slots (C_{min}^k) of k^{th} FCS.

$$\frac{T_\mu}{N_c^k T_{\lambda_{ph}^k}} < 1 \tag{4.10}$$

$$N_c^k > T_\mu / T_{\lambda_{ph}^k} \tag{4.11}$$

Since, N_c^k is an integer quantity, therefore, minimum number of slots at each FCS is given by

$$N_{c_{min}}^k = \left\lceil T_\mu / T_{\lambda_{ph}^k} \right\rceil \tag{4.12}$$

The flowchart for the computation of slots of each candidate location is given in Fig. 4.1. Once the size of each FCS is known, the total expected EV charging demand at any time t of each FCS can be calculated using equation (3.53) and (3.54).

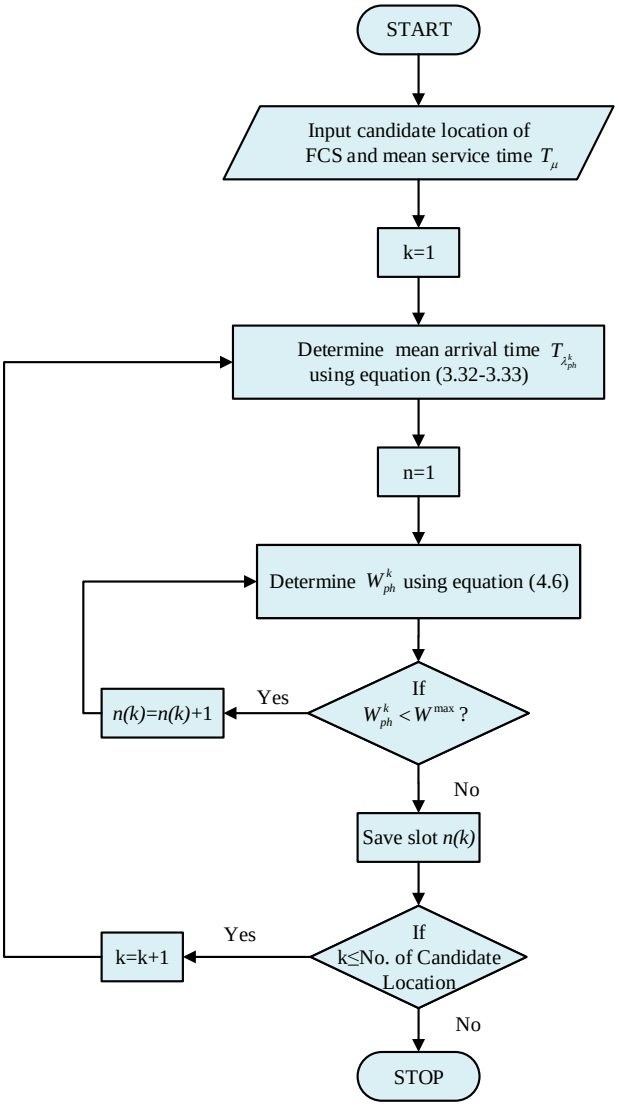

FIGURE 4.1: Flowchart for the computation of identical slots of FCS

4.2.3 Optimization Model for FCS Planning

The objective of the planning of FCS is to determine the location and sizes of FCS to be built. In this study, the FCSs are synergistically planned in the distribution system coupled with transportation network. A multi-objective synergistic planning framework is proposed with the aim of minimizing the power losses and the voltage deviations in the distribution system and maximizing the EV traffic flows served by the FCS. The first two objectives helps in reducing the negative impact of FCS on the distribution system due to the increased charging load while the last objective improves service quality and the increased utilization of FCS. The detailed objective formulation is given below:

4.2.3.1 Minimization of the Voltage Deviation and the System Power Losses

The deployment of FCS in the distribution system will increase load demand and thus will result in increased power losses and may also deviate the voltage from its ideal values. The proper planning of FCS in the distribution system can assist in reducing its negative impact. Therefore, the power losses and voltage deviation are minimized given in equation (4.14) and (4.15).

$$Minimize: \tag{4.13}$$

$$F_1 = P_{loss} \tag{4.14}$$

$$F_2 = \frac{1}{N_B} \sum_{t=1}^{24} \sum_{i=1}^{N_B} \frac{|V_{i,t} - V_0|}{V_0} \times 100\% \tag{4.15}$$

where

$$P_{loss} = \frac{1}{2} \sum_{t=1}^{24} \sum_{i=1}^{N_B} \sum_{j=1}^{N_B} G_{ij} \left(V_{i,t}^2 + V_{j,t}^2 - 2V_{i,t}V_{j,t} \cos\left(\theta_{ij,t}\right) \right)$$

Subject to:

a) *Power Balance Constraint:* The demand-supply balance constraint for both active and reactive power is given by the load flow depicted in equation (4.16). As stated in chapter 3, the exponential load model is the better representation of charging demand of FCS. Therefore, active power balance equation in power flow analysis is modified to incorporate the voltage-dependent exponential characteristic of FCS load. However, the reactive supply-demand balance constraint remains same as the additional EV fast charging demands only active power due to the unity power factor correction feature of EV fast charger.

$$P_{G_{i,t}} = P_{D0_{i,t}} + \psi^k E[P_{FCS_t^k}]\left[a_p\left(\frac{V_{i,t}}{V_o}\right)^{n_p} + b_p\right] + V_{i,t}\sum_{j=1}^{N_B} V_{j,t}\left(G_{ij}\cos\left(\theta_{ij,t}\right) + B_{ij}\sin\left(\theta_{ij,t}\right)\right) \quad (4.16a)$$

$$Q_{G_{i,t}} = Q_{D0_{i,t}} - V_{i,t}\sum_{j=1}^{N_B} V_{j,t}\left(G_{ij}\sin\left(\theta_{ij,t}\right) - B_{ij}\cos\left(\theta_{ij,t}\right)\right) \quad (4.16b)$$

For the distribution system coupled with transportation network, there are few common nodes which are part of both the distribution system and the transportation network. These common nodes are termed as the coupled nodes of the two networks. They will serve traditional fixed demand at node i and the requested fast charging EV load. This interface is expressed by (4.16a) in which the first part is traditional demand at node i and second part is FCS demand where the binary variable ψ^k associated with it represents that k^{th} FCS on path OD is located at node i.

b) *Bus Voltage Constraint:* The voltage magnitude of each bus are constrained within the permissible limit.

$$V_{i,min} \leq V_{i,t} \leq V_{i,max} \quad \forall i \in N_B \quad (4.17)$$

c) *Thermal limit Constraint:* The current of each branch must not exceed the predefined thermal rating.

$$I_{ij,t} \leq I_{ij}^{max} \; \forall ij \in N_L \; (lines\ of\ the\ system) \quad (4.18)$$

where $V_{i,t}, V_{j,t}$ are the voltage magnitude of bus i and j, $\theta_{j,t}$ is the phase angle difference between bus i and j, $P_{G_{i,t}}$ and $Q_{G_{i,t}}$ are active and reactive power generations of generators at bus i, $P_{D0_{i,t}}$ and $Q_{D0_{i,t}}$ are active and reactive loads at bus i, $I_{ij,t}$ is the line current of line ij at time t, G_{ij} and B_{ij} are conductance and susceptance of line between bus i and j, V_i^{min} and V_i^{max} are the voltage limits of bus i, I_{ij}^{max} is the current permissible for branch ij and N_B, N_L are set of distribution system buses and lines.

4.2.3.2 Maximization of EV Flow Served by FCS

To improve the service quality and increased utilization of FCS, it is expected that it can serve as many EVs as possible. The maximal covering location model locates facilities to serve maximum node based demand [143]. However, the demand is not always expressed at nodes and the mobility of EVs results in dynamic demand. Therefore, it is better to model the EV charging demand as traffic flows in the transportation network. The EV traffic flows is the total number of EVs that travel on the path connecting the nodes.

FCS at a node in the network serves all the EV flow that passes through that node. The objective function for maximum serving of EV flow-based [143] charging load demand by FCS is given in (4.19).

$$Maximize: \quad F_3 = \sum_{t=1}^{24} \sum_{O \in N_T} \sum_{D \in N_T} f_{OD,t} \tau_{OD} \tag{4.19}$$

Subject to:

$$\sum \psi^k \geq \tau_{OD} \tag{4.20}$$

where τ_{OD} is 1 if the EV flow on path OD is served otherwise zero. The constraint (4.20) implies that the EV flow on path OD is served only if atleast one FCS exists on path OD.

The whole planning problem is further constrained with the service radius of the FCS to account the convenience, range anxiety of EV owners and reduction in charging resource wastage. The distance between any two adjacent FCS should not be too far and distance between adjacent FCS should not be too close given by equation (4.21). The two FCS are said to be adjacent when the actual distance between them considering the shortest route is smallest as compared to the others.

$$d_{SR} \leq d_{FCS} \leq 2 * d_{SR} \tag{4.21}$$

4.3 Proposed Methodology for FCS Planning

In this section, service radius incorporating uncertainties is utilized for the rational planning of FCS in order to minimize the power losses and voltage deviation of distribution system and maximizing the served EV flow for customer convenience. Then, recently introduced Multi-Objective Grey Wolf Optimization (MOGWO) algorithm is implemented as an optimization technique for FCS planning. The impact of important parameters such as service radius and waiting time is also investigated for the proper planning of FCS. The objectives F_1 and F_2 minimizes the power loss and bus voltage deviation while F_3 maximizes the traffic flow served by the FCS. The third objective conflicts the other two objectives. Therefore, it is important to transform the objectives as

$$\begin{aligned} F(x) &= \left[F_1^{min}(x),\ F_2^{min}(x),\ F_3^{max}(x)\right]^T \\ F'(x) &= \left[F_1^{min}(x),\ F_2^{min}(x),\ -F_3^{min}(x)\right]^T \end{aligned} \tag{4.22}$$

The developed mathematical model for the planning of FCS is a $MINLP$ constrained optimization problem.

$$\begin{aligned} &Minimize: \quad F'(x) \\ &Subject\ to: \ g_i(x) \geq 0 \ \forall i = 1, 2, ...m \\ &h_i(x) = 0 \ \forall i = 1, 2, ...n \\ &L_i \leq x_i \leq U_i \ \forall i = 1, 2, ...p \end{aligned} \tag{4.23}$$

where, x is the vector consisting of binary decision variables. The inequality constraints $g_i(x) \geq 0$ is written as $-g_i(x) \leq 0$, $h_i(x) = 0$ as $h_i(x) \leq 0$ and $-h_i(x) \leq 0$, $x_i \geq L_i$ as $-(x_i - L_i) \leq 0$ and $x_i \leq U_i$ as $x_i - U_i \leq 0$. Therefore, the problem is transformed into optimization problem with inequality constraints and can be generalized as $g_i(x) \leq 0 \ \forall i = 1, 2, ...m + n + p$.

The constrained $MINLP$ optimization problem can be solved using deterministic or stochastic approach. Deterministic method such as generalized gradient descent and feasible direction method requires the objective function to be continuous and differentiable. Thus, stochastic methods such as evolutionary algorithms have gained more importance recently to tackle the constrained optimization problems. The stochastic methods are developed for the unconstrained optimization.

4.3.1 Handling Constraints

There are different methods to incorporate the constraints into the objective function like Lagrange method and penalty functions. The Lagrange method requires the constraint to be differentiable and continuous. Therefore, in this study, penalty method is used to handle the constraints. The constrained problem is converted into unconstrained by penalizing the constraints and developing a single objective function which is further optimized using unconstrained stochastic optimization algorithm. In this method, penalty value is added whenever the constraint is violated. In this study, the penalty values are dynamically modified in each iteration and the same is also reported in the literature that dynamic penalty value is better than the fixed penalty value. Determining penalty value is the main concern as the high penalty values may result in minimization problem to get trapped in local minima and low value may not be able to detect the feasible solutions. The penalty values are selected using trial and error method. The modified objective function with penalized constraint are given as

$$F''(x) = F'(x) + h(z)H(x) \tag{4.24}$$

where $F'(x)$ is the original objective function, $h(z)$ is dynamically modified penalty value, z is the current iteration number and $H(x)$ is the penalty factor given as:

$$H(x) = \sum_{i=1}^{m+n+p} \theta(q_i(x)) q_i(x)^{\gamma(q_i(x))} \tag{4.25}$$

where $q_i(x) = max(0, g_i(x))\ \forall i = 1, 2, ...m+n+p$. The function $q_i(x)$ is a relative violated function of the constraints, $\theta(q_i(x))$ is a multistage assignment function and $\gamma(q_i(x))$ is the power of the penalty function. The functions $h(.)$, $\theta(.)$ and $\gamma(.)$ are problem dependent. In this study, if $q_i(x) < 1$, then $\gamma(q_i(x)) = 1$, otherwise 2. If $q_i(x) < 0.001$ then $\theta(q_i(x)) = 1$, else, if $q_i(x) < 0.1$ then $\theta(q_i(x)) = 10$, else, if $q_i(x) < 1$ then $\theta(q_i(x)) = 20$, otherwise $\theta(q_i(x)) = 100$. $h(z) = \sqrt{z}$ is considered for this problem.

4.3.2 Multi-objective Grey Wolf Optimizer Algorithm

As mentioned above, the metaheuristic are independent of system complexity and do not require past knowledge of the problem. A recently developed efficient metaheuristic MOGWO algorithm is employed to solve the multi-objective optimization problem. It is proved in [144] that computational complexity of MOGWO is equal to other well known algorithms like Non-dominated Sorted Genetic Algorithm (NSGA-II) and Multi-Objective Particle Swarm Optimization (MOPSO) and has better computational complexity compared to NSGA and Strength Pareto Evolutionary Algorithm (SPEA). The solutions obtained by MOGWO has better coverage in search space and fast convergence compared to the MOPSO and Multi-Objective Evolutionary Algorithm/Decomposition (MOEA/D). MOGWO is the modified version of the original Grey Wolf Optimizer (GWO) algorithm to perform the multi-objective optimization. The original Grey Wolf Optimizer (GWO) algorithm [145] is a search based bio-inspired optimization technique which mimics the social hierarchy and hunting technique of pack of grey wolves. The hunting behaviour of grey wolves involves the following series of events:

- They track, chase and approach the prey
- The prey is encircled and harassed until it becomes stationary
- The prey is attacked

The social hierarchy of grey wolves is mathematically modelled by considering three consecutive best solutions as alpha (α), beta (β) and delta (δ) wolves. The remaining probable solutions are assumed to be omega (ω) wolves who are guided by α, β and δ wolves in search for the optimal solution. The encircling behaviour of grey wolves around

the prey during hunting is defined as:

$$\vec{D} = \left|\vec{C}.\vec{X}_p(y) - \vec{X}(y)\right| \tag{4.26}$$

$$\vec{X}(y+1) = \vec{X}_p(y) - \vec{A}.\vec{D} \tag{4.27}$$

where y denotes current iteration, $\vec{A}$ and $\vec{C}$ denotes coefficient vectors, $\vec{X}_p$ denotes position of the prey and $\vec{X}$ denotes the vector position of grey wolves around the prey. The coefficient vectors $\vec{A}$ and $\vec{C}$ are determined as:

$$\vec{A} = 2\vec{a}.\vec{r1} - \vec{a} \tag{4.28}$$

$$\vec{C} = 2.\vec{r2} \tag{4.29}$$

$$\vec{r1}, \vec{r2} \in [0, 1] \tag{4.30}$$

where $\vec{a}$ linearly decreases from 2 to 0 to employ the exploratory behaviour during the initial stage and exploitation behaviour during the final stage while $\vec{C}$ ensures exploration during the whole course of iteration. To find the optimal solution, the first three fittest solutions are stored as α, β and δ wolves and the other search agents are guided based on their position as:

$$\vec{D}_\alpha = \left|\vec{C}_1.\vec{X}_\alpha - \vec{X}\right| \tag{4.31a}$$

$$\vec{D}_\beta = \left|\vec{C}_2.\vec{X}_\beta - \vec{X}\right| \tag{4.31b}$$

$$\vec{D}_\delta = \left|\vec{C}_3.\vec{X}_\delta - \vec{X}\right| \tag{4.31c}$$

$$\vec{X}_1 = \vec{X}_\alpha - \vec{A}_1.\vec{D}_\alpha \tag{4.31d}$$

$$\vec{X}_2 = \vec{X}_\beta - \vec{A}_1.\vec{D}_\beta \tag{4.31e}$$

$$\vec{X}_3 = \vec{X}_\delta - \vec{A}_1.\vec{D}_\delta \tag{4.31f}$$

$$\vec{X}(z+1) = \frac{\vec{X}_1 + \vec{X}_2 + \vec{X}_3}{3} \tag{4.31g}$$

The wolves update their real valued position in the search space bounded by the constraints in continuous GWO. However, the proposed problem is $MINLP$ problem and solution variables are binary in nature. Therefore, continuous GWO is modified to map the real valued wolf position by the binary wolf position. This is ensured by passing the real valued wolf position to a transfer function as follows:

$$X_d\,(z+1) = \begin{Bmatrix} 1 & if\ \frac{1}{1+e^{-X_d(z)}} \geq rand \\ 0 & otherwise \end{Bmatrix} \tag{4.32}$$

where *rand* is a random number between 0 and 1 drawn from uniform distribution, $X_d(z)$ is the updated binary position in dimension d in z^{th} iteration. The solutions in single objective can be easily compared due to the single fitness values obtained from the objective function. The solution X is better than Y if $f(X) < f(Y)$, where $f(X)$ and $f(Y)$ are the fitness values of the minimization function f. However, the solutions obtained in the multi-objective optimization cannot be easily ranked as multi-objective provides multiple fitness values. The solution of multi-objective is better if and only if it provides better or equal fitness value of all the objectives and also provides better fitness value in atleast one objective function. This concept is known as Pareto dominance and the set of solutions obtained are the Pareto-optimal solutions also known as non-dominated solutions. To perform multi-objective optimization, new components are added in the binary *GWO* algorithm as:

- *Archive:* stores non-dominated Pareto optimal solutions obtained so far.
- *Leader Selection Mechanism:* It assists in choosing the α, β and δ leaders from the least crowded segment in the archive.

The pseudo code of MOGWO algorithm is given in Algorithm 1.

4.3.3 Normalization of the Objectives

The multi-objective optimization techniques have difficulty in finding a set of uniformly distributed non-dominated solutions over the entire Pareto front when each objective are separately scaled. Thus, each objective is normalized as given in (4.33).

$$F_{i,norm} = \frac{F_i - F_{i,min}}{F_{i,max} - F_{i,min}} \ \forall i = 1, 2, 3 \tag{4.33}$$

where, $F_{i,min}$ and $F_{i,max}$ are the minimum and maximum values of i^{th} objective function. The values corresponding to each objective are obtained by solving each objective individually. The solution to the multi-objective is not unique solution but provides a set of trade-off solutions. Therefore, a subjective selection has to be made to choose one solution over the set of solutions based on the decision-maker preference.

Algorithm 1: Pseudo code for MOGWO algorithm

Initialize the grey wolf position X_i $i = 1, 2, ...n$ Initialize a, A and C;
Evaluate fitness values of each wolf;
Store the position of the wolf that represent non-dominated vectors in the archive;
Generate hypercubes of the search space explored so far and locate the wolves using these hypercubes as a coordinate system where each wolf's coordinates are defined according to fitness values of its objectives;
Assign the probability P_i to each hypercube as

$$P_i = \frac{c}{N_i} \tag{4.34}$$

where c is a constant number greater than 1 and N_i are the number of wolves in the i^{th} hypercube;
Apply roulette wheel method to select a hypercube. The probability P_i will ensure that the hypercube with least number of wolves has higher chances of getting selected;
Assign z=1;
while $z <$ *Maximum number of iterations* **do**
    Randomly select any three wolves from the i^{th} hypercube and assign it to α, β and δ wolves;
    if $N_i >= 3$ **then**
        Select least crowded hypercube to choose the leaders;
    else if $N_i < 3$ **then**
        Select the leader from another least crowded hypercube
    else
        Select the leader from the third least crowded hypercube
    end
    for $i = 0$ **to** *Number of Wolf* **do**
        Update the position of the current wolf by equation (4.24–4.30);
    end
    Update a, A and C;
    Find the non-dominated solutions and update the archive with respect to the obtained non-dominated solutions;
    if *Archive is full* **then**
        Generate the hypercubes of search space. Find the most crowded segment and omit one of its solution randomly;
        Add new solution to the least crowded hypercube;
    end
    z=z+1;
end
return Archive;

4.3.4 Fuzzy Satisfaction Based Method for Final Decision-Making

After the determination of non-dominated solutions, the compromise solution has to be selected among a set of solutions. The fuzzy satisfying decision-making approach [146] is used to make the final decision such that performance of group of solutions are ranked and the best one is selected. Fuzzy decision-based method can assist decision-maker in choosing the final scheme from non-dominated solutions such that desirable level of each objective is achieved. The membership functions are used to describe the fuzzy sets whose values ranges from 0 to 1. These values represent the degree of membership in a fuzzy and indicates the compatibility within the set. The 0 membership values suggests incompatibility and 1 implies full compatibility within the set. In fuzzy satisfying method, the continuous monotonically decreasing function is assigned to each objective such as linear, exponential and hyperbolic. In this study, continuous linear decreasing membership function is used for all the objectives as follows:

$$\mu_{F_i}(\bar{x}) = \begin{Bmatrix} 0 & F_i(\bar{x}) > F_{i,max} \\ \frac{F_{i,max} - F_i(\bar{x})}{F_{i,max} - F_{i,min}} & F_{i,min} \leq F_i(\bar{x}) \leq F_{i,max} \\ 1 & F_i(\bar{x}) < F_{i,min} \end{Bmatrix} \tag{4.35}$$

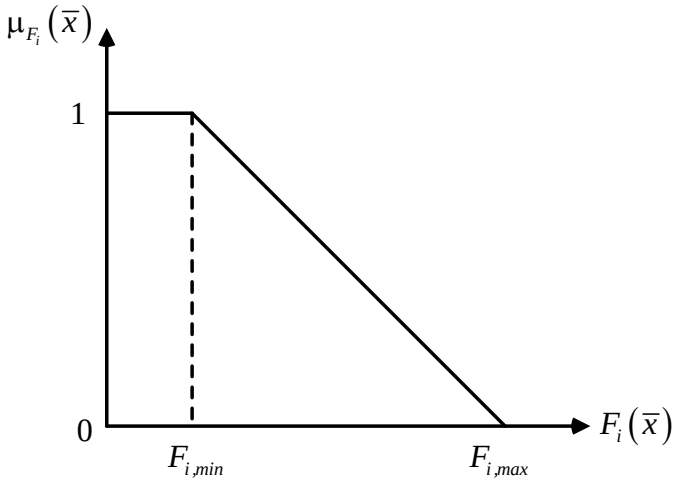

FIGURE 4.2: Continuous monotonically linear descreasing membership function

The graph of linear membership function is shown in Fig. 4.2. The selection of membership function will influence the final solution. If the exponential function is assigned to one of its objectives, then it will prioritize this objective with respect to other objectives in case of minimization as it will assign smaller membership value compared to the linear type. Therefore, to give equal importance to each objectives, continuous linear decreasing membership function is assigned to all the objectives. The value of the membership

function $\mu_{F_i}(\bar{x})$ lies in the range [0,1] where value of membership indicates to what extent a solution is satisfying the objective F_i. $\mu_{F_i} = 1$ indicates the solution fully satisfies the objective and 0 indicates that the solution does not satisfy the objective at all. The final solution from the non-dominated solution is selected by maximizing the objective function given by:

$$Maximize: \quad \prod_{i=1}^{3} \mu_{F_i}(\bar{x}) \tag{4.36}$$

The advantage of maximizing the product over the summation of the membership values of the objective is that, the product of the membership values will try to provide a trade-off value in which all the objectives are satisfied equally while the summation may result in one objective satisfied more that the others. Optimization technique employed in the planning of FCS can be used for any test system due to its simplicity and problem independent nature. Further, desirable value chosen in fuzzy satisfaction-based decision making approach provides decision maker an opportunity to choose the final planning scheme according to their choice.

The complete framework for the planning of FCS is shown in Fig. 4.3 which consists of spatial-temporal distribution of EVs, sizing of FCS, estimation of service radius of FCS and the siting and sizing of FCS.

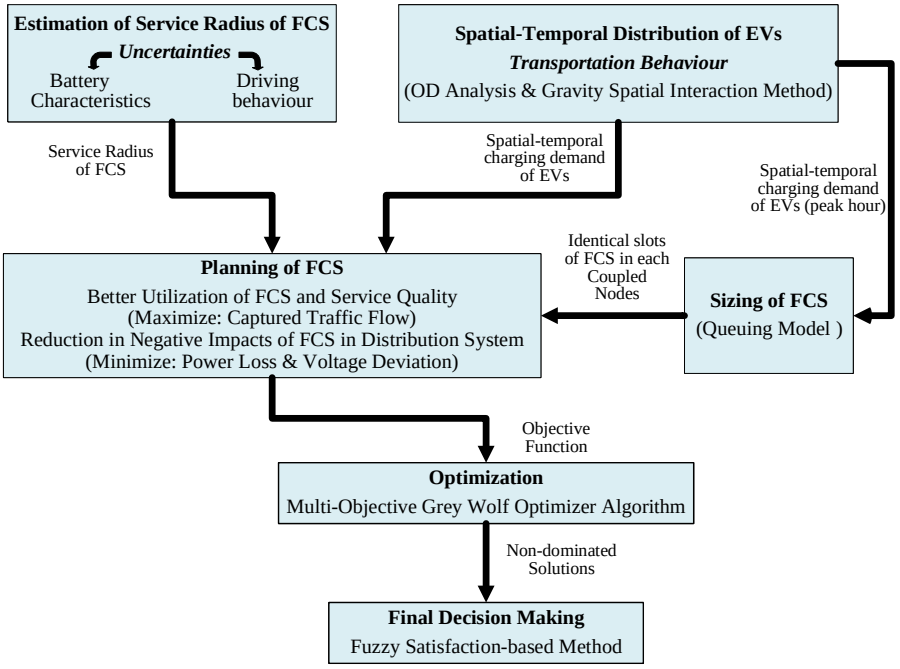

FIGURE 4.3: Synergistic planning framework of FCS in distribution system coupled with transportation network

4.4 Results and Discussions

4.4.1 Test System and Parameter Setting

The IEEE 123-bus distribution system [139] coupled with 25-node transportation network [143] is used to demonstrate the effectiveness of the proposed methodology. It has 85 spot loads and 118 distribution lines. The IEEE 123-bus distribution system is modified to integrate the residential houses, distribution transformers, FCS and each feeder length is multiplied by 1000 to increase the feeder length as the feeder is small. The parameters of exponential load model for the fast charging EVs and methodology for spatial-temporal charging demand of EVs obtained in Chapter 3 are used in this study. It is modelled in openDSS. Few of the nodes of the distribution system is coupled with 25-node transportation network. The node coupling relationship is given in Table 4.1 and the candidate locations of FCS are the coupled nodes of the two systems.

TABLE 4.1: Coupled Nodes of the Two Networks

C_i(**DB-TN**)	C_1(1-22)	C_2(13-14),	C_3(18-10),	C_4(23-9),	C_5(47-3),
	C_6(51-2),	C_7(52-19),	C_8(57-13),	C_9(67-12),	C_{10}(81-25),
	C_{11}(86-24),	C_{12}(89-23),	C_{13}(97-7),	C_{14}(99-6),	C_{15}(105-5)

C_i- Coupled Node Pair, DB-Distribution Bus, TN-Transportation Node

The number of EVs charging at FCS governs the siting and sizing of FCS in planning area. It will depend on the distribution of EVs on the road during the day. This data is obtained from the mobility survey of Waterloo region [57]. The planning of FCS is also effected by the load during the day. Fig. 4.4 shows the vehicle distribution on the road and load pattern during the day. It is observed that the peak of both the patterns occur at the same time.

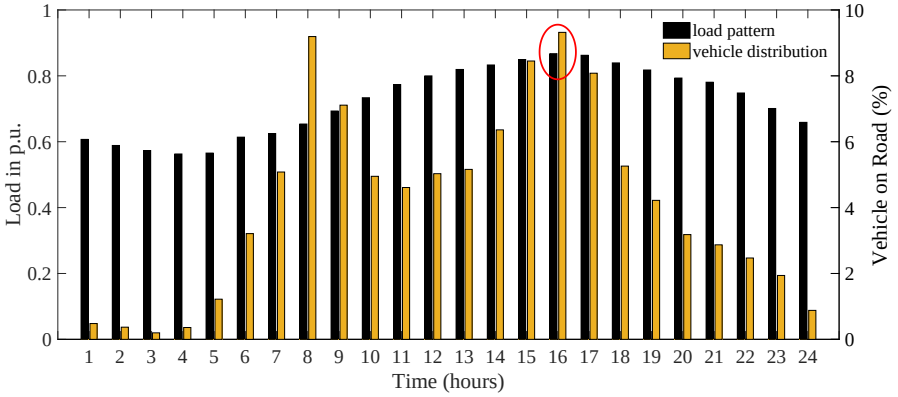

FIGURE 4.4: 24-hour vehicle distribution on the road and load pattern

The simulation parameters are listed in Table 4.2.

TABLE 4.2: Simulation Parameter Settings

Parameters	**Values**	**Parameter**	**Values**
η	0.5-1	C_{bat} (kWh)	24
SOC_d	0.3-0.5	C_{rate}	1C
SOC_{min}	0.2	W^{max} (min)	5
d_{max} (miles)	84	$\sum_{t=1}^{24} f_{total,t}$	1000
(1-α)	0.95	P_{FCS} (kW)	30
ϵ (kWh/mile)	0.272	$a_p, b_p,$ n_p	0.0246, 0.9754, 1.839
d_μ (miles)	40	$V_{min}, V_{max},$ V_0	0.95,1.05, 1.0

The service radius of FCS is obtained by fitting normal distribution on d_{SC} distribution using maximum likelihood estimation algorithm to determine mean and standard deviation of the travel range (d_{SC}) when EV needs to recharge. The mean and standard deviation are used to determine the service radius of FCS using equation (4.3). Fig. 4.5 shows the distribution of distance d_{SC} that EVs can travel when they need to be recharged and service radius of 5.97 *miles* is obtained for 95% confidence level.

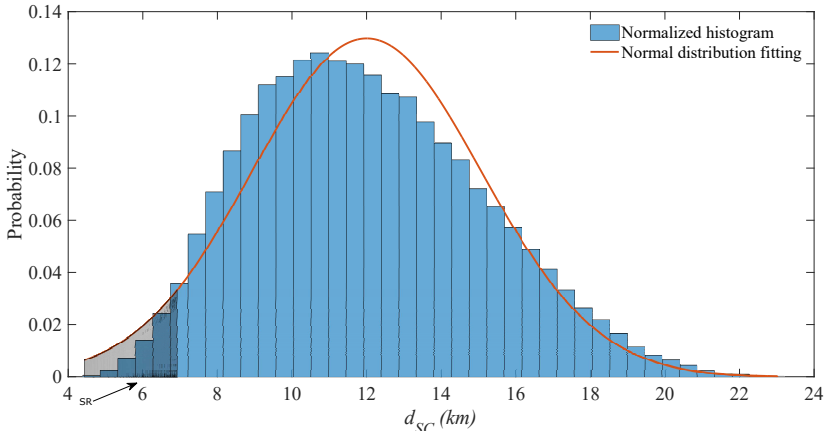

FIGURE 4.5: The d_{SC} distribution

4.4.2 Planning Results

Planning of FCS needs estimation of service radius and spatial-temporal charging demand of EVs. The service radius of FCS for the given confidence level is estimated in the previous section and the spatial-temporal charging demand model developed in Chapter 3 is utilized here to estimate the charging demand occurring at FCS. The demand during the peak hour is used to obtain the identical charging slots of FCS at each candidate location.

Table 4.3 lists the number of identical charging slots for each coupled nodes for the peak hour for 5 minute waiting time.

TABLE 4.3: Number of Charging Slots of Coupled Nodes during Peak Time Interval

Coupled Node	**Charging Spots**	**Coupled Node**	**Charging Spots**	**Coupled Node**	**Charging Spots**
C_1	14	C_6	9	C_{11}	9
C_2	20	C_7	10	C_{12}	10
C_3	13	C_8	6	C_{13}	4
C_4	7	C_9	7	C_{14}	2
C_5	7	C_{10}	1	C_{15}	4

This is further used to determine the optimal location of FCS in the system. MOGWO algorithm is employed to solve the multi-objective planning problem. The initial parameter chosen for MOGWO is given in Table 4.4.

TABLE 4.4: Simulation Parameter Settings for MOGWO Algorithm

Parameters	**Values**	**Parameter**	**Values**
Maximum iteration	500	nGrid	10
Search agents	40	Leader Selection Pressure Parameter	4
Archive Size	40	Repository Member Selection Pressure	2
Grid Inflation Parameter	0.1	Number of variables	15

The algorithm is run for 50 times and multi-period power flow is carried out to precisely calculate the power losses and voltage deviation. The optimization results gives the non-dominated solutions. Backward forward sweep power flow method is used due to high R/X ratio and unbalancing of the distribution system. To determine the final planning scheme, one solution is selected from the set of non-dominated solutions by using fuzzy satisfaction-based method. To apply the fuzzy satisfying method, the decision maker should determine the minimum and the maximum values for each objective which are required for the normalization of the objective. These values are determined by optimizing the objective functions individually. The idea is to find the best trade-off solution such that it provides maximum satisfaction to each objectives. The best trade-off solution is obtained corresponding to the maximum μ_F value. The best 10 results according to the μ_F values are listed in Table 4.5.

The top solution is selected for the final planning scheme which results in maximum capturing of EV flow of all the cases. However, the power loss and voltage deviation is

TABLE 4.5: Planning Results of FCS of the Multi-Objective Optimization

Locations	**Power Loss (MWh)**	**Voltage Deviation (%)**	**Served EV Flow (%)**	μ_F
C_1, C_6, C_7, C_9, C_{14}, C_{15}	1.1870	1.9308	69.76	0.8591
C_1, C_3, C_4, C_7, C_{14}, C_{15}	1.1689	2.2395	66.30	0.8472
C_1, C_4, C_7, C_9, C_{14}, C_{15}	1.1093	1.9490	64.33	0.8464
C_3, C_7, C_9, C_{10}, C_{11}, C_{14}	1.2707	1.7931	64.71	0.8428
C_3, C_7, C_{10}, C_{12}, C_{14}, C_{15}	1.2253	1.8260	60.11	0.8278
C_1, C_6, C_7, C_{10}, C_{11}, C_{15}	1.2303	1.8929	62.85	0.8254
C_3, C_7, C_9, C_{10}, C_{12}, C_{14}	1.2969	1.7829	64.24	0.8231
C_3, C_7, C_{11}, C_{12}, C_{14}, C_{15}	1.1457	1.8535	58.89	0.8229
C_1, C_4, C_6, C_7, C_{11}, C_{12}	1.2452	1.8955	62.32	0.8222
C_4, C_6, C_7, C_9, C_{10}, C_{12}	1.3015	1.7975	62.50	0.8218

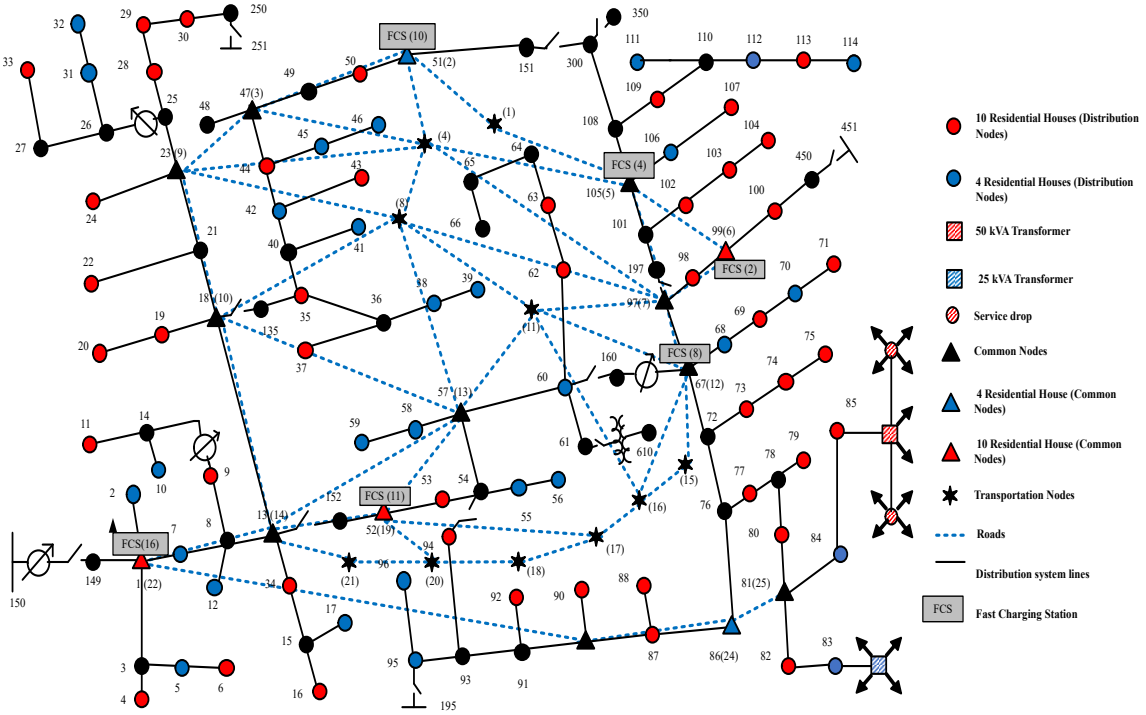

FIGURE 4.6: Final Planning Scheme of FCS in IEE 123-Bus Distribution System Coupled with Transportation Network

more than some cases. This suggests that none of the solution is superior than the others. The selected scheme for the planning of FCS is graphically represented as shown in Fig. 4.6 where the number indicated in the symbol of FCS is same as the number of charging slots of corresponding FCS.

4.4.3 Effectiveness of the Proposed Method

To verify the effectiveness and efficacy of the proposed optimization approach, the proposed planning model has also been solved using MOPSO [147] and MOEA/D [148] algorithms using Matlab 2015b on a 3.19 GHz computer. The parameters for MOPSO and MOEA/D algorithm are given in Table 4.6 and Table 4.7 respectively. For all the algorithms, 40 search agents, a maximum of 500 iterations are utilized and each algorithm is run 50 times.

TABLE 4.6: Simulation Parameter Settings for MOPSO Algorithm

Parameters	**Values**	**Parameter**	**Values**
Inertia weight	0.4 to 0.9	nGrid	10
Search agents	40	Leader Selection Pressure Parameter	4
Archive Size	40	Repository Member Selection Pressure	2
Grid Inflation Parameter	0.1	Number of variables	15
Cognitive constant	2	social constant	2

TABLE 4.7: Simulation Parameter Settings for MOEA/D Algorithm

Parameters	**Values**	**Parameter**	**Values**
Subproblems	40	Number of Neighbours	0.1*subproblems
Crossover Parameter	0.5	Mutation rate	0.5

The performance of multi-objective algorithm can be assessed by determining the closeness to the true Pareto front, spread (distribution) along the Pareto front and the number of solutions in the non-dominated set. The distance based metric for the convergence analysis is not determined due to the unavailability of true Pareto-set. Performance metrics like metric of spread (MS) and metric of spacing (SP) [144] are employed to quantify the spread along the Pareto front. SP provides information regarding how well non-dominated solutions are distributed. SP value zero indicates that all non-dominated solutions are equidistantly spaced. MS indicates distance between the boundary solutions and the space covered by the solutions in objective space. Higher values of SP represents better space coverage. Table 4.8 and 4.9 shows the SP and MS values for all the three algorithms.

TABLE 4.8: Metric of Spacing

	MOGWO	**MOPSO**	**MOEA/D**
Average	0.2423	0.2468	0.2980
STD. Dev.	0.0118	0.0131	0.0282
Best	0.2125	0.2215	0.2275
Worst	0.2526	0.2698	0.3546

TABLE 4.9: Metric of Spread

	MOGWO	**MOPSO**	**MOEA/D**
Average	0.6461	0.6458	0.5395
STD. Dev.	0.0341	0.0359	0.0701
Best	0.7626	0.7551	0.7067
Worst	0.5752	0.5653	0.3705

From the Table 4.8, it is observed that MOGWO algorithm provides minimum value of metric of spacing and standard deviation compared to MOPSO and MOEA/D algorithms, thus, showing that the non-dominated solutions obtained by MOGWO are better distributed while the performance of MOGWO and MOPSO algorithm are comparable. From the Table 4.9, it is observed that maximum value of metric of spread is obtained using MOGWO algorithm compared to the other algorithm while minimum standard deviation is obtained indicating that MOGWO provides better space coverage. Therefore, MOGWO outperforms the other two algorithms in terms of distribution and coverage. Further, total number of non-dominated solutions were determined and it was found that 40, 39 and 19 non-dominated solutions were obtained for MOGWO, MOPSO and MOEA/D algorithm respectively for the best case. This also validates MOGWO algorithm is better compared to other algorithm. However, the performance of MOGWO and MOPSO are comparable.

4.4.4 Sensitivity Analysis

The location and sizes of FCS are sensitive to the objectives considered, service radius and the waiting time. Therefore, in this section, the sensitivity analysis is performed for analysing the impact of different parameters on the planning of FCS.

4.4.4.1 Impact of Different Objectives

The objectives considered will effect the planning of FCS. As the FCS couples distribution and transportation network, thus, the planning objectives can effect the distribution

system and the transportation network performance. The transportation network performance is assessed in terms of the served EV flow by the FCS also representing the customer convenience. This section explores the effect of different objectives on the planning of FCS to validate the effectiveness of the considered multi-objective planning model. Four cases are studied and results of planning of FCS in the system for all the cases is given in Table 4.10.

(i) Case 1: To obtain minimum power losses, only objective F_1 is considered.

(ii) Case 2: To obtain minimum voltage deviation, only objective F_2 is considered.

(iii) Case 3: To serve maximum EV flow, only objective F_3 is considered.

(iv) Case 4: Both distribution system and transportation network operation parameters are considered. Objectives F_1, F_2 and F_3 are considered simultaneously.

TABLE 4.10: Planning Results for Different Cases

Case Number	**Location**	**Power Loss (MWh)**	**Voltage Deviation (%)**	**Served EV Flow (%)**
1	C_1, C_4, C_{10}, C_{11}, C_{14}, C_{15}	1.1060	1.9721	41.08
2	C_3, C_4, C_9, C_{12}, C_{14}, C_{15}	1.3321	1.7591	55.35
3	C_1, C_3, C_6, C_7, C_{14}, C_{15}	1.2284	2.2176	74.10
4	C_1, C_6, C_7, C_9, C_{14}, C_{15}	1.1870	1.9308	69.76
Without FCS	–	0.7579	2.1854	–

(i) **Case-1:** It aims to minimize the power losses occurring in distribution system due to the addition of fast charging EV load demand by locating and sizing the FCS accordingly. In this case, minimum power losses is obtained compared to the other cases. The system losses will be less when the demand seen by the system is less or the load is located near to the substation so that the feeder length gets reduced. In this case, the load served by the system is less as evident from the served EV flow. The loads are not located near to the substation as planning problem is solved with the FCS service radius constraint. The voltage deviation is more as the load added to the system is less, thus, resulting in less voltage drop.

(ii) **Case-2:** This case results in low voltage deviation amongst all the other cases. The less voltage deviation indicates that bus voltages of the system are nearer to the reference voltage 1.0 p.u. Bus voltages in distribution system are generally less

than 1.0. p.u. indicating that bus voltages improves if the load is connected to the stronger buses or the load is less. However, as mentioned in the Chapter 3, the test system considered in this thesis has voltage regulators which maintains the bus voltages more than 1.0 p.u. This suggest that the voltage deviation will be low if the load in the system is more or the load is connected to the weak buses of the system. Further, the load connected to the weak buses of the system will result in higher losses. The similar observation is made in Table 4.10. The losses are maximum for this case as well as the EVs served are more than case-1 but less than other cases implying that the load is connected to the weak buses of the system.

(iii) **Case-3:** It aims to maximize the served EV flow. This means that this case will result in maximum load demand as seen by the distribution system. This will result in increased system losses. From the Table 4.10, it is observed that maximum EV flow is served in this case. The system losses is less than case-1 and more than the other cases. Further, it is also observed that the voltage deviation is maximum amongst all the other cases. There should be reduction in voltage deviation when the additional load is more. However, the voltage deviation increases indicating that the location of FCS has caused the tap adjustment of the voltage regulators so that the bus voltages are towards higher side.

(iv) **Case-4:** This case tries to find a trade-off solution such that the power losses and voltage deviation are minimized while maximizing the served EV flow. It is observed that there is slight decrement in served EV flow and the losses and voltage deviation are slightly higher than that of Case 1 and Case 2.

The study suggests that the planning objectives effects the location and sizes of FCS consequently affecting the system performance. Case 1 and Case 2 focus on the distribution system performance resulting in minimum power loss for case 1 and less voltage deviation for case 2. However, the traffic network is ignored which results in less capture of EV flow compared to the Case 3 and Case 4. Thus, causing inconvenience to the EV drivers. Case 3 considers the traffic network and improved convenience for EV drivers is observed as the EV flow capture increases to 74.10%. The power losses and voltage deviation also increases in Case 3 affecting the distribution system performance. Case 4 takes into account both distribution system and transportation network. Case 4 does not provide the best solution for any of the objectives but gives the rational trade-off between different objectives of distribution system and transportation network. Further, 24-hour served traffic flow, active power losses and voltage profile of 123-bus distribution system for all

the cases are determined to investigate the effectiveness of the proposed multi-objective planning model as shown in Fig. (4.7-4.10).

From Fig. 4.7, it is clear that maximum EV flow is served in Case 3 and slightly less in Case 4 for 24-hours. Similar observation is made for the losses in Fig. 4.8 and 4.9, where active and reactive losses are slightly more in Case 4 compared to Case 1. Better voltage profile is obtained in Case 2 as all the buses are closer to reference voltage of 1 *p.u.* and it is slightly poor in Case 4 as compared to Case 2 as shown in Fig. 4.10. This further confirm that the proposed method provides better trade-off between different objectives of traffic network and distribution system. From Fig. 4.8, 4.9 and 4.10, it can be concluded that addition of FCS to the distribution system decreases voltage deviation in the system but increases the system losses.

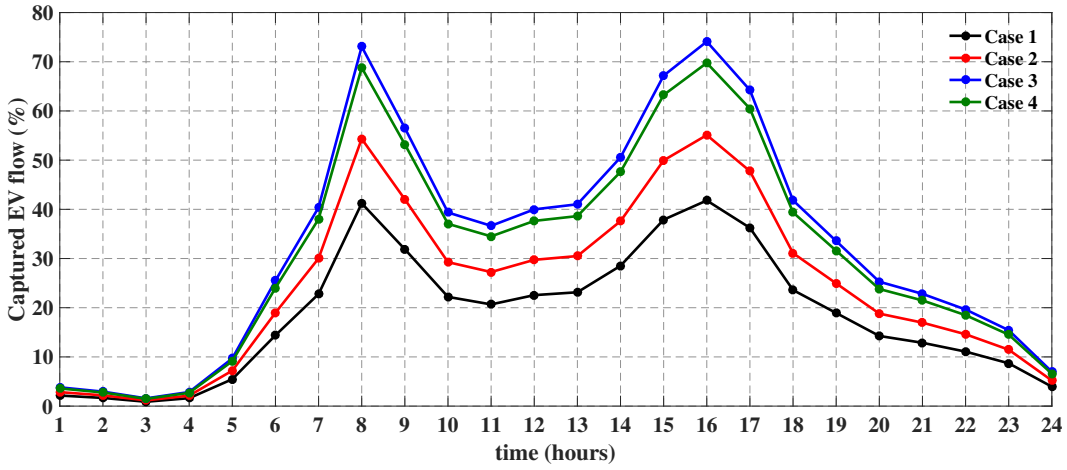

FIGURE 4.7: 24-hour served EV flow for different cases

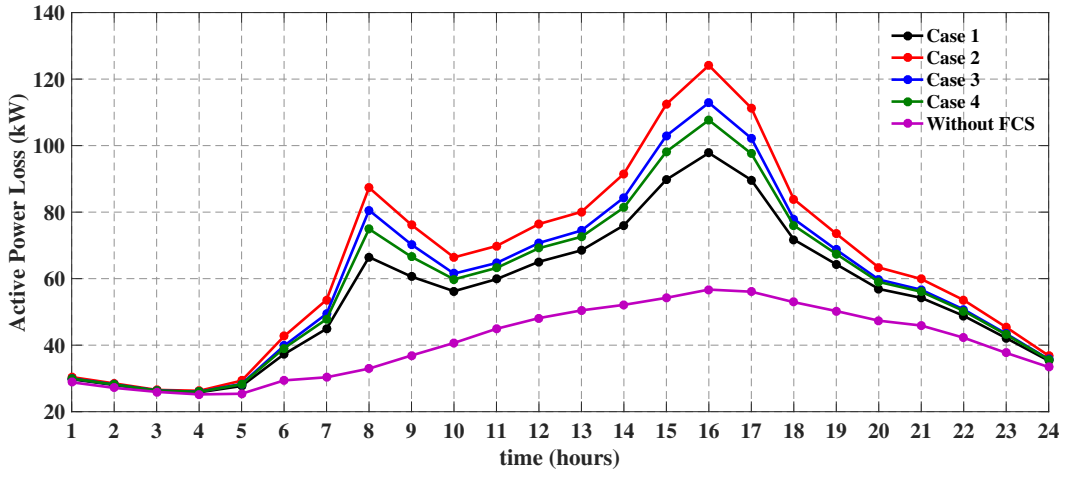

FIGURE 4.8: 24-hour active power loss for different cases

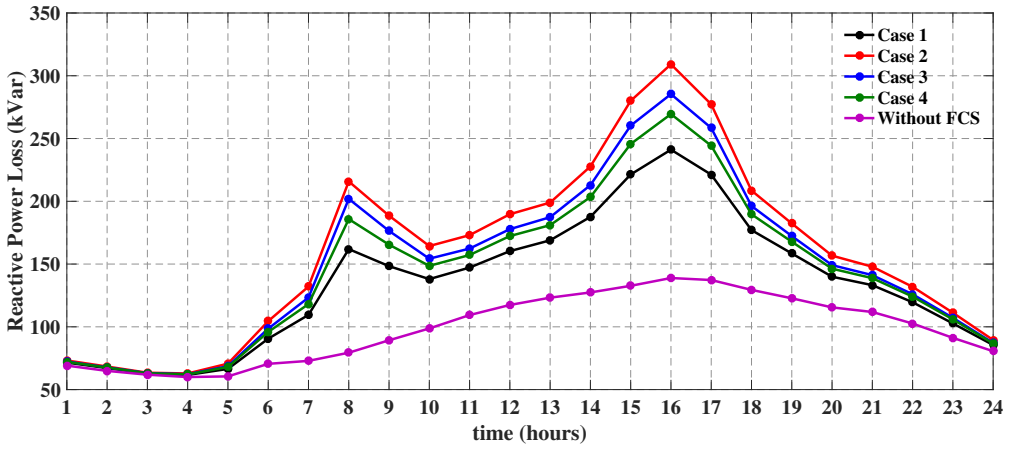

FIGURE 4.9: 24-hour reactive power loss for different cases

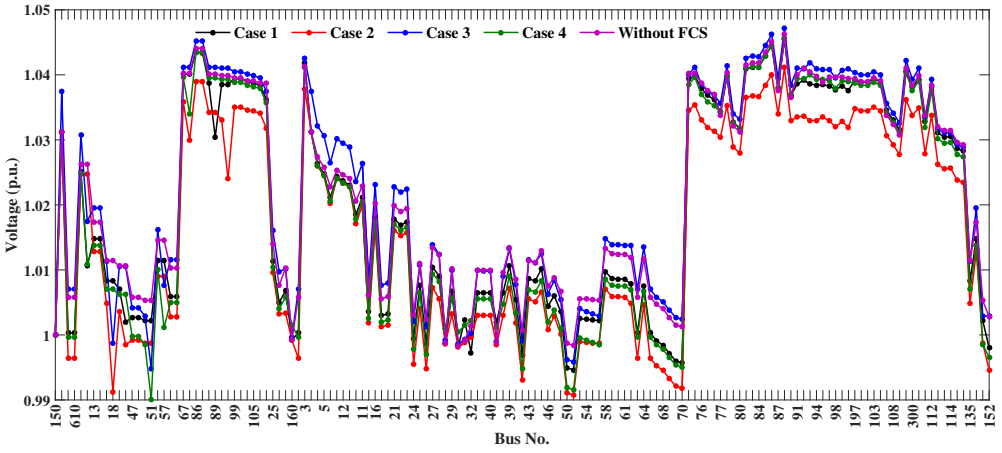

FIGURE 4.10: Voltage profile of IEEE 123-bus distribution system for different cases

4.4.4.2 Effect of Service Radius

The effect of service radius on the planning of FCS is investigated in this section. The service radius are obtained for confidence levels 80%, 85%, 90%, 95% and 99%. The planning results are given in Table 4.11 for waiting time of 5 minutes. Following observations are made:

1. It is observed that service radius decreases with increase in confidence level. It is expected that the number of FCS installed in the system should also increase with decrease in service radius in accordance with the distance between the two adjacent FCS as specified in equation (4.21). However, it is observed that the number of FCS is 5 for confidence level 80%, 85% and 90% as well as the location remains same for these confidence level. This is due to the transportation network topology which is able to satisfy the constraint (4.21) for the service radius corresponding to the confidence level of 80%, 85% and 90%. This results in same losses, voltage deviation, identical slots

and served EV flow. It is also observed that the active and reactive power losses and waiting time is highest for these confidence levels.

2. The confidence level of 95% requires 6 FCS to be installed in the system and gives maximum value of fuzzy satisfaction indicator as compared to the other cases. The active and reactive losses and the average waiting time obtained is minimum for 95% confidence level and maximum EV flow is served. However, the voltage deviation is maximum for this confidence level which suggests that the voltage profile obtained deviates from the reference voltage value. This is due to the voltage regulators present in the distribution system that adjust the system bus voltage towards the higher side.
3. The confidence level of 99% requires 7 FCS to be installed in the system and results in increased network losses and average waiting time as well as the fuzzy satisfaction indicator value decreases.

This indicates that increasing the confidence level more than 95% does not improve the system performance and requires more FCS to meet service radius constraint. Based on the obtained results, it can be said that the service radius of 5.97 miles corresponding to 95% confidence level is the better choice for the planning problem.

4.4.4.3 Effect of Waiting Time

The waiting time will effect the number of slots of FCS and may violate the distribution system operation constraint. This will result in locations of FCS to vary for different waiting time. Therefore, the effect of waiting time on planning results needs to be investigated. The different value of waiting time for sensitivity analysis considered are 1, 2, 5, 10, 15, 20 minutes. The results are obtained for 95% confidence level given in Table 4.12. Following observations are made:

1. Two coupled nodes C_9 and C_{15} are obtained in all the cases. It is found that the number of identical slots decreases with increase in waiting time. The average waiting time increases and is within the allowed waiting time for all the cases.
2. The fuzzy satisfaction indicator initially increases and then decreases after 10 minutes of waiting time.
3. Higher EV flow is served corresponding to the waiting time of 10 minutes and lower power losses are obtained for the waiting time of 2 minutes. The power loss increases with increase in waiting time except for the case 1 while voltage deviation increases with increase in waiting time. However, the voltage deviation decreases for the case 6.
4. Similar observations are made for the served EV flow which increases up to 10 minute waiting time and then decreases.

TABLE 4.11: Planning Results for Different Service Radius

Confidence Level (%)	**Service Radius (miles)**	**Location/ Charging Slots**	**Active Power Loss (MW)**	**Reactive Power Loss (MVAr)**	**Voltage Deviation (%)**	**Served EV Flow (%)**	μ_F	**Average Waiting Time (minutes)**
80	8.06	$C_3/13$, $C_7/7$, $C_9/10$, $C_{10}/10$, $C_{12}/1$	1.2591	3.1069	1.7976	65.79	0.8502	2.7461
85	7.57	$C_3/13$, $C_7/7$, $C_9/10$, $C_{10}/10$, $C_{12}/1$	1.2591	3.1069	1.7976	65.79	0.8502	2.7461
90	6.94	$C_3/13$, $C_7/7$, $C_9/10$, $C_{10}/10$, $C_{12}/1$	1.2591	3.1069	1.7976	65.79	0.8502	2.7461
95	5.97	$C_1/14$, $C_6/9$, $C_7/10$, $C_9/7$, $C_{14}/2$, $C_{15}/4$	1.1870	2.9269	1.9308	69.76	0.8591	2.1074
99	4.07	$C_3/12$, $C_7/6$, $C_9/7$, $C_{10}/1$, $C_{11}/9$, $C_{14}/2$, $C_{15}/4$	1.2335	3.0324	1.7371	57.64	0.7974	2.1700

TABLE 4.12: Planning Results for Different Waiting Time

Waiting Time (Minutes)	**Locations/ Charging Slots**	**Active Power Loss (MW)**	**Reactive Power Loss (MVAr)**	**Voltage Deviation (%)**	**Served EV Flow (%)**	μ_F	**Average Waiting Time (Minutes)**
1	$C_3/15$, $C_9/8$, $C_{10}/1$, $C_{11}/11$, $C_{14}/2$, $C_{15}/5$	1.1909	2.9273	1.7605	50.86	0.7555	0.3636
2	$C_1/15$, $C_4/7$, $C_7/11$, $C_9/8$, $C_{14}/2$, $C_{15}/4$	1.1563	2.8497	1.8909	64.33	0.8423	1.0503
5	$C_1/15$, $C_6/9$, $C_7/10$, $C_9/7$, $C_{14}/2$, $C_{15}/4$	1.1870	2.9269	1.9308	69.76	0.8591	2.1074
10	$C_1/12$, $C_3/11$, $C_7/9$, $C_9/6$, $C_{14}/1$, $C_{15}/3$	1.1890	2.9413	1.9408	72.84	0.8790	6.5373
15	$C_1/12$, $C_4/5$, $C_6/8$, $C_7/8$, $C_9/6$, $C_{15}/3$	1.1898	2.9405	1.9526	71.85	0.8706	6.6696
20	$C_3/11$, $C_7/8$, $C_9/6$, $C_{12}/8$, $C_{14}/1$, $C_{15}/3$	1.2765	3.1499	1.8070	68.43	0.8462	12.5356

From the table, a set pattern of conclusions cannot be drawn as the location and number of slots changes in order to satisfy the system operational constraints of the planning problem. However, fuzzy satisfaction-based indicator and average waiting time can be utilized to decide the allowable waiting time. It can be said that the waiting time of 5, 10 and 15 minutes are the good choice for the allowed waiting time.

TABLE 4.13: FCS Utilization and Idle Proportion of Time

Average Waiting Time (minutes)	**Maximum FCS Utilization (%)**	**Minimum FCS Utilization (%)**	**Average FCS Utilization (%)**	**Maximum FCS Idle Time (%)**	**Minimum FCS Idle Time (%)**	**Average FCS Idle Time (%)**
1	66.48	4.15	37.55	95.85	33.52	62.44
2	72.93	9.03	50.88	90.97	27.07	49.12
5	77.67	12.97	56.58	87.03	22.33	43.42
10	85.67	16.81	64.66	83.19	14.32	35.34
15	88.26	17.46	66.82	82.54	11.74	33.18
20	90.41	17.74	69.49	82.26	9.58	30.50

This is further analysed by determining the proportion of time for which the FCS is utilized and remains idle. Table 4.13 shows the maximum, minimum and average proportion of time for which FCS is utilized and maximum, minimum and average proportion of time for which FCS remains idle. The high utilization indicates better efficiency of the system, however, it also suggest that customer has to wait more if utilization is more. The probability of finding a FCS idle when customer arrives is less. Also, idle time has to be less for better efficiency of the system while it should be more for reduced waiting time. From the Table 4.13, following observations are made:

1. Maximum, minimum and average utilization increase with the increase in waiting time. The variation in FCS utilization reduces with increase in waiting time. This indicates that increasing the waiting time after some point will not greatly improve the FCS utilization.
2. Maximum, minimum and average FCS idle time reduces with increase in waiting time signifying better utilization of FCS. This will also cause more customer inconvenience as probability of finding the FCS idle reduces. The variation in FCS idle time reduces with increase in waiting time implying that the increase in waiting time will not significantly reduce the FCS idle time and it will cause more inconvenience as the average waiting time increases.

It is concluded that the allowed waiting time of more than 10 minutes does not significantly effect the utilization and idle time of FCS. Further, a knee point of average idle time is

determined to find the optimal waiting time for the considered test case as shown in Fig. 4.11. From the figure it is observed that knee point occurs at 10 minute waiting time suggesting that allowed waiting time of 10 minutes is suitable choice for the planning of FCS.

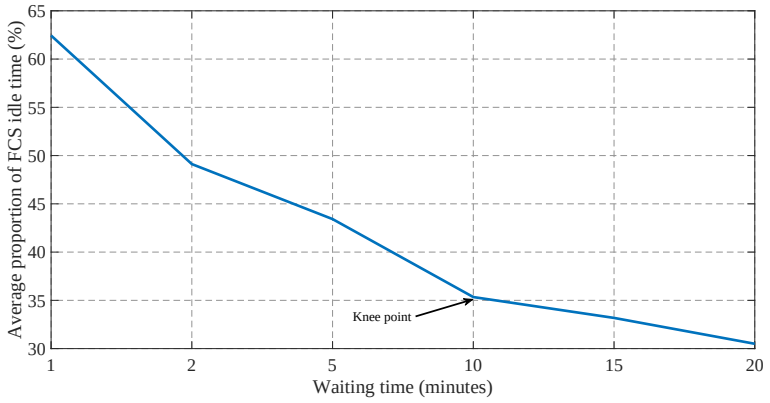

FIGURE 4.11: Knee point of average proportion FCS idle time

4.5 Summary

The adoption of EVs can be increased in the future by suitably planning the FCS in the system to meet the range anxiety of the EV customers. The planning of FCS requires determination of location and sizes of FCS where size represents the identical charging slots of each installed FCS. The charging infrastructure affects the behaviour of EV owners, distribution system and transportation network operations. Therefore, in this chapter, a multi-objective synergistic planning model is proposed for determining the location and sizes of FCS in the distribution system coupled with the transportation network. The proposed multi-objective problem is solved by MOGWO algorithm and final decision is made using fuzzy satisfaction-based method. Finally, the effectiveness of the proposed model is investigated on IEEE 123-bus distribution system coupled with 25-node transportation network. To consider FCS charging demand, more suitable exponential load model is considered for the assessment of the performance of distribution system. The main conclusions and highlights of this study are:

1. The proposed multi-objective problem attempts to minimize the power loss and voltage deviation and maximize the EV flow served by the FCS. It considers the customer convenience by reducing the waiting time at the FCS and range anxiety by introducing service radius of FCS in the proposed model. The uncertainties associated with the driving behaviour and weather conditions in estimation of service radius and waiting time is considered to represent the realistic scenario.

2. The MOGWO optimization algorithm utilized for solving multi-objective planning problem performs better than MOPSO and MOEA/D algorithms.

3. It is found that 95% of EVs can recharge with remaining battery SOC when service radius of FCS is 5.97 miles. The selected planning scheme results in 69.76% of served EV flow but also causes 1.1870 MWh power losses and 1.9308% voltage deviation. The obtained values of system losses and voltage deviation are not the minimum values signifying that the planning scheme is not able to provide optimal values of different objectives considered. Thus, it can be inferred that the multi-objective problems does not give optimal solution with respect to each objective but gives trade-off solution.

4. It is observed that different objectives affects the planning of FCS. Considering one network affects the performance of other suggesting importance of considering both distribution system and transportation network in the problem formulation of planning of FCS.

5. The confidence level will effect the service radius of FCS, thereby, affecting the planning of FCS. The service radius also decides the number of FCS to be located in the system. It is found that 95% confidence level is suitable choice for the planning of FCS.

6. Waiting time effects the number of identical charging slots, further, varying the location of FCS. It is found that value of fuzzy satisfaction-based indicator increases and then decreases after waiting time of 10 minutes. Higher utilization of FCS and lower idle time of FCS is achieved by increasing the waiting time. However, the variation is low and customer convenience decreases with increased waiting time. It is inferred that waiting time of 10 minutes is good choice for the planning of FCS as beyond this value, the utilization of FCS does not increase much while simultaneously causes more inconvenience to the customers.

7. The presented approach provides decision maker an opportunity to make a proper trade-off between the power losses, voltage deviation and the served EV flow. The proposed method also suggest the way to select proper service radius and waiting time.

Chapter 5

Distribution System Performance Analysis with FCS and Wind Generation

5.1 Introduction

Rapid depletion of fossil fuels, environmental concerns, volatility in fuel prices and advancement in the battery technologies led to fast growth of Electric Vehicles (EVs) and proper planning of charging infrastructure will favour the adoption of EVs in the system. It is expected that the penetration of level III infrastructure known as Fast Charging Station (FCS) will increase in the future [95]. With increased penetration of FCS, high demand level is expected that may overload the distribution system equipment and can cause low voltages in the system. Therefore, impact analysis of FCS on the performance of distribution system becomes important to assist the distribution planners in decision making incase of any system violations. Further, the introduction of renewable generation at the local end can reduces the stress on the centralized generation and charging with renewable can further reduce the green house gas emissions related to the transportation sector. Currently, wind generation is the fastest growing clean source of renewable energy [48]. Despite its numerous economic and environmental benefits, its intermittent nature introduces technical challenges. The amount of wind power a distribution system can absorb compared to the power supplied by the distribution system known as wind penetration will depend on the intermittency associated with it [149].

Various studies have been conducted to study the impact of EV charging on the load profile of the power system [11–13, 104–108, 110–112], overloading of system components [7–11], voltage profile [6,17,36,46,53,113], phase unbalance [114,115] and system losses [11,13,116, 117]. Further, the integration of wind generation in the distribution system can diminish the negative impact of FCS but it can also cause reverse power flow and voltage rise problem. Many studies have studied the interaction between the EVs and the renewables in smart grid environment [119–121]. This requires intelligent charging techniques by effectively utilizing two-way communication. However, the intelligent charging technology is not mature enough and consumers are preferring convenient way of charging. Very few studies have attempted to analyse the impact of EV charging and renewable simultaneously [48, 126–129].

Literature survey shows that installation of FCS will add an extra demand on the existing distribution system, thus causing change in load profile, increase in peak load demand, increased voltage deviation and unbalance, overloading of the system components and increased system losses. It is concluded from the literature that the probabilistic approaches incorporating uncertainties associated with the driving patterns needs to be considered for the assessment of performance of distribution system in presence of FCS. The impact analysis is mostly done for the slow charging EVs while very few authors have attempted to analyse the impact of fast charging EVs on the distribution system performance. Integration of renewable in the distribution system may lessen the negative impacts of FCS but it may also cause reverse power flow and voltage rise problem. It is mentioned in the literature that wind will be used in conjunction with FCS in the future. However, the uncertainty associated with the wind speed further complicates the impact assessment of wind generation on the performance of distribution system. Most of the literature has considered Constant Power Load (CPL) model in the power flow analysis but it is proved in Chapter 3 that exponential load model is better load model of FCS compared to the CPL model. Therefore, in this chapter, impact of FCS and wind generation on the distribution system performance are analysed individually and simultaneously by evaluating performance indices. Exponential load model is considered in this study to avoid the misrepresentation of performance parameters of distribution system. The objectives of this chapter are:

1. To develop Weibull Probability Distribution Function (PDF) for the wind speed and estimate the parameters of wind speed PDF using maximum likelihood estimator.
2. To estimate daily expected wind power output incorporating uncertainties associated with wind speed for different scenarios .
3. To propose performance indicators for impact analysis of FCS and wind generation on distribution system performance.
4. To integrate the spatial-temporal FCS charging demand with exponential load model for power flow analysis developed in Chapter 3 and expected wind power output in IEEE 123-bus distribution system.
5. To investigate the performance of IEEE 123-bus distribution system with FCS and wind generation using proposed performance indicators for different cases.
6. To perform synergy analysis to study the interaction between FCS and wind generation.

5.2 Output Power Model of Wind Generation

The kinetic energy of the wind is converted into mechanical energy that changes wind force into a torque acting on the rotor blades. The power generated by the wind will depend on

the volume of the air, speed of air and mass of the air. The power that can be extracted from wind is proportional to the cube of wind speed [150] given by equation (5.1).

$$P_{wind} \propto v^3 \tag{5.1}$$

where, v is the average wind velocity. From equation (5.1), it can be inferred that a small variation in wind speed will create a large variation in power produced. Therefore, it is important to have information about the wind speed to estimate the power output of the wind for its impact analysis on the distribution system performance. The wind speed is erratic in nature. Thus, it becomes important to develop the wind speed models from the available wind speed data. The distribution of wind speed is often represented by the Weibull Probability Distribution Function (PDF) [149]. In this study, the PDF of wind speed data is developed separately for each hour. At t^{th} hour, it is given by [150]:

$$f_t(v) = \left(\frac{l_t}{c_t}\right)\left(\frac{v_t}{c_t}\right)^{l_t-1} e^{-\left(\frac{v_t}{c_t}\right)^{l_t}} \tag{5.2}$$

where, v_t is the average wind speed in (m/s) at t^{th} hour, l_t and c_t are the Weibull shape and scale parameters respectively at t^{th} hour. The shape parameter will affect the shape of the distribution function and scale parameters affects the spread of the distribution function. The Weibull scale and shape parameters are estimated by maximum likelihood estimator. The shape parameter can be estimated by solving equation (5.3) numerically.

$$0 = \sum_{i=1}^{n} \frac{(v_{i,t})^{l_t} \ln(v_{i,t})}{v_{i,t}} - \frac{1}{l_t} - \frac{1}{n}\sum_{i=1}^{n} \ln(v_{i,t}) \tag{5.3}$$

Then the value of c_t is given by equation (5.4):

$$c_t = \frac{\bar{v_t}}{\Gamma\left(1 + \frac{1}{l_t}\right)} \tag{5.4}$$

where, $\bar{v_t}$ is the mean of wind speed at t^{th} hour and Γ is the gamma function. This results in continuous PDF for each hour. To integrate the wind generation in the distribution system, the continuous PDF of wind speed is divided into m states. The wind speed in each state is bounded by the upper and lower limits. The number of states m is chosen such that it is neither small nor large. Discrete function with small number of states will lose information about the continuous distribution function and large number of states will increase the problem complexity. In this work, the step is adjusted to 1 m/s as shown in Table 5.1.

TABLE 5.1: Wind Speed States

Weibull state (m)	**Wind speed limits** (m/s)
1	0-1
2	1-2
⋮	⋮
Last state	v_{max-1} to v_{max}

The probability of wind speed being in State (S) m at t^{th} hour is calculated using equation (5.5) for wind speed limits v_{m1} and v_{m2} of state m:

$$P\left(S_m^t\right) = \int_{v_{m1}}^{v_{m2}} f_t(v)dv \tag{5.5}$$

The power curve of wind turbine is used to calculate the power output of the wind with respect to the wind speed. The power available in the wind cannot be fully utilized by the wind turbine for the generation of electricity. To consider this physical characteristic, a power index coefficient C_p is introduced. It is defined as the fraction of the available wind power that can be extracted by the rotor blades. According to [151], the power curve regions can be described as follows:

- Optimum constant C_p region, where power increases with increasing wind speed
- Limited power region, generating a constant power, even during the high wind speed
- Region of power shutdown, where power generation is decelerated to zero when wind speed approaches the cut-out limit.

This is well described by equation (5.6). It is used to determine the output power of wind corresponding to each state m.

$$P_m^w(v) = \begin{Bmatrix} 0 & if & 0 \le v_{am} \le v_{ci} \\ P_{rated} \times \left(\frac{v_{am}-v_{ci}}{v_r-v_{ci}}\right) & if & v_{ci} < v_{am} \le v_r \\ P_{rated} & if & v_r < v_{am} \le v_{co} \\ 0 & if & v_{co} < v_{am} \end{Bmatrix} \tag{5.6}$$

where, v_{am} is the average wind speed of state m, v_{ci} , v_r and v_{co} are the cut–in, rated and cut–off speed of wind turbine. To incorporate the wind generation in the distribution system, expected power output is calculated for t^{th} hour given by:

$$P_{exp,t}^w = \sum_m P_m^w(v) \times P\left(S_m^t\right) \tag{5.7}$$

The flowchart for estimation of expected power output is shown in Fig. 5.1.

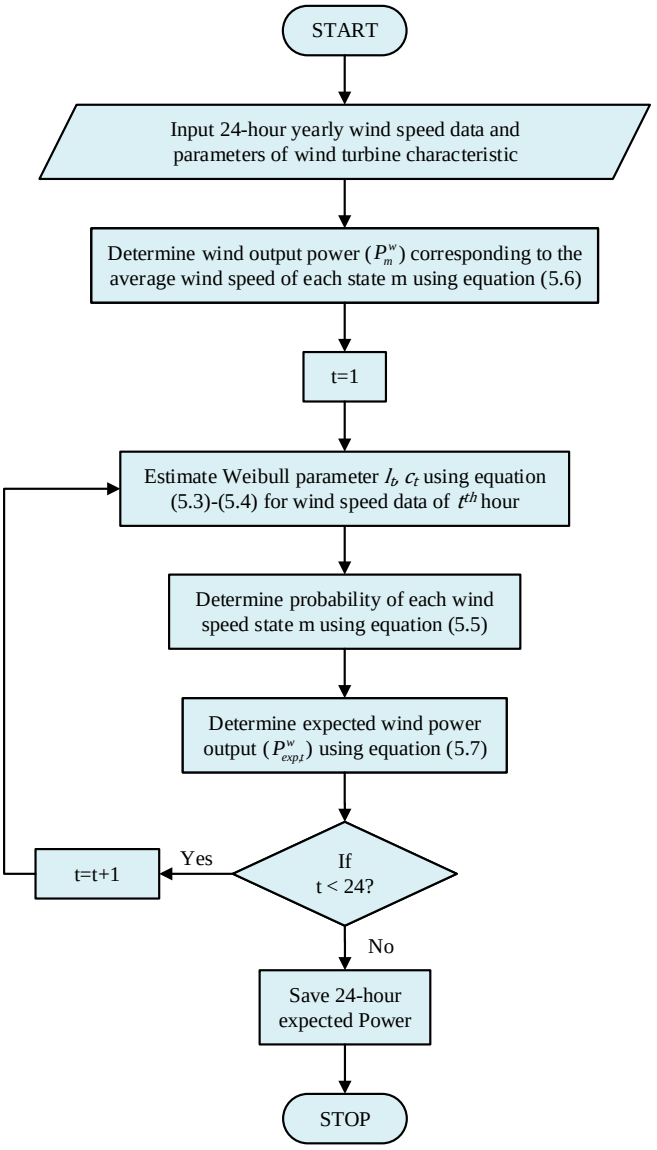

FIGURE 5.1: Flowchart for the expected output power of wind generation

5.3 Proposed Performance Indices

In order to serve the FCS charging demand, additional power will be drawn from the distribution system. This may negatively impact the distribution system performance. The voltage profile and system power losses are the important operational parameters of the distribution network. However, the additional load may also result in phase unbalancing and overloading of the distribution system components like distribution lines and

transformers. The introduction of intermittent wind generation in the distribution system to further reduce the CO_2 emissions can have both positive and negative impact on the performance of distribution system. Therefore, in this chapter, several indices are computed to describe the impact of FCS charging demand and wind generation on the distribution system performance. Synergy between FCS charging demand and wind generation is also studied in this chapter.

5.3.1 Load Profile

The load profile of the distribution system changes due to the additional FCS charging demand. The intelligent charging technology is still in its early stage, thus, it is expected that the convenient charging will take place mostly. The additional load may increase the peak of the load profile and/or can shift the peak demand loading. Aggregated EV Charging Profile (AECP) developed in the Section 3.3 is used to investigate the effect of EV fast charging on the load profile of the distribution system which has both spatial and temporal characteristics. The 24-hour load profile of the distribution system is given by:

$$P_{D_t} = \left(\sum_{k=1}^{K} E\left[P_{FCS_t^k} \right] + \sum_{i=1}^{N_B} P_{D0_{i,t}} \right) \tag{5.8}$$

where, P_{D_t} is total active load of the system, $P^w_{exp,t}$ is the total wind power generation determined using equation (5.7) and $E\left[P_{FCS_t^k}\right]$ is the total expected FCS charging demand determined using equation (3.54) at time t and K is the total number FCS present in the distribution system.

5.3.2 Line Congestion

As a consequence of additional FCS charging load demand, the current flows may increase in the distribution lines and might congest some lines of the distribution system. However, the incorporation of wind generation in the distribution system may decrease the current flows in some section as it supplies power near to the loads. To quantify the line congestion due to FCS and wind generation, line congestion indices are introduced. Line congestion indices are calculated based on the maximum current carrying capacity of the conductors. It provides important information about the level of currents through the network regarding

the maximum capacity of conductors.

$$CI_{avg} = \frac{1}{T * N_L} \left(\sum_{t=1}^{T} \sum_{l=1}^{N_L} \frac{|I_{ij,t}|}{I_{ij}^{max}} \right) \tag{5.9}$$

$$CI_{max} = Max \left(\frac{|I_{ij,t}|}{I_{ij}^{max}} \right) \quad \begin{matrix} for\ t = 1 \sim T \\ ij = 1 \sim N_L \end{matrix} \tag{5.10}$$

where, CI_{avg} and CI_{max} are the average and maximum congestion indices of all the lines, $I_{ij,t}$ and I_{ij}^{max} are the current of line ij at time t and current rating of line ij, T is the number of time intervals and N_L is the number of branches in distribution system. The value of CI_{max} less than one indicates that none of the branches are overloaded and the value of CI_{avg} closer to zero indicates that the system can take up additional load and it has loading capacity available.

5.3.3 Voltage Deviation and Unbalance

Additional load due to EV fast charging will cause more voltage drop in the system. This results in bus voltage of the distribution system to decrease. However, the integration of wind generation in the system will cause bus voltage to rise. This imply that FCS and wind generation can either improve or worsen the voltage profile of the system. The voltage profile is said to be better if the bus voltages of the system are closer to reference voltage. This is quantified by determining voltage deviation index given by

$$VDI_{avg} = \frac{1}{T * N_B} \left(\sum_{t=1}^{T} \sum_{i=1}^{N_B} \left| \frac{V_0 - V_{i,t}}{V_0} \right| \right) \tag{5.11a}$$

$$VDI_{max} = Max \left(\left| \frac{V_0 - V_{i,t}}{V_0} \right| \right) \quad \begin{matrix} for\ t = 1 \sim T \\ i = 1 \sim N_B \end{matrix} \tag{5.11b}$$

where, VDI_{avg} and VDI_{max} are the average and maximum voltage deviation indices, $V_{i,t}$ and V_0 are the bus voltage and reference voltage of i^{th} bus at time t and N_B is the number of buses of the distribution system. VDI_{avg} and VDI_{max} closer to one indicates better voltage profile of the system. Further, the voltage unbalance may occur due to the connection of single phase loads. It can cause overheating of electrical components and can lead to higher currents in the neutral. Voltage unbalance in a three-phase system is defined as the ratio of the maximum deviation of rms voltage from the average rms voltage to the average rms voltage. It is expressed in percent as given in equation (5.12) using

phase to phase measurements [152].

$$VU_{L-N}^{avg} = \frac{1}{T}\sum_{t=1}^{T}\frac{max\left(V_{t,\phi-N} - V_{t,L-N}^{avg}\right)}{V_{t,L-N}^{avg}} \times 100\ \%\ \phi \in A,B,C \tag{5.12a}$$

$$VU_{L-N}^{max} = Max\left(\frac{max\left(V_{t,\phi-N} - V_{t,L-N}^{avg}\right)}{V_{t,L-N}^{avg}}\right) \times 100\ \%\ for\ t = 1 \sim T \tag{5.12b}$$

where,

$$V_{t,L-N}^{avg} = \frac{|V_{A-N}| + |V_{B-N}| + |V_{C-N}|}{3}$$

where, VU_{L-N}^{avg} and VU_{L-N}^{max} are the average and maximum voltage unbalance, $V_{t,\phi-N}$ is the phase to neutral voltage at time t. It is recommended that voltage unbalance should not exceed 3% [152].

5.3.4 Power Losses

The addition of new FCS charging load demand requires more power transmission causing more power losses in the distribution system while the integration of wind generation may result in reduction in power losses. However, the excess power from wind generation can cause reverse power flows resulting in higher losses. Active and reactive power losses indices given by equation (5.13) and (5.14) can provide the information about the positive and negative impacts of FCS and wind generation on the performance of distribution system regarding system losses.

$$PL_{avg} = \frac{1}{T}\sum_{t=1}^{T}\frac{\Re(losses_t)}{\Re(losses_t^0)} \tag{5.13a}$$

$$PL_{max} = Max\left(\frac{\Re(losses_t)}{\Re(losses_t^0)}\right) \qquad for\ t = 1 \sim T \tag{5.13b}$$

$$QL_{avg} = \frac{1}{T}\sum_{t=1}^{T}\frac{\Im(losses_t)}{\Im(losses_t^0)} \tag{5.14a}$$

$$QL_{max} = Max\left(\frac{\Im(losses_t)}{\Im(losses_t^0)}\right) \qquad for\ t = 1 \sim T \tag{5.14b}$$

where, PL_{avg} and PL_{max} are the average and maximum active loss indices, QL_{avg} and QL_{max} are the average and maximum reactive loss indices, $losses_t$ is the complex power losses with FCS and wind generation, $losses_t^0$ is the total power loss without FCS and wind generation at time t, $\Re(.)$ and $\Im(.)$ are the real and imaginary parts of complex term. The value of PL_{avg}, PL_{max}, QL_{avg} and QL_{max} less than one signify that there is reduction

in losses and more than one signify that there is increment in losses when FCS and wind generation are present in the distribution system.

5.3.5 Synergy Analysis

Wind generation is integrated in the distribution system so as to serve the EV fast charging load. However, intermittency associated with the wind generation does not provide power to the FCS at all times. Further, the power generation from the wind generation may not even satisfy the traditional load demand at some time while may exceed the total load demand of the system. Synergy analysis between FCS charging demand and wind generation is done by carrying out following analysis:

5.3.5.1 Excess Wind Power Generation

The amount of active and reactive power of wind generation exceeding the total FCS charging demand is termed as excess wind power generation. It is given by:

$$EPG_t^w = P_{exp,t}^w - \sum_{k=1}^{K} E\left[P_{FCS_t^k}\right] \tag{5.15}$$

where, EPG_t^W is the excess active wind power generation. Here, excess reactive wind power generation is not calculated as it is assumed that the EVs will draw negligible reactive power as compared to the active power.

5.3.5.2 Assessment of Reverse Power Flow

Reverse power will occur when the power generated by the wind generation exceeds the total load demand of the system. In this case, the power flows back to the substation. Reverse power flow can cause the current in the distribution lines to increase. This will result in increased system losses. This is given by:

$$RP_t = max\left(0, P_{exp,t}^w - \left(\sum_{k=1}^{K} E\left[P_{FCS_t^k}\right] + \sum_{i=1}^{N_B} P_{D0_{i,t}}\right)\right) \tag{5.16}$$

where, $P_{D0_{i,t}}$ is the active power demand of bus i at time t

5.4 Numerical Results and Discussions

The impact of uncontrolled EV charging at FCS on the distribution system with and without wind generation is investigated on IEEE 123-bus distribution system [139]. The system has 85 spot load and 118 distribution lines. The peak load and power factor of

the system is 3855.257 kVA and 0.9391 respectively. The standard system is modified to integrate the residential houses, distribution transformers, FCS and wind generation. The modification of standard distribution system is explained in detail in Section 3.4.3. The location and size of installed FCS is considered same as obtained in Chapter 4. The feeder length of the system is small, therefore, it is assumed that the wind generation can be installed at any location as well as the wind speed profile remains same throughout the area. The number and location of wind generation are set according to Ref. [48]. The study also investigates the synergy between the FCS and wind generation.

5.4.1 Output Power of Wind Generation

Total wind power output in the system will depend on the number of wind generation installed in the distribution system and wind speed. It is already stated that the feeder length of distribution system is small, therefore, the location of wind generation will not significantly affect the output power of the wind. The location of wind generation are set according to Ref. [48]. Four scenarios are considered to estimate the expected wind power output given as:

(i) **Scenario 1:** 1 Wind generator installed at bus 42

(ii) **Scenario 2:** 2 Wind generator installed at bus 42 and 57

(iii) **Scenario 3:** 3 Wind generator installed at bus 42, 57 and 60

(iv) **Scenario 4:** 4 Wind generator installed at bus 42, 57, 60 and 97

The estimation of wind speed is required to model the power output of wind generation. One-year hourly wind speed data of Phoenix is extracted for the year 2014 [153]. Phoenix is the capital city of Arizona State U.S., located at 112°4′26″W longitude and 33°26′54″N latitude. The resulting data set consists of 365 day × 24 hour records. The wind speed is shown in Fig. 5.2. From the figure, it is observed that wind speed is highly erratic in nature and does not follow any set pattern. Thus, the estimation of wind speed becomes difficult.

To estimate the wind speed, Probability Distribution Function (PDF) is developed for each hour. Weibull distribution function is used to represent the frequency of occurrence of wind speeds for each hour. It requires estimating two parameters of Weibull distribution function namely: shape and scale parameters. For this, Weibull distribution function is fitted on the past record of wind speed data and shape and scale parameter values are estimated using maximum likelihood estimator for each hour given in Table 5.2.

From the table, it is observed that scale parameter ranges from 5.0155–5.9669 and shape parameter ranges from 2.1051–2.6542. Small variation in shape and scale parameters is

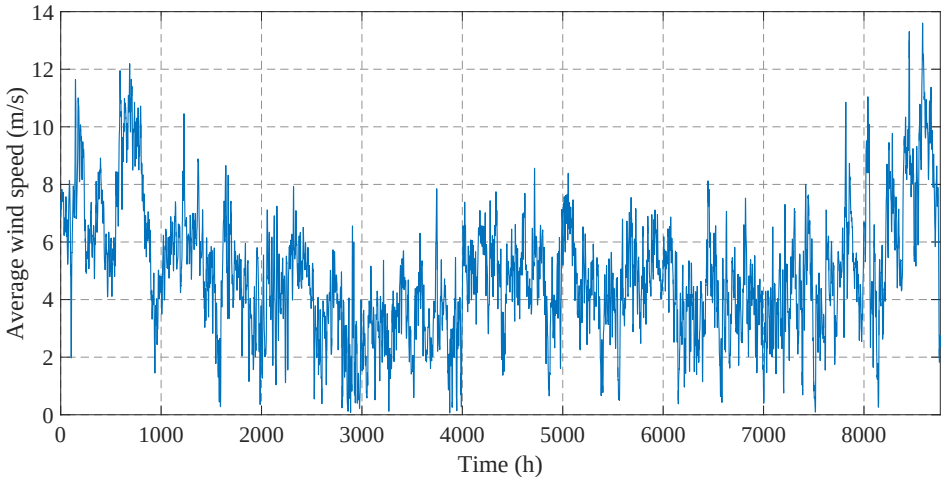

FIGURE 5.2: Average wind speed averaged (hourly)

observed for different hours. Maximum value of shape and scale parameter are observed for 15^{th} hour. The large scale parameter suggest that the distribution function is more stretched out to the right and peak is low compared to the other obtained Weibull distribution for different hours. The mean of the wind speed is maximum during this hour. Minimum value of scale parameter is observed for 9^{th} hour as well as mean of the wind speed data is minimum for this hour. Weibull distribution fitted on wind speed data for different hours is shown in Fig. 5.3.

Once the PDF for each hour is developed, then 24-hour expected power for different penetration of wind generation is determined using equation (5.6) and (5.7). Equation (5.6) gives power output for a given wind speed. It depends on the type of generator used. For the sake of simplicity, only one type of wind turbine is assumed for the study. The simulation parameters of wind turbine [154] is given in Table 5.3.

The expected wind power output for different scenarios is shown in Fig. 5.4. From the figure, it is observed that variation in 24-hour wind power increases with increase in number of wind generations integrated in the distribution system. It is also observed that wind power output is maximum during 15^{th} hour of the day and minimum during 9^{th} hour of the day. Further, it is also noted that the variation in daily expected power output of the wind increases with increase in wind generation.

TABLE 5.2: Shape and Scale Parameters of Weibull Distribution Function

Hour	**Scale Parameter** (c_t)	**Shape Parameter** (l_t)
1	5.4576	2.4013
2	5.4977	2.3621
3	5.5474	2.3057
4	5.5113	2.2472
5	5.4099	2.1983
6	5.2696	2.1261
7	5.1486	2.1051
8	5.0570	2.1234
9	5.0155	2.1424
10	5.1097	2.1997
11	5.3078	2.3001
12	5.5420	2.4455
13	5.7244	2.5492
14	5.8642	2.6163
15	5.9669	2.6542
16	5.9018	2.6359
17	5.7320	2.5657
18	5.5859	2.4987
19	5.4783	2.4691
20	5.4040	2.4640
21	5.3615	2.4710
22	5.3834	2.4635
23	5.4404	2.4497
24	5.4800	2.4318

TABLE 5.3: Characteristics of Wind Turbine

Features	**Values**
Rated Power (kW)	250
Cut-in speed (m/s)	3
Rated speed (m/s)	7
Cut-out speed (m/s)	11

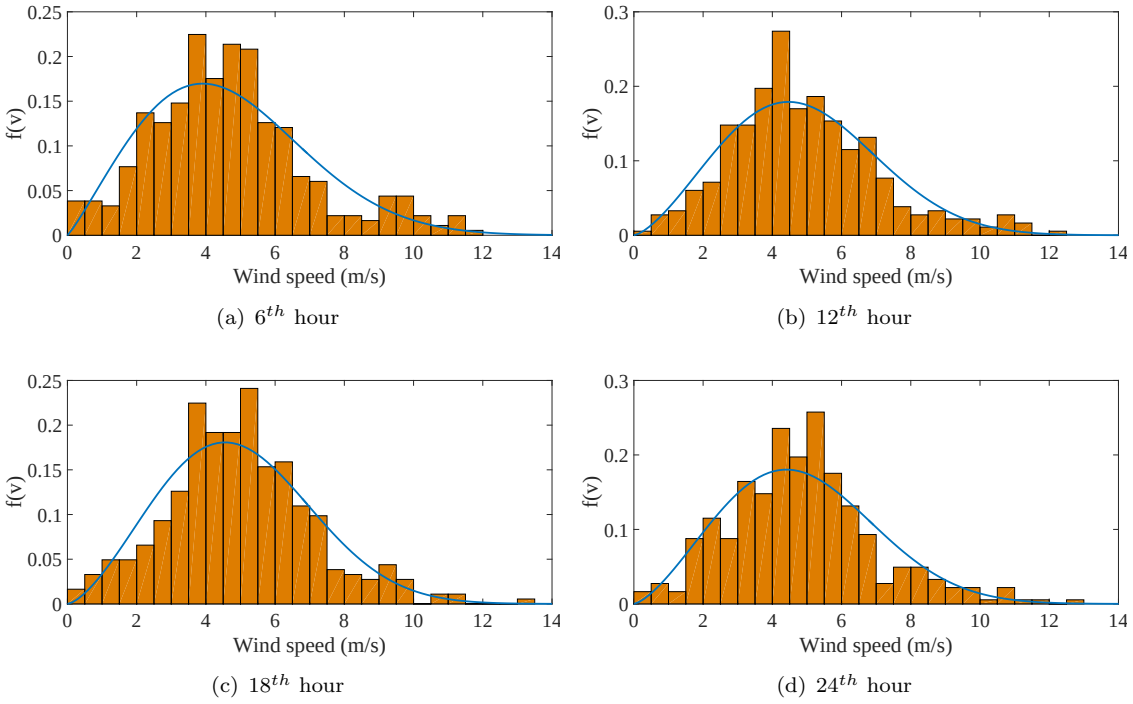

(a) 6^{th} hour (b) 12^{th} hour

(c) 18^{th} hour (d) 24^{th} hour

FIGURE 5.3: *PDF* of wind speed for different hour

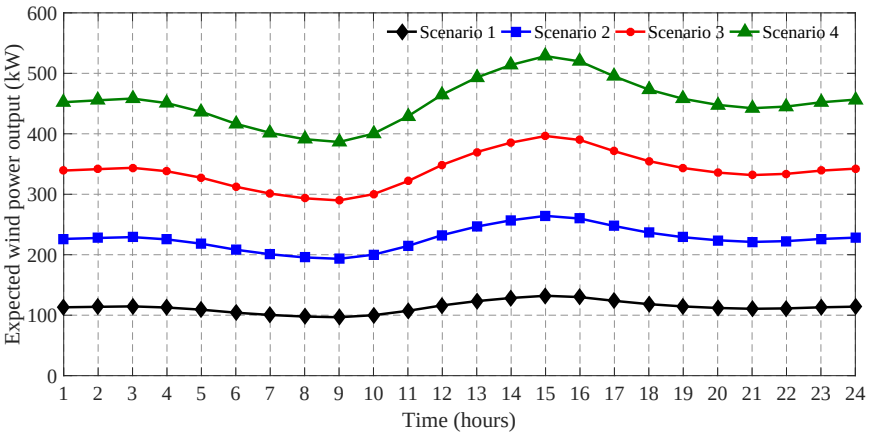

FIGURE 5.4: Daily expected wind power output

5.4.2 Performance Investigation of Distribution System with FCS and Wind Generation

In Chapter 4, it is suggested that the waiting time of 10 minutes and service radius corresponding to 95% confidence level are the suitable choice for the planning of FCS. Hence, the location and sizes corresponding to these parameters are used in this chapter to investigate the performance of distribution system with FCS.

5.4.2.1 Impact on Load Profile

The spatial-temporal charging demand of FCS represented by exponential load model in power flow analysis developed in Chapter 3 corresponding to the location and sizes obtained in Chapter 4 are utilized to develop the new load profile of the distribution system. The load profile of FCS is developed for 20%–100% penetration level of EVs in step of 20% as shown in Fig. 5.5.

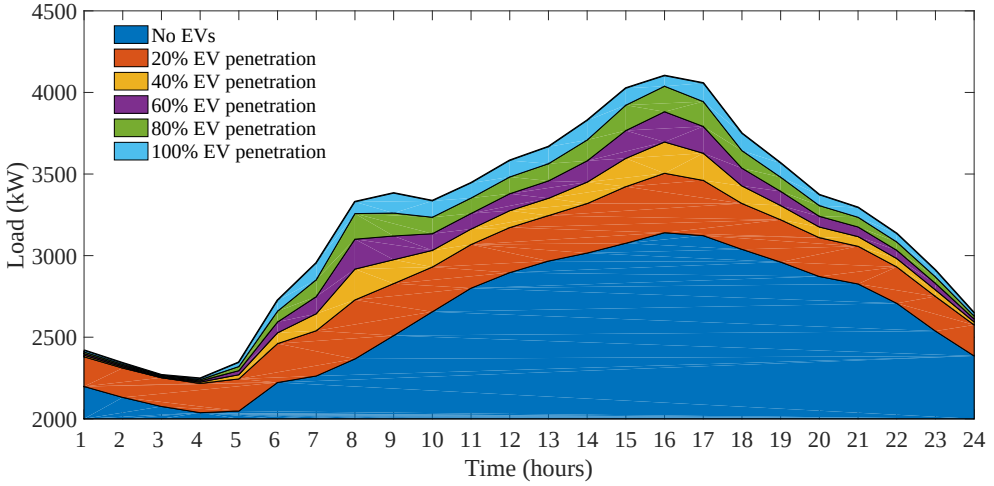

FIGURE 5.5: 24-hour load profile of distribution system for different EV penetration level

From the Fig. 5.5, it is observed that the peak of the load profile increases with the EV penetration level and occurs at 16^{th} hour of the day. However, there is no shift in peak of the load profile. This is expected as the peak of the load profile with no EVs and the vehicle distribution on the road coincides. It is also observed that the change in load demand due to FCS with increase in EV penetration level decreases. This is anticipated as the FCS is not able to serve all the EVs at higher penetration level. The variation in load demand for different EV penetration level is not noticeable from 23:00-05:00 as the distribution of vehicles on the road during this time is low. Further, the impact of fast charging EVs on the load profile of distribution system is analysed in terms of peak load and Peak to Average Ratio (PAR) given in Table 5.4. PAR value should be closer to one. Higher PAR requires substantial cost increment for utilities in long-term since it requires new investment in generation and transmission capacities to serve higher peak load. Table 5.4 demonstrates that growing EV penetration level leads to a significant increment in peak load .

The increment in peak load demand is more than the increment in average load demand causing increment in PAR more. However, decrease in PAR value for 100% EV penetration

TABLE 5.4: Peak load and PAR for different EV penetration level

	No EVs	**20% EV**	**40% EV**	**60% EV**	**80% EV**	**100% EV**
Peak Load (kW)	3140.2	3504.5	3696.3	3881.7	4038.0	4102.2
PAR	1.1991	1.2182	1.2476	1.2736	1.2906	1.2832

level is observed compared to the 80% EV penetration level as the change in peak demand is less than the change in average value.

5.4.2.2 Performance Indices

The performance of distribution system is investigated in presence of FCS and wind generation. The EV penetration level is varied from 0 to 100% in steps of 20%. Four wind generation are integrated in the distribution systems and five cases are considered to study the impact of FCS and wind generation given as:

(i) **Case–1:** No Wind generator installed

(ii) **Case–2:** One Wind generator installed at bus 42

(iii) **Case–3:** Two Wind generator installed at bus 42 and 57

(iv) **Case–4:** Three Wind generator installed at bus 42, 57 and 60

(v) **Case–5:** Four Wind generator installed at bus 42, 57, 60 and 97

- **Case–1: No wind generator**

In this case, no wind generation is installed in the distribution system and performance of distribution system is investigated only in the presence of FCS. Performance indices related to the conductor capacities, voltage drop and unbalance and system losses are given in Table 5.5 to investigate the performance of distribution system in presence of FCS and wind generation. From the Table 5.5, following observations are made:

1. The values of CI_{avg} and CI_{max} increases with increase in EV penetration level implying that power flow increases in the conductor and reserve capacity of conductor decreases. The value of IC_{max} is 0.9642 which is very close to 1, signifying that the conductors are very close to being overloaded. However, none of the branches are overloaded.
2. The values of VDI_{avg} and VDI_{max} decreases with increase in EV penetration level suggesting that the system voltage profile improves with the EV penetration level. As mentioned in Chapter 3, bus voltages of the considered test system are towards the higher side and additional load due to FCS will cause more voltage drop. Thus, bringing the bus voltages closer to the reference voltage 1.0 p.u. and improving the voltage profile of the system.

TABLE 5.5: Performance Indices for IEEE 123-Bus Distribution System for Case–1

Penetration → **Level (%)** **Indices ↓**	**0**	**20**	**40**	**60**	**80**	**100**
CI_{avg}	0.1101	0.1151	0.1171	0.1190	0.1209	0.1225
CI_{max}	0.6833	0.7591	0.8235	0.8870	0.9414	0.9642
VDI_{avg}	1.6325	1.5388	1.5053	1.4725	1.4416	1.4160
VDI_{max}	4.4900	4.2200	4.1600	4.1000	4.0400	3.9800
VU_{L-N}^{avg}	0.8144	0.8380	0.8472	0.8563	0.8651	0.8731
VU_{L-N}^{max}	0.9895	1.0111	1.0176	1.0253	1.0349	1.0467
PL_{avg}	1.0000	1.1695	1.2405	1.3178	1.3976	1.4680
PL_{max}	1.0000	1.2867	1.4888	1.7159	1.9355	2.0443
QL_{avg}	1.0000	1.1809	1.2547	1.3344	1.4162	1.4883
QL_{max}	1.0000	1.3049	1.5146	1.7480	1.9719	2.0822

3. The value of VU_{L-N}^{avg} and $VU_{L_N}^{max}$ increases with increase in EV penetration level implying that voltage unbalancing increases. However, the voltage unbalancing is within the permissible limit of 3% even for 100% EV penetration level. As FCS is a three-phase load, therefore, EV fast charging has negligible impact on the phase unbalancing of the system.
4. PL_{avg}, PL_{max}, QL_{avg} and QL_{max} provides similar results and value more than 1 implies that both active and reactive losses increases with increase in EV penetration level.

- **Case–2: One Wind generator installed at bus 42**

In this case, single wind generator of 250 kW rated capacity is installed at bus 42. The performance indices for this case are given in Table 5.6 and following observations are made:

1. The values of CI_{avg} and CI_{max} increases with increase in EV penetration level implying that power flow increases in the conductor and reserve capacity of conductor decreases. The value of CI_{max} is 0.9640 which is very close to 1, signifying that the conductors are very close to being overloaded. However, none of the branches are overloaded. The value of CI_{avg} and CI_{max} are less for all EV penetration level compared to the case when no wind generation are present. This imply that with the addition of wind generation, the power flow in the branches decreases, thus, increasing available loading capacity of conductor.

2. The values of VDI_{avg} and VDI_{max} decreases with increase in EV penetration level suggesting that the system voltage profile improves with the EV penetration level. However, voltage deviation is more compared to the case–1. This indicate that the addition of wind generator has caused smaller voltage drops and thus, worsening the voltage profile of the distribution system.
3. The value of VU_{L-N}^{avg} and $VU_{L_N}^{max}$ increases with increase in EV penetration level implying that voltage unbalance increases. It is also observed that there is less voltage unbalance compared to the case–1. However, significant improvements are not observed and hence, it can be said that the integration of FCS and wind generation plays negligible role in voltage unbalancing of the system.
4. PL_{avg}, PL_{max}, QL_{avg} and QL_{max} provides similar results and value more than 1 implies that both active and reactive losses increases with increase in EV penetration level. But the values of performance indices are less than one when there are no EVs present in the system. This indicate that the system losses has decreased for 0% EV penetration level. For higher EV penetration level, even though the system losses increases, the value of power loss indices are less as compared to case–1 suggesting that the introduction of wind generation has resulted in decreased system losses for all the EV penetration level.

TABLE 5.6: Performance Indices for IEEE 123-Bus Distribution System for Case–2

Penetration → **Level (%)** **Indices ↓**	**0**	**20**	**40**	**60**	**80**	**100**
CI_{avg}	0.1083	0.1133	0.1153	0.1173	0.1192	0.1208
CI_{max}	0.6601	0.7590	0.8234	0.8868	0.9412	0.9640
VDI_{avg}	1.6538	1.5553	1.5204	1.4863	1.4542	1.4274
VDI_{max}	4.5300	4.2500	4.1900	4.1300	4.0700	4.0100
VU_{L-N}^{avg}	0.8043	0.8289	0.8371	0.8469	0.8562	0.8634
VU_{L-N}^{max}	0.9769	0.9998	1.0065	1.0183	1.0275	1.0360
PL_{avg}	0.9466	1.1121	1.1820	1.2582	1.3368	1.4064
PL_{max}	0.9532	1.2305	1.4298	1.6541	1.8712	1.9788
QL_{avg}	0.9383	1.1143	1.1866	1.2649	1.3453	1.4161
QL_{max}	0.9463	1.2392	1.4452	1.6748	1.8955	2.0043

- **Case–3: Two Wind generator installed at bus 42 and 57**

In this case, two wind generation are installed at bus 42 and 57 of the distribution system. The rated capacity of 250 kW is considered for both the wind generators. The performance indices are given in Table 5.7 and following observations are made:

1. The values of CI_{avg} and CI_{max} increases with increase in EV penetration level implying that power flow increases in the conductor and available loading capacity of conductor decreases and is less than case–1 and 2 for all EV penetration level. This signifies that the available loading capacity of conductor increases with increase in wind generations as well as the system can handle more load without getting overloaded.
2. The values of VDI_{avg} and VDI_{max} decreases with increase in EV penetration level suggesting that the system voltage profile improves with the EV penetration level. The voltage profile is poor compared to the case–1 and 2.
3. The value of VU_{L-N}^{avg} and $VU_{L_N}^{max}$ increases with increase in EV penetration level implying that voltage unbalance has increased. However, these values are less compared to case–1 and 2 indicating that the voltage unbalance decreases with increase in wind generation.
4. PL_{avg}, PL_{max}, QL_{avg} and QL_{max} are more than 1 for all EV penetration level except for 0% EV penetration level indicating that the active and reactive losses are less than the base case when there are no EVs in the system. Further, the lower values of loss indicators suggest that the system losses are less compared to the case–1 and 2.

TABLE 5.7: Performance Indices for IEEE 123-Bus Distribution System for Case–3

Penetration → **Level (%)** **Indices ↓**	**0**	**20**	**40**	**60**	**80**	**100**
CI_{avg}	0.1063	0.1113	0.1133	0.1152	0.1171	0.1187
CI_{max}	0.6368	0.7143	0.7785	0.8418	0.8961	0.9188
VDI_{avg}	1.6956	1.5927	1.5567	1.5215	1.4884	1.4609
VDI_{max}	4.6200	4.3400	4.2700	4.2100	4.1500	4.0900
VU_{L-N}^{avg}	0.7915	0.8150	0.8237	0.8332	0.8417	0.8499
VU_{L-N}^{max}	0.9681	0.9883	0.9957	1.0049	1.0137	1.0255
PL_{avg}	0.8858	1.0444	1.1119	1.1855	1.2618	1.3293
PL_{max}	0.9000	1.1624	1.3553	1.5734	1.7851	1.8902
QL_{avg}	0.8709	1.0393	1.1090	1.1846	1.2625	1.3312
QL_{max}	0.8873	1.1636	1.3629	1.5858	1.8007	1.9068

- **Case–4: Three Wind generators installed at bus 42, 57 and 60**

In this case, three wind generators are installed at bus 42, 57 and 60 of the distribution system. The rated capacity of 250 (kW) is considered for all the wind generation. The

performance indices are given in Table 5.8. Similar observations are made as the earlier cases. The important findings are:

1. The value of CI_{max} is 0.8730 for 100% EV penetration level is less than the case–1,2 and 3 indicating that the addition of third wind generator will further increase the available loading capacity of the conductors.
2. The increased value of average voltage deviation to 1.5085 for 100% EV penetration level indicates that the voltage profile of the system has further worsened compared to the other cases.
3. The unbalancing in the voltage of the system has reduced with the addition of wind generation, however, not much variation is observed.
4. It is also observed that the values of PL_{avg} and QL_{avg} are less than one for 0 and 20% EV penetration level indicating that the active and reactive losses of the distribution system for 20% EV are less than when there are no EVs present in the system. But the values PL_{max} and QL_{max} greater than one indicate that the maximum losses of the system are more than the base case.

TABLE 5.8: Performance Indices for IEEE 123-Bus Distribution System for Case–4

Penetration → **Level (%)** **Indices ↓**	**0**	**20**	**40**	**60**	**80**	**100**
CI_{avg}	0.1040	0.1089	0.1109	0.1128	0.1147	0.1163
CI_{max}	0.6134	0.6791	0.7332	0.7962	0.8504	0.8730
VDI_{avg}	1.7535	1.6455	1.6079	1.5716	1.5372	1.5085
VDI_{max}	4.7500	4.4700	4.3800	4.3200	4.2600	4.2000
VU_{L-N}^{avg}	0.7810	0.8047	0.8131	0.8219	0.8309	0.8387
VU_{L-N}^{max}	0.9551	0.9773	0.9857	0.9941	1.0033	1.0144
PL_{avg}	0.8104	0.9599	1.0240	1.0943	1.1674	1.2322
PL_{max}	0.8332	1.0767	1.2613	1.4711	1.6756	1.7773
QL_{avg}	0.7917	0.9507	1.0171	1.0894	1.1640	1.2300
QL_{max}	0.8174	1.0737	1.2645	1.4790	1.6865	1.7893

- **Case–5: Four wind generators installed at bus 42, 57, 60 and 97**

In this case, four wind generators are installed at bus 42, 57, 60 and 97 of the distribution system. The rated capacity of 250 kW is considered for all the wind generation. The performance indices are given in Table 5.9. Similar observations are made as the earlier cases. The important findings are:

1. The value of CI_{max} is 0.87270 which is less than the case–(1–4) indicating that the addition of fourth wind generator has further increased the reserved capacity of the conductors.
2. The increased value of average voltage deviation to 1.5660 for 100% EV penetration level indicates that the voltage profile of the system has further worsened compared to the other cases.
3. The unbalancing in the voltage of the system has reduced with the addition of wind generation, however, not much variation is observed.
4. It is also observed that the values of PL_{avg} and QL_{avg} less than one for 0, 20%, 40% and 60% EV penetration level indicating that the active and reactive losses of the distribution system for 0 to 60% EV penetration are less than when there are no EVs present in the system. Further, the values PL_{max} and QL_{max} less than one for 20% EV penetration imply that the integration of four wind generation in the distribution system has caused the maximum losses of the system less than the base case.

TABLE 5.9: Performance Indices for IEEE 123-Bus Distribution System for Case–5

Penetration → **Level (%)** **Indices ↓**	**0**	**20**	**40**	**60**	**80**	**100**
CI_{avg}	0.1011	0.1060	0.1079	0.1099	0.1117	0.1133
CI_{max}	0.5902	0.6553	0.6904	0.7505	0.8045	0.8270
VDI_{avg}	1.8211	1.7089	1.6688	1.6310	1.5958	1.5660
VDI_{max}	4.9000	4.6200	4.5100	4.4500	4.3900	4.3300
VU_{L-N}^{avg}	0.7693	0.7934	0.8021	0.8104	0.8191	0.8259
VU_{L-N}^{max}	0.9435	0.9642	0.9736	0.9830	0.9948	1.0029
PL_{avg}	0.7333	0.8722	0.9326	0.9991	1.0684	1.1300
PL_{max}	0.7641	0.9868	1.1617	1.3618	1.5578	1.6556
QL_{avg}	0.7119	0.8603	0.9230	0.9914	1.0624	1.1253
QL_{max}	0.7461	0.9809	1.1620	1.3668	1.5660	1.6649

The performance indicators for different cases are shown graphically in Fig. 5.6–Fig. 5.15. From the Fig. 5.6 and Fig. 5.7, it is observed that CI_{avg} and CI_{max} linearly increases with the EV penetration level and decreases with increase in number of wind generation. It is found that with four wind generators, value of CI_{avg} for 60% EV penetration level becomes less than the base case value. However, CI_{max} less than base case is observed for 40% EV penetration level. Further, it is to be noted that integration of only one wind generator does not result in significant changes in CI_{max} compared to the case when no

wind generator is present in the system while increased variation in CI_{avg} is observed with the increment in number of wind generator.

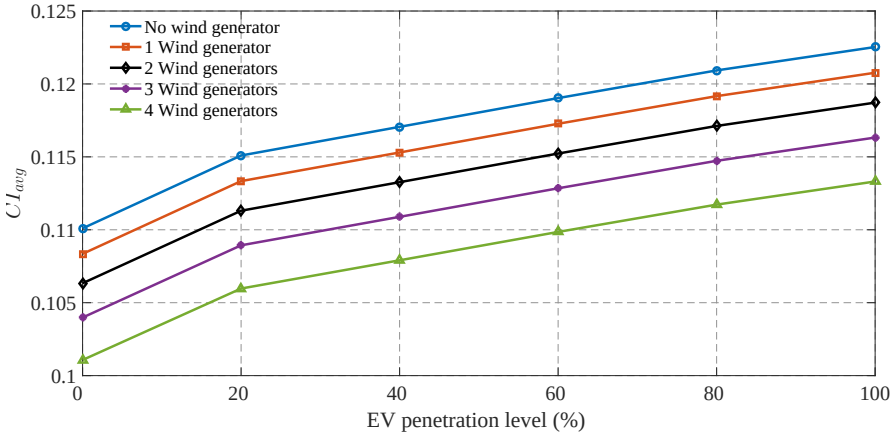

FIGURE 5.6: Comparison of average congestion indices

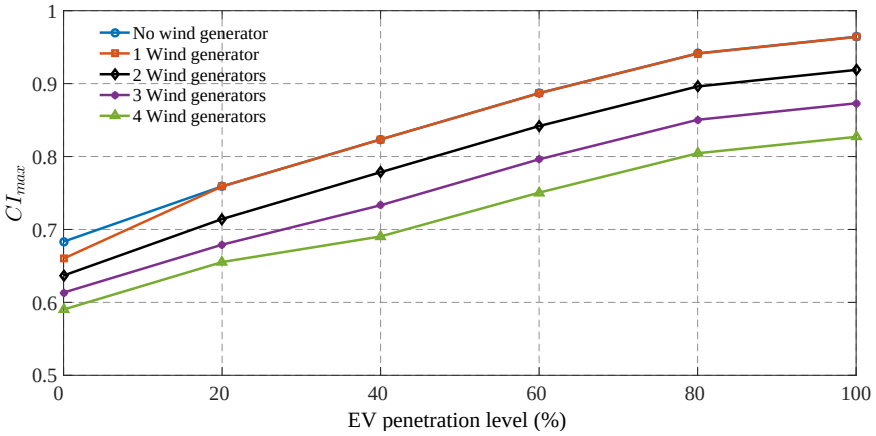

FIGURE 5.7: Comparison of maximum congestion indices

From Fig. 5.8 and Fig. 5.9, it is observed that voltage deviation from the reference value linearly decreases with the increase in EV penetration level while increases with increase in number of wind generation. It is to be noted that with the addition four wind generators, value of VDI_{avg} and VDI_{max} becomes less than the case when no wind generation is present in the system for 80% EV penetration level. Further, increment in variation of VDI_{avg} and VDI_{max} are observed with increased number of wind generation.

From Fig. 5.10, it is observed that the value of VU_{L-N}^{avg} linearly increases with EV penetration level while it decreases with increase in number of wind generation. Significant variation in VU_{L-N}^{avg} is not observed for different EV penetration level and number of wind generation and the voltage unbalance is within the permissible limit of 3%. From Fig. 5.11,

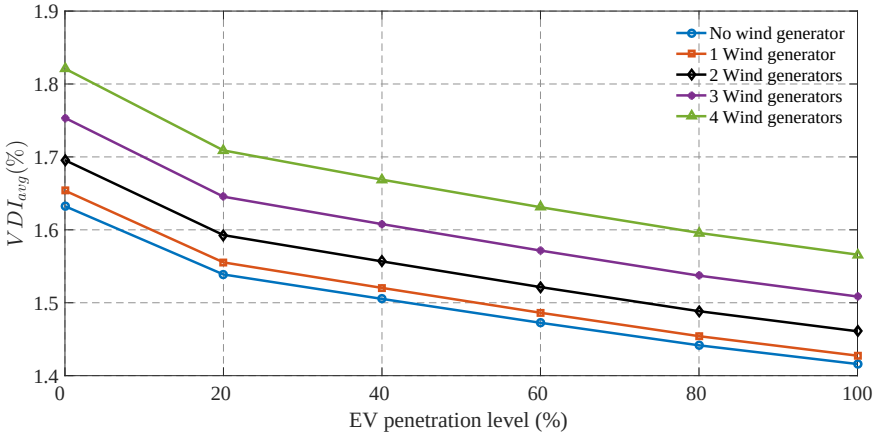

FIGURE 5.8: Comparison of average voltage deviation indices

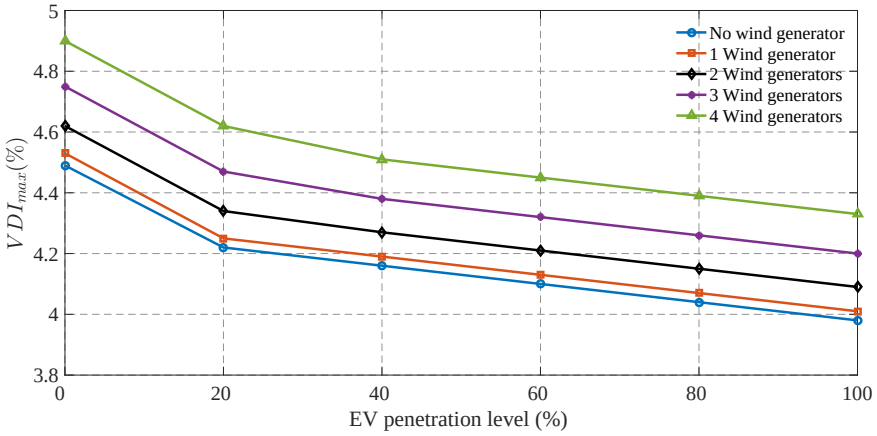

FIGURE 5.9: Comparison of maximum voltage deviation indices

it is observed that the value of VU_{L-N}^{max} increase with increase in EV penetration level while decreases with the number of wind generation. Maximum voltage unbalance is also within the permissible limit of 3%.

Fig. 5.12 and Fig. 5.13 shows the average and maximum active loss indices for different EV penetration level and number of wind generation. From Fig. 5.12, it is observed that active loss increases linearly with EV penetration level while decreases with the increase in number of wind generation. The increment in loss reduction is observed with increased with generation and it is to be noted that average losses are less than the base case loss for four wind generation and 60% EV penetration level. Similar observations are made in PL_{max}. However, the increment in maximum loss reduction is less compared to the increment in average loss reduction. Further, change in slope of PL_{max} is observed after 80% EV penetration level. This can be justified by observing the load profile of

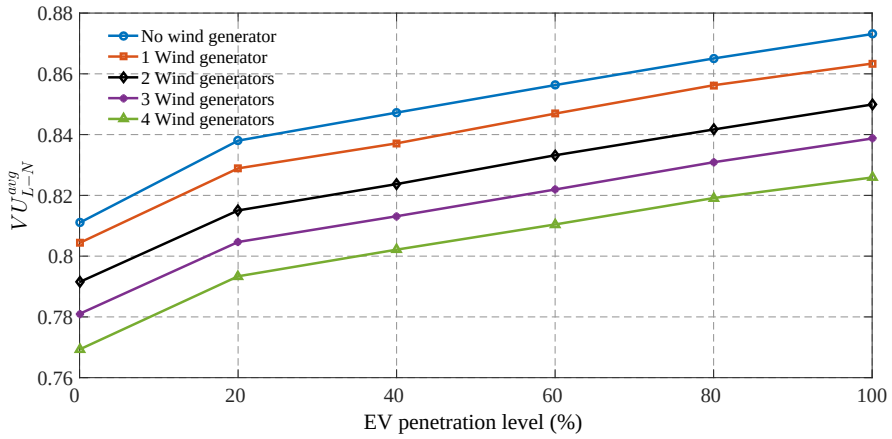

FIGURE 5.10: Comparison of average voltage unbalance indices

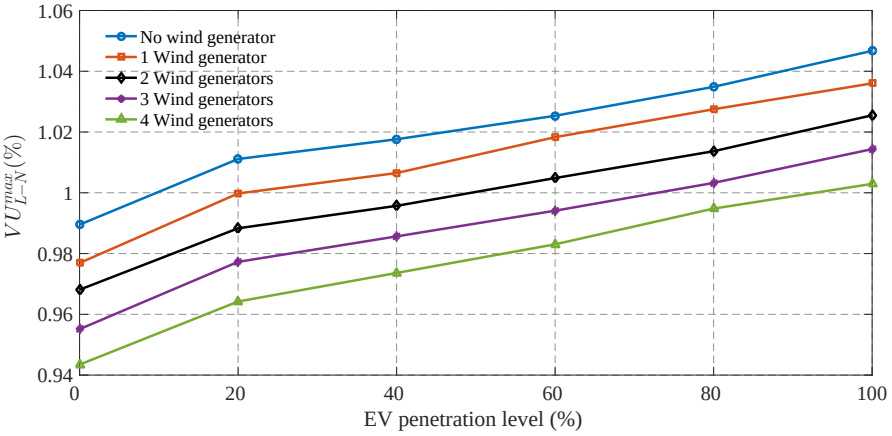

FIGURE 5.11: Comparison of maximum voltage unbalance indices

the distribution system which shows decrease in increment of peak load for 100% EV penetration level. Thus, the increment in losses due to increased EV penetration level also decreases.

Fig. 5.14 and Fig. 5.15 shows the average and maximum reactive loss indices for different EV penetration level and number of wind generation. The curve of QL_{avg} and QL_{max} follows the similar pattern as of PL_{avg} and PL_{max}. Therefore, same conclusions are drawn for average and maximum reactive power losses.

5.4.3 Synergy Analysis

Synergy analysis is carried out to study the interaction between FCS and wind generation in terms of active and reactive energy flows and reverse power flow. The key findings of the synergy analysis are as follows:

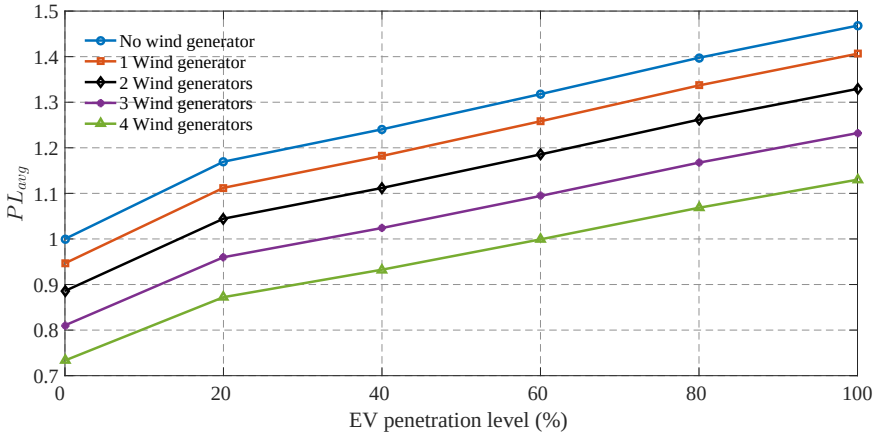

FIGURE 5.12: Comparison of average active power loss indices

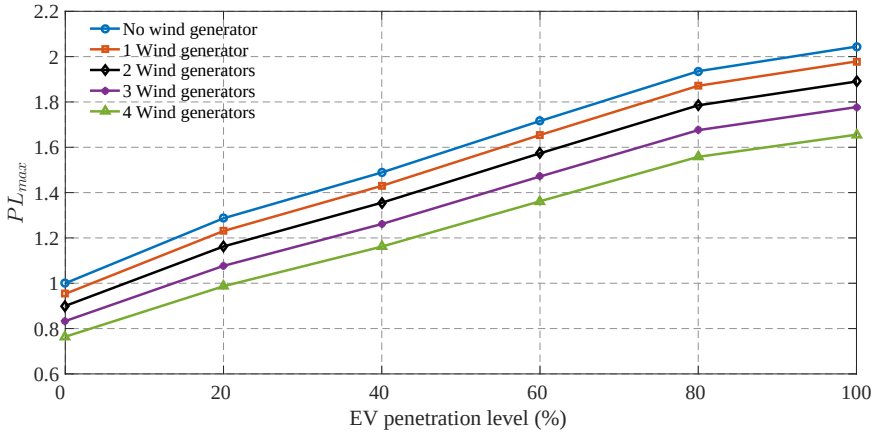

FIGURE 5.13: Comparison of maximum active power loss indices

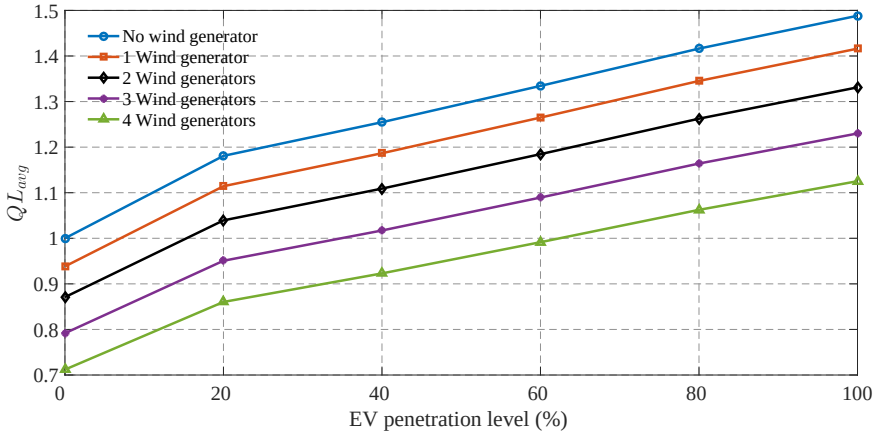

FIGURE 5.14: Comparison of average reactive power loss indices

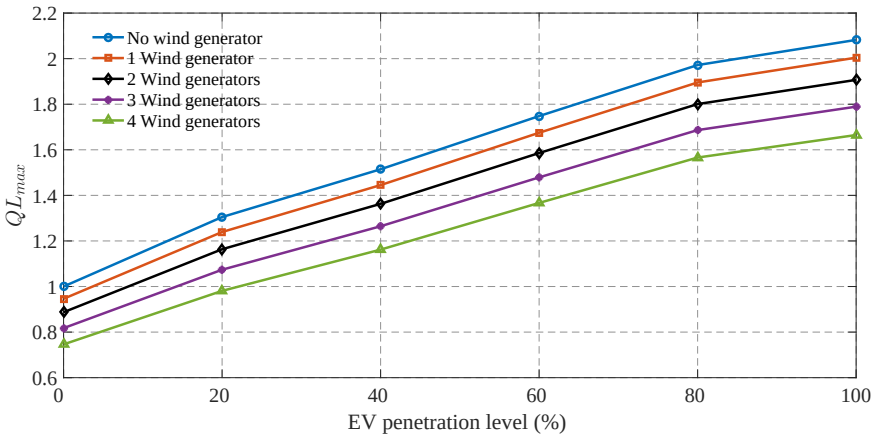

FIGURE 5.15: Comparison of maximum reactive power loss indices

- **Excess Wind Power Generation**

In order to determine the daily amount of excess active power output from wind generation, interaction between FCS daily demand and the active power output of wind generation are compared at different EV penetration level. The daily amount of excess wind energy with 100% EV for different penetration of wind generation is shown in Fig. 5.16.

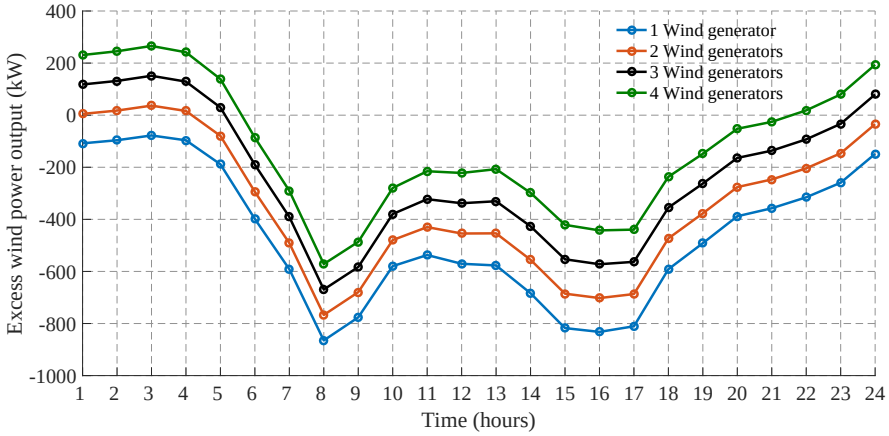

FIGURE 5.16: Daily excess output power of wind generator

Positive excess wind power output imply that the power output available from wind generation is more than the FCS charging demand while negative excess wind power output imply that the power output available from the wind generation is less than the FCS charging demand. From the Fig. 5.16, it is observed that depending on the number of wind generation and the time of the day, EV fast charging load may be totally or partially supplied by the wind generation. It shows that four wind generation are not sufficient to satisfy the FCS charging demand during the peak hours of demand. The unsatisfied

FCS demand will be satisfied by importing the power from substation. Fig. 5.17 shows the daily active energy drawn from substation in p.u. for different penetration of EVs and number of wind generations. Three observations are made: i) the active energy imported from substation decreases with increase in number of wind generation ii) the active energy imported from substation increase with increase in EV penetration level iii) there is linear relationship between the active energy from substation and EV penetration level. This linear relationship can be used to estimate the substation active energy for any EV penetration level. Fig. 5.17 shows the daily active energy drawn from substation in p.u. for different penetration of EVs and number of wind generations. The variation in reactive power import from substation is negligible compared to the active power import from the substation. This is anticipated because the power factor of the EV fast charging load is close to one as well as it is assumed that the wind generation provides only active power.

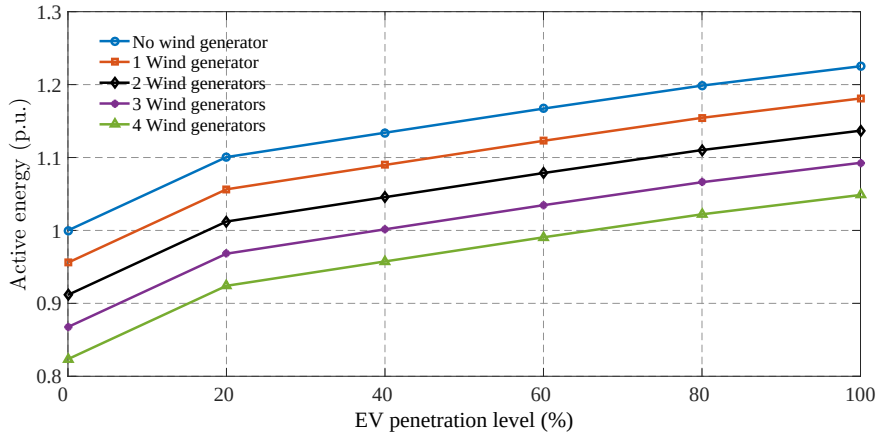

FIGURE 5.17: Substation active energy in per unit

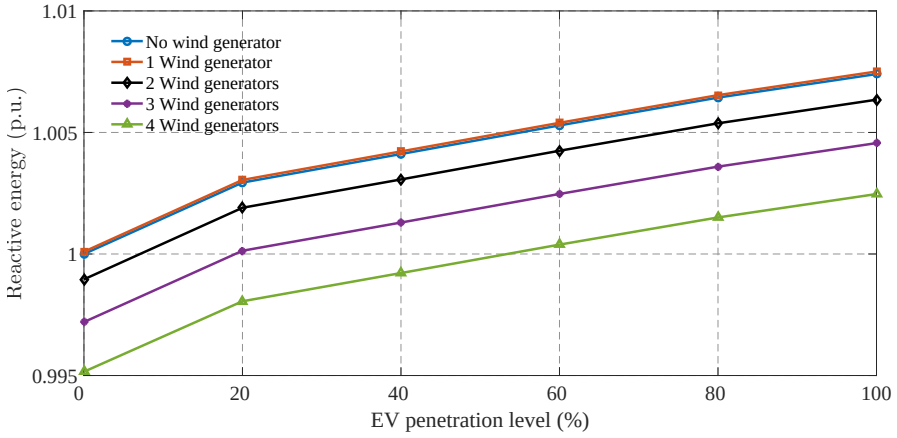

FIGURE 5.18: Substation reactive energy in per unit

- **Reverse Power Flow**

Reverse power flow is the amount of power that flows back to the substation. Fig. 5.19 shows the daily active power flow at the substation with 0% EV penetration level for different number of wind generation. The active power flow of substation is always positive even for the distribution system with four wind generation and zero EVs. It implies that there is no reverse power flow. Therefore, RP_t measures zero for all the cases.

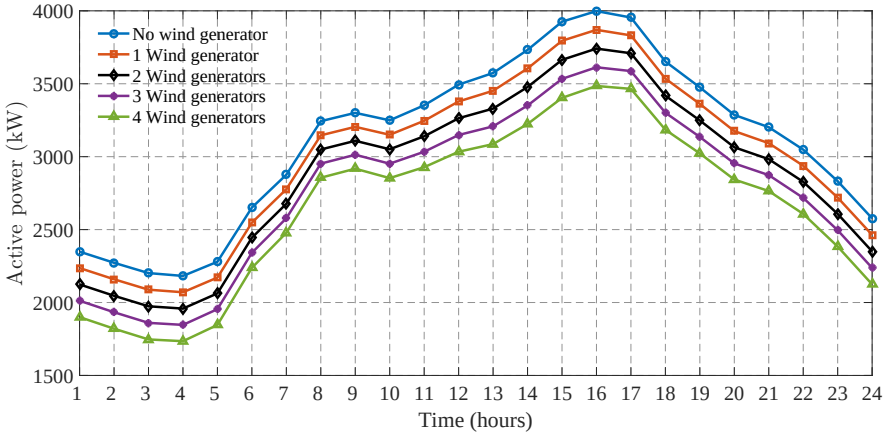

FIGURE 5.19: Substation daily active power

5.5 Summary

The additional load demand due to the integration of FCS may degrade the performance of distribution system. The inclusion of wind generation can reduce the environment pollution but it may affect the performance of distribution of system positively or negatively due to the intermittency associated with it. Therefore, it is important to study the impact of FCS and wind generation to assist the distribution planner in decision making in case of any system violations. In this chapter, wind generator power output is modelled incorporating the uncertainties associated with the wind speed using Weibull distribution function. Different performance indices characterizing the impact of FCS and wind generator on load profile, congestion of conductor, voltage deviation and unbalance and system losses are proposed. The proposed performance indices are determined for IEEE 123-bus distribution system. Load demand due to FCS developed in chapter 3 having spatial-temporal characteristic with suitable exponential load model is utilized to assess the performance of the distribution system. Further, synergy analysis is also carried out to study the interaction between FCS and wind generation. The main conclusions and highlights of this study are:

1. Daily expected output power of wind generation is determined incorporating uncertainties associated with the wind speed using Weibull distribution function. Two Weibull parameters namely: shape and scale parameters are estimated for each hour using maximum likelihood estimator. The mean of the wind speed is maximum during 15^{th} hour and minimum during 9^{th} hour of the day. Therefore, it is expected that expected output power of wind generation will be maximum during 15^{th} and minimum during 9^{th} hour of the day. Small variation in shape and scale parameters are observed indicating small variation in daily expected output power of wind generation. However, the variation increases with increase in number of wind generation.

2. It is found that peak of the load profile of distribution system increases with increase in EV penetration level and occurs at 16^{th} hour of the day. But shift in peak load demand is not observed as the peak of the original load pattern and distribution of vehicles on the road coincides during this hour. Increment in load demand decreases with increased EV penetration level as the FCS is unable to serve all the EVs at higher penetration level. Further, PAR value increases with increased EV penetration level except for 100% EV penetration level.

3. It is inferred that congestion indices have positive linear relationship with EV penetration level while it decreases with increase in number of wind generation. Based on the IC_{max} value, it is inferred that none of the distribution lines are overloaded even for 100% EV penetration level.

4. The voltage profile of the system improves with increased EV penetration level while it worsens with increased number of wind generations. However, bus voltages are within the permissible limit of $\pm$ 5% even for extreme scenarios like 100% EV penetration level or four wind generation in the system

5. The impact of FCS and wind generation of voltage unbalance of the system is not significant as the FCS is three-phase load. Thus, causing no unbalance.

6. Active and reactive losses of the system increases with increase in EV penetration level and decreases with increased wind generation. It is found that with addition of four wind generators in the distribution system with 60% EV penetration level causes less power losses as compared to the base case.

7. It is observed from excess wind power generation that even four wind generation are unable to satisfy the FCS charging demand during peak hours. However, four wind generation results in daily energy imported from substation less than the base case for 60% EV penetration level. Also, zero reverse power flow is observed for all the cases.

8. Based on the substation active energy and power system losses, it can be said that the distribution system with four wind generator can take additional 60% penetration level of EV loads without requiring extra active energy from the substation during the day.

9. From the above observations, it can be inferred that increased EV penetration level will cause the degradation in performance of distribution system in terms of congestion, losses and load profile while improves the voltage profile of the system. The integration of wind generation has positive impact on the distribution system performance except for the voltage profile of the system. But the intermittency associated with the wind does not satisfy the EV fast charging demand at all times. Thus, it can be concluded that wind will act only as partial solution and for maintaining power balance, the support from the main grid may be required for satisfying the FCS load demand.

Chapter 6

Conclusions

The increased environment pollution and energy crisis has led the governments around the world to promote Electric Vehicles (EVs). However, the growth of EV is hindered due to more charging time and less driving range compared to the Internal Combustion Engine (ICE) vehicles and lack of proper charging infrastructure. The charging time can be improved with the advancement of technology while driving range anxiety can be dealt by planning proper fast charging infrastructure known as Fast Charging Station (FCS). The planning of FCS depends on the charging demand, power system and transportation network operational constraint. Therefore, there is a need to develop stochastic EV charging profile as well as establishing proper load model of FCS for power flow analysis to correctly assess the operational parameters of distribution system. The integration of FCS will add extra load demand on the distribution system. This additional demand can degrade the performance of distribution system. Moreover, the increased wind integration in the power system due to environment concerns can have both positive and negative impacts on the performance of distribution system. Thus, impact analysis of FCS and wind generation is required to obtain the operational characteristic of distribution system.

This thesis attempts to determine the load model of EV fast charging for power flow analysis and develop Aggregated EV Charging Profile (AECP) of FCS. The thesis proposes a multi-objective synergistic planning model of FCS in distribution system coupled with transportation network and analyses its impact on distribution system performance. Further, synergy between wind generation and FCS are also investigated. The thesis work is organised in six chapters. In chapter-1 a brief introduction of the proposed research work is presented. Chapter 2 presents a comprehensive literature survey of significant works in the areas of load modelling of FCS, planning of FCS and impact analysis of FCS and wind generation on distribution system performance from technical reports and research publications. On the basis of literature survey, the research objectives are framed. In this chapter, the main findings and contributions of this thesis are summarized and some possible future research scope is also presented.

In Chapter 3, a mathematical relationship between the active power consumption and supply voltage is identified for fast charging EVs. The derived relationship is validated by simulating a fast charger with a rated capacity of 30 KW. The power vs voltage characteristics obtained from the simulated fast charger is used to estimate the parameters

of two standard load models for power flow analysis namely: exponential and ZIP load model. The EV charging demand depends on different uncertain factors like location, time, duration of charging and driving behaviour of the EV owners. Therefore, stochastic Aggregated EV Charging Profile (AECP) of FCS is developed which has both spatial and temporal characteristic as well as incorporates the uncertainties. The effect of different load models on the distribution system is carried out on the IEEE 123-bus distribution system to demonstrate the effectiveness of the proposed voltage-dependent load model and stochastic charging demand. Following conclusions are drawn from this chapter:

1. The derived mathematical relationship states that the active power consumption decreases with increase in supply voltage and increases with increase in SOC. The power vs voltage characteristics for different values of SOC obtained from the simulated fast charger shows that the power demand decreases with increase in supply voltage and increases with increase in battery SOC. Thus verifying the derived mathematical relationship.

2. The parameters of voltage dependent exponential and ZIP load model for different values of SOC are estimated and it is found that the parameters of these load models vary slightly with the SOC. Based on the MAE values, it is concluded that the exponential load model is the best representation of voltage-dependent behavioural characteristic of EV fast charging load and MAE value also suggest that single set of parameters might be sufficient to represent the load models for different values of SOC. This is confirmed by the power vs voltage characteristics and the most appropriate single set of parameters are selected for exponential load model.

3. The developed stochastic FCS charging demand shows that the demand by the FCS will depend on its location and the time of charging during the day. Thus, having spatial-temporal characteristics. It is also found that the charging demand depends on the penetration level of EVs and initial SOC has little effect on the charging demand. However, the initial SOC governs the charging time, thereby effecting the mean charging time of each FCS. This will further effect the number of EVs charging simultaneously at each FCS and thus affecting the charging demand of FCS.

4. It is found that the different load models affects the increment in energy demand, energy losses, voltage profile and power factor of the system due to the additional EV fast charging demand. It is observed that the exponential load and ZIP load model results in less energy demand. The exponential and ZIP load model will not necessarily result in less energy demand than the CPL model but will be governed by the system

voltages. The distribution performance parameters like power losses, voltage profile and power factor depends on the load demand, therefore, it can be inferred that different load models will effect the distribution performance parameters.

In Chapter 4, a multi-objective synergistic planning model is proposed for determining location and sizes of FCS in the distribution system coupled with the transportation network. The multi-objective model attempts to minimize power losses and voltage deviation of the distribution system and maximizes EV flow served by the FCS. Service radius is introduced in the planning model in order to ensure that EVs can reach its nearest FCS with the available battery SOC. Further, better service quality is provided by reducing the waiting time. The developed multi-objective problem is solved by $MOGWO$ algorithm and final decision is made using fuzzy satisfaction-based method. The efficacy of proposed planning model is carried out on modified IEEE 123-bus distribution system coupled with 25 node transportation network. The FCS is integrated in the distribution system using more suitable exponential load model. Moreover, sensitivity analysis is carried out to determine the effect of different objective functions, service radius and waiting time on the planning of FCS in the system. Following conclusions are drawn from this chapter:

1. The proposed multi-objective problem tries to minimize the power loss and voltage deviation and maximize the EV flow served by the FCS. It considers the customer convenience by reducing the waiting time at the FCS and range anxiety by introducing service radius of FCS in the proposed model. The uncertainties associated with the driving behaviour and weather conditions in estimation of service radius and waiting time is considered to represent the realistic scenario.

2. The MOGWO optimization algorithm utilized for solving multi-objective planning problem performs better than MOPSO and MOEA/D algorithms.

3. The service radius is obtained for different confidence level and it is observed that service radius decreases with increase in confidence level. The desirable solution amongst the non-dominated solutions obtained using fuzzy satisfaction based method show that system losses and voltage deviation are not the minimum values signifying that the planning scheme is not able to provide optimal values of different objectives considered. Thus, it can be inferred that the multi-objective problems does not give optimal solution with respect to each objective but gives trade-off solution.

4. It is observed that different objectives affects the planning of FCS. Considering one network affects the performance of other suggesting importance of considering both

distribution system and transportation network in the problem formulation of planning of FCS.

5. The confidence level affects the service radius of FCS, thereby, affecting the planning of FCS. The service radius also decides the number of FCS to be located in the system.

6. Waiting time effects the number of identical charging slots, further, varying the location of FCS. It is inferred that lower waiting time increases service quality while decreases utilization of FCS, thus, wasting the resource. On the other hand, higher waiting time worsens service quality while increasing the utilization of FCS. Therefore, a trade-off waiting time is determined.

7. The presented approach provides decision maker an opportunity to make a proper trade-off between the power losses, voltage deviation and the served EV flow. The proposed method also suggest the way to select proper service radius and waiting time.

In Chapter 5, the performance analysis of distribution system is carried out in presence of FCS and wind generation. For integrating wind generator in the distribution system, wind power output is modelled considering wind speed uncertainties. Also, performance indices characterizing the impact of FCS and wind generation on load profile, congestion of conductor, voltage deviation and unbalance and system losses are proposed. The FCS and wind generation are integrated in modified IEEE 123-bus distribution system and impact assessment is investigated by determining performance indices. Simulations are carried out for different penetration level of EVs and number of wind generator. Load demand developed in Chapter 3 having spatial-temporal characteristic with suitable exponential load model is utilized to assess the performance of the distribution system. Further, synergy analysis is also carried out to study the interaction between FCS and wind generation. Following conclusions are drawn from this chapter:

1. The developed model of expected output power of wind, models wind speed uncertainty, is effective in obtaining daily output power of wind for different scenarios. Small variations in hourly wind speed profile is observed, thus, reflecting the same in expected power output of the wind. However, the variation increases with increase in number of wind generation.

2. The daily load profile of distribution system is significantly affected by the FCS charging additional demand. Increment in peak of the load profile is observed, however, there is no shift in peak. Further, PAR of the daily load profile worsens with the increased

penetration level of EVs implying that addition of FCS has resulted in poor load profile of the system.

3. It is inferred that congestion indices have positive linear relationship with EV penetration level while it decreases with increase in number of wind generation. However, none of the lines of distribution system are overloaded even for the worst case scenario.

4. Improvement in voltage profile of the distribution system is observed with the increased penetration of EVs while worsening is observed with increased number of wind generation. The impact of FCS and wind generation of voltage unbalance of the system is not significant as the FCS is three-phase load. Thus, causing no unbalance.

5. The addition of FCS demand causes increased active and reactive power losses in the distribution system while decreased system losses are obtained with increased number of wind generation.

6. It is observed from excess wind power generation that even four wind generation are unable to satisfy the FCS charging demand during peak hours. However, four wind generation results in daily energy imported from substation less than the base case for 60% EV penetration level. Also, zero reverse power flow is observed for all the cases. Based on the substation active energy and power system losses, it can be said that the distribution system with four wind generator can take additional 60% penetration level of EV loads without requiring extra active energy from the substation during the day.

7. From the above observations, it can be inferred that increased EV penetration level will cause the degradation in performance of distribution system in terms of congestion, losses and load profile while improves the voltage profile of the system. The integration of wind generation has positive impact on the distribution system performance except for the voltage profile of the system. But the intermittency associated with the wind does not satisfy the EV fast charging demand at all times. Thus, it can be concluded that wind will act only as partial solution and for maintaining power balance, the support from the main grid may be required for satisfying the FCS load demand.

FUTURE RESEARCH SCOPE

The adoption of EVs will not only benefit the environment but also reduce reliance on the oil markets, thus, dealing with energy crisis. It also has economic and smart grids benefits. However, cost, driving range and charging time are still major concerns of EV users. Proper planning of charging infrastructure can reduce the charging time and driving range anxiety. But, the fast charging of EVs can greatly affect the performance of distribution system.

Thus, impact analysis of FCS on the distribution system performance is required to provide information about the operational characteristics of distribution system so that they can take necessary actions in case of any system violations. This thesis attempts to address the key issues of load modelling, planning and impact analysis of FCS in distribution system. The possible future extensions of this thesis are as follows:

1. The proposed study has determined load model of single fast charging EV for power flow analysis. However, aggregated load model of FCS can also be incorporated in the study. Further, the load model of FCS can also be determined considering voltage stability studies.

2. The simulated traffic flows are used in the proposed model of stochastic charging demand of FCS. However, real-time traffic flows or different methods for simulating traffic flows can be explored to develop stochastic charging demand.

3. The optimal location and sizing of FCS require cost function and good optimization techniques. The heuristic technique used for proposed planning of FCS efficiently solves the multi-objective problem. However, each optimization techniques has its benefits and drawbacks. Therefore, different optimization techniques can be explored to solve this problem. The research can be extended by enhancing the cost function, analysing the sensitiveness of techniques to variopus optimization parameters and exploring other optimization and decision making techniques .

4. The impact analysis of FCS is carried out in conjunction with wind generation. However, other clean energy sources like photovoltaic etc. can also be incorporated in this study.

5. The integration of distributed generation like wind and solar can mitigate the negative impacts of EV fast charging load on the distribution system. Therefore, simultaneous planning of FCS and distributed generation can be incorporated in this study while considering the uncertainty of distributed generation and EV charging demand at FCS.

6. The impact analysis shows the worsening of load profile and other adverse affects on the distribution system. Further, the wind generation is unable to satisfy the FCS load demand during peak hours. This can be resolved by employing intelligent charging strategies which can coordinate both EVs and renewable sources. Further, battery storage can be used to deal with supply-demand mismatch due to uncertainty associated with EVs and renewable sources.

Appendix A

IEEE 123-Bus Distribution System

The simulations in this study are carried out on the IEEE-123 bus distribution system. This distribution test system and its data are referred from [139]. It operates at a nominal voltage of 4.16 kV. The system has both underground and overhead lines, characterized by unbalance loading with constant power, impedance and current loads, four voltage regulators, shunt capacitor banks, and multiple switches. The base load of the system is 4023.524 kVA with a power factor of 0.8761 and served by 5000 kVA transformer. The line diagram of IEEE 123-bus distribution system is given in Fig. A.1.

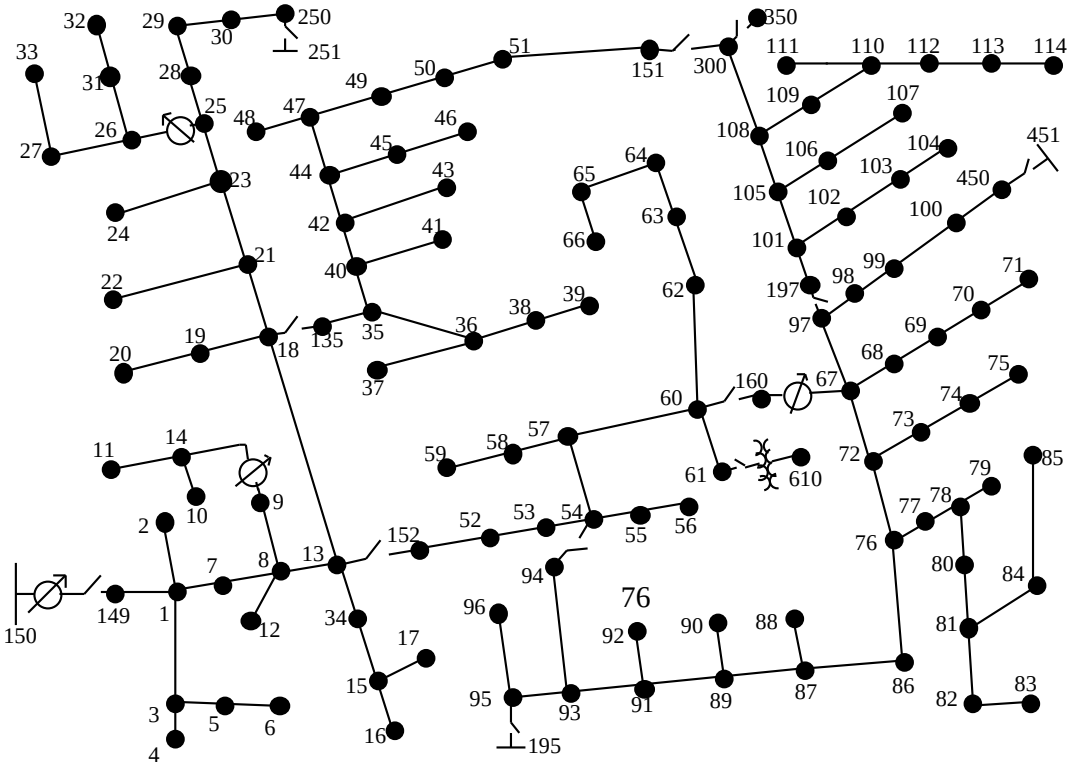

FIGURE A.1: Line diagram of IEEE 123-bus distribution system

Table A.1: Overhead Line Configurations of IEEE 123-Bus Distribution System

Configuration	Phasing	Phase Conductor ACSR	Neutral Conductor ACSR	Spacing ID
1	A B C N	336,400 26/7	4/0 6/1	500
2	C A B N	336,400 26/7	4/0 6/1	500
3	B C A N	336,400 26/7	4/0 6/1	500
4	C B A N	336,400 26/7	4/0 6/1	500
5	B A C N	336,400 26/7	4/0 6/1	500
6	A C B N	336,400 26/7	4/0 6/1	500
7	A C N	336,400 26/7	4/0 6/1	505
8	A B N	336,400 26/7	4/0 6/1	505
9	A N	1/0	1/0	510
10	B N	1/0	1/0	510
11	C N	1/0	1/0	510

Table A.2: Underground Line Configurations of IEEE 123-Bus Distribution System

Configuration	Phasing	Cable	Spacing ID
12	A B C	1/0 AA, CN	515

Table A.3: Line Data of IEEE 123-Bus Distribution System

Node A	Node B	Length (kft.)	Configuration
1	2	175	10
1	3	250	11
1	7	300	1
3	4	200	11
3	5	325	11
5	6	250	11
7	8	200	1
8	12	225	10
8	9	225	9
8	13	300	1
9	14	425	9
13	34	150	11
13	18	825	2
14	11	250	9
14	10	250	9
15	16	375	11
15	17	350	11
18	19	250	9

Continued...

Table A.3 – *Continued...*

Node A	**Node B**	**Length (kft.)**	**Configuration**
18	21	300	2
19	20	325	9
21	22	525	10
21	23	250	2
23	24	550	11
23	25	275	2
25	26	350	7
25	28	200	2
26	27	275	7
26	31	225	11
27	33	500	9
28	29	300	2
29	30	350	2
30	250	200	2
31	32	300	11
34	15	100	11
35	36	650	8
35	40	250	1
36	37	300	9
36	38	250	10
38	39	325	10
40	41	325	11
40	42	250	1
42	43	500	10
42	44	200	1
44	45	200	9
44	47	250	1
45	46	300	9
47	48	150	4
47	49	250	4
49	50	250	4
50	51	250	4
51	151	500	4
52	53	200	1
53	54	125	1
54	55	275	1
54	57	350	3
55	56	275	1
57	58	250	10

Continued...

Table A.3 – *Continued...*

Node A	Node B	Length (kft.)	Configuration
57	60	750	3
58	59	250	10
60	61	550	5
60	62	250	12
62	63	175	12
63	64	350	12
64	65	425	12
65	66	325	12
67	68	200	9
67	72	275	3
67	97	250	3
68	69	275	9
69	70	325	9
70	71	275	9
72	73	275	11
72	76	200	3
73	74	350	11
74	75	400	11
76	77	400	6
76	86	700	3
77	78	100	6
78	79	225	6
78	80	475	6
80	81	475	6
81	82	250	6
81	84	675	11
82	83	250	6
84	85	475	11
86	87	450	6
87	88	175	9
87	89	275	6
89	90	225	10
89	91	225	6
91	92	300	11
91	93	225	6
93	94	275	9
93	95	300	6
95	96	200	10
97	98	275	3

Continued...

Table A.3 – *Continued...*

Node A	Node B	Length (kft.)	Configuration
98	99	550	3
99	100	300	3
100	450	800	3
101	102	225	11
101	105	275	3
102	103	325	11
103	104	700	11
105	106	225	10
105	108	325	3
106	107	575	10
108	109	450	9
108	300	1000	3
109	110	300	9
110	111	575	9
110	112	125	9
112	113	525	9
113	114	325	9
135	35	375	4
149	1	400	1
152	52	400	1
160	67	350	6
197	101	250	3

Table A.4: Spot Load Data of IEEE 123-Bus Distribution System

Node	Load Model	Ph-1 kW	Ph-1 kVAr	Ph-2 kW	Ph-2 kVAr	Ph-3 kW	Ph-4 kVAr
1	Y-PQ	40	20	0	0	0	0
2	Y-PQ	0	0	20	10	0	0
4	Y-PR	0	0	0	0	40	20
5	Y-I	0	0	0	0	20	10
6	Y-Z	0	0	0	0	40	20
7	Y-PQ	20	10	0	0	0	0
9	Y-PQ	40	20	0	0	0	0
10	Y-I	20	10	0	0	0	0
11	Y-Z	40	20	0	0	0	0
12	Y-PQ	0	0	20	10	0	0
16	Y-PQ	0	0	0	0	40	20

Continued...

Table A.4 – *Continued...*

Node	Load Model	Ph-1 kW	Ph-1 kVAr	Ph-2 kW	Ph-2 kVAr	Ph-3 kW	Ph-4 kVAr
17	Y-PQ	0	0	0	0	20	10
19	Y-PQ	40	20	0	0	0	0
20	Y-I	40	20	0	0	0	0
22	Y-Z	0	0	40	20	0	0
24	Y-PQ	0	0	0	0	40	20
28	Y-I	40	20	0	0	0	0
29	Y-Z	40	20	0	0	0	0
30	Y-PQ	0	0	0	0	40	20
31	Y-PQ	0	0	0	0	20	10
32	Y-PQ	0	0	0	0	20	10
33	Y-I	40	20	0	0	0	0
34	Y-Z	0	0	0	0	40	20
35	D-PQ	40	20	0	0	0	0
37	Y-Z	40	20	0	0	0	0
38	Y-I	0	0	20	10	0	0
39	Y-PQ	0	0	20	10	0	0
41	Y-PQ	0	0	0	0	20	10
42	Y-PQ	20	10	0	0	0	0
43	Y-Z	0	0	40	20	0	0
45	Y-I	20	10	0	0	0	0
46	Y-PQ	20	10	0	0	0	0
47	Y-I	35	25	35	25	35	25
48	Y-Z	70	50	70	50	70	50
49	Y-PQ	35	25	70	50	35	20
50	Y-PQ	0	0	0	0	40	20
51	Y-PQ	20	10	0	0	0	0
52	Y-PQ	40	20	0	0	0	0
53	Y-PQ	40	20	0	0	0	0
55	Y-Z	20	10	0	0	0	0
56	Y-PQ	0	0	20	10	0	0
58	Y-I	0	0	20	10	0	0
59	Y-PQ	0	0	20	10	0	0
60	Y-PQ	20	10	0	0	0	0
62	Y-Z	0	0	0	0	40	20
63	Y-PQ	40	20	0	0	0	0
64	Y-I	0	0	75	35	0	0
65	D-Z	35	25	35	25	70	50
66	Y-PQ	0	0	0	0	75	35

Continued...

Table A.4 – *Continued...*

Node	Load Model	Ph-1 kW	Ph-1 kVAr	Ph-2 kW	Ph-2 kVAr	Ph-3 kW	Ph-4 kVAr
68	Y-PQ	20	10	0	0	0	0
69	Y-PQ	40	20	0	0	0	0
70	Y-PQ	20	10	0	0	0	0
71	Y-PQ	40	20	0	0	0	0
73	Y-PQ	0	0	0	0	40	20
74	Y-Z	0	0	0	0	40	20
75	Y-PQ	0	0	0	0	40	20
76	D-I	105	80	70	50	70	50
77	Y-PQ	0	0	40	20	0	0
79	Y-Z	40	20	0	0	0	0
80	Y-PQ	0	0	40	20	0	0
82	Y-PQ	40	20	0	0	0	0
83	Y-PQ	0	0	0	0	20	10
84	Y-PQ	0	0	0	0	20	10
85	Y-PQ	0	0	0	0	40	20
86	Y-PQ	0	0	20	10	0	0
87	Y-PQ	0	0	40	20	0	0
88	Y-PQ	40	20	0	0	0	0
90	Y-I	0	0	40	20	0	0
92	Y-PQ	0	0	0	0	40	20
94	Y-PQ	40	20	0	0	0	0
95	Y-PQ	0	0	20	10	0	0
96	Y-PQ	0	0	20	10	0	0
98	Y-PQ	40	20	0	0	0	0
99	Y-PQ	0	0	40	20	0	0
100	Y-Z	0	0	0	0	40	20
102	Y-PQ	0	0	0	0	20	10
103	Y-PQ	0	0	0	0	40	20
104	Y-PQ	0	0	0	0	40	20
106	Y-PQ	0	0	40	20	0	0
107	Y-PQ	0	0	40	20	0	0
109	Y-PQ	40	20	0	0	0	0
111	Y-PQ	20	10	0	0	0	0
112	Y-I	20	10	0	0	0	0
113	Y-Z	40	20	0	0	0	0
114	Y-PQ	20	10	0	0	0	0

Table A.5: Transformer Data of IEEE 123-Bus Distribution System

	kVA	**kV-high**	**kV-low**	**R – %**	**X – %**
Substation	5,000	115 – D	4.16 Gr–W	1	8
XFM – 1	150	4.16 – D	.480 – D	1.27	2.72

Table A.6: Regulator Data of IEEE 123-Bus Distribution System

Regulator ID	**1**	**2**	**3**		**4**		
Line Segment	150 – 149	9 – 14	25 – 26		160 – 67		
Location	150	9	25		160		
Phases	A–B–C	A	A-C		A–B–C		
Connection	3–Ph, Wye	1-Ph, L-G	2-Ph, L-G		3–Ph, LG		
Monitoring Phase	A	A	A–C		A–B–C		
Bandwidth	2.0 volts	2.0 volts	1		2		
PT Ratio	20	20	20		20		
Primary CT Rating	700	50	50		300		
Compensator	Ph–A	Ph–A	Ph–A	Ph-C	Ph-A	Ph–B	Ph–C
R – Setting	3	0.4	0.4	0.4	0.6	1.4	0.2
X – Setting	7.5	0.4	0.4	0.4	1.3	2.6	1.4
Voltage Level	120	120	120	120	124	124	124

Table A.7: Switch Data of IEEE 123-Bus Distribution System

Node A	**Node B**	**Normal**
13	152	closed
18	135	closed
60	160	closed
61	610	closed
97	197	closed
150	149	closed
250	251	open
450	451	open
54	94	open
151	300	open
300	350	open

Table A.8: Shunt Capacitor Data of IEEE 123-Bus Distribution System

Node	**Ph–A kVAr**	**Ph–B kVAr**	**Ph–C kVAr**
83	200	200	200
88	50	–	–
90	–	50	–
92	–	–	50

Appendix B

25-Node Transportation Network

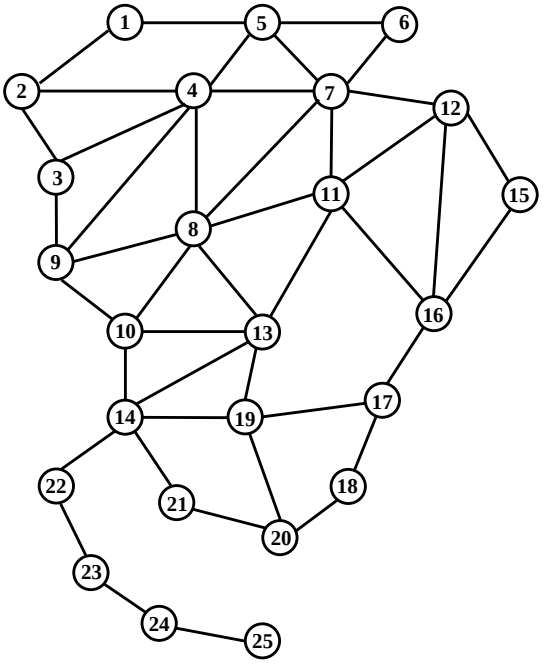

FIGURE B.1: Line diagram of 25-node transportation network

TABLE B.1: Line Parameter of 25-Node Transportation Network

Node–1	**Node–2**	**Length (miles)**
‘ 1	2	4
1	5	5
2	3	3
2	4	4
3	4	4
3	9	4
4	9	7
4	8	5
4	7	5
4	5	3
5	6	5
5	7	5
6	7	3

Continued...

Table B.1 – *Continued...*

Node–1	**Node–2**	**Length (miles)**
7	8	3
7	11	8
7	12	9
8	9	6
8	10	6
8	11	7
8	13	7
9	10	6
10	13	6
10	14	3
11	13	3
11	16	7
11	12	2
12	15	4
12	16	4
13	14	7
13	19	4
14	19	7
14	21	2
14	22	4
15	16	4
16	17	4
17	18	3
17	19	3
18	20	3
19	20	3
20	21	2
22	23	3
23	24	3
24	25	8

TABLE B.2: Node Weight Data of 25-Node Transportation Network

Node	**Weight**	**Node**	**Weight**
1	0.05	14	0.059
2	0.082	15	0.017
3	0.023	16	0.022

Continued...

Table B.2 – *Continued...*

Node	**Weight**	**Node**	**Weight**
4	0.032	17	0.038
5	0.023	18	0.104
6	0.003	19	0.07
7	0.007	20	0.036
8	0.061	21	0.018
9	0.013	22	0.073
10	0.052	23	0.011
11	0.013	24	0.134
12	0.052	25	0.002
13	0.005	–	–

Publications

Journals

1. Akanksha Shukla, Kusum Verma and Rajesh Kumar, "Voltage Dependent Modelling of Fast Charging Electric Vehicle Load Considering Battery Characteristics", *IET Electrical Systems in Transportation*, 2018, vol. 8, no. 4, pp. 221–230
2. Akanksha Shukla, Kusum Verma and Rajesh Kumar, " Impact of EV Fast Charging Station on Distribution System Embedded with Wind Generation", *The Journal of Engineering (IET)*, 2019, vol. 2019, no. 18, pp. 4692–4697.
3. Akanksha Shukla, Kusum Verma and Rajesh Kumar, "Multi-Objective Synergistic Planning of EV Fast Charging Stations in Distribution System Coupled with Transportation Network", *IET Generation, Transmission & Distribution*, 2019, vo. 13, no. 15, pp. 3421–3432.
4. Akanksha Shukla, Kusum Verma and Rajesh Kumar, "Aggregate Load Modelling of EV Fast Charging Stations Considering Exponential Battery Charging Behavior", *International Transactions on Electrical Energy Systems*, 2019. (Communicated)
5. Akanksha Shukla, Kusum Verma and Rajesh Kumar, "Planning of Fast Charging Stations in Distribution System Coupled with Transportation Network for Capturing EV flow", *IEEE Transactions on Industry Application*, 2019. (Communicated)

Conferences

1. Akanksha Shukla, Kusum Verma and Rajesh Kumar, "Planning of EV Fast Charging Stations for Distribution System Coupled with Transportation Network", in IEEE PES General Meeting, Atlanta, 4-8 Aug. 2019.
2. Akanksha Shukla, Kusum Verma and Rajesh Kumar,"Planning of Fast Charging Stations in Distribution System Coupled with Transportation Network for Capturing EV flow" in IICPE 2018, 8th IEEE India International Conference on Power Electronics (IICPE 2018), Jaipur, 13-15 Dec. 2018.
3. Akanksha Shukla, Kusum Verma and Rajesh Kumar, "Impact of EV Fast Charging Station on Distribution System Embedded with Wind Generation" in IET RPG 2018, 7th International Conference on Renewable Power Generation, Denmark, 26-27 Sept. 2018.
4. Akanksha Shukla, Kusum Verma and Rajesh Kumar,"Multi-Stage Voltage Dependent Load Modelling of Fast Charging Electric Vehicle" in IEEE 6th International Conference on Computer Applications in Electrical Engineering-Recent Advances (CERA 17), Roorkee, 5-7 Oct. 2017.
5. Akanksha Shukla, Kusum Verma and Rajesh Kumar, "Consumer Perspective based Placement of Electric Vehicle Charging Stations by Clustering Techniques" in IEEE 19th National Power Systems Conference (NPSC 2016), Bhubaneswar, 19-21 Dec. 2016.

Bibliography

[1] "International energy agency (iea) . co2 emissions from fuel combustion." Tech. Rep.

[2] S. Juyal, M. Singh, S. Singh, S. Pal *et al.*, "India leaps ahead: transformative mobility solutions for all," Tech. Rep., 2017.

[3] "Global ev outlook 2018: Towards cross-modal electrification," "International Energy Agency", Tech. Rep. [Online]. Available: https://www.iea.org/gevo2018/

[4] J. Y. Yong, V. K. Ramachandaramurthy, K. M. Tan, and N. Mithulananthan, "A review on the state-of-the-art technologies of electric vehicle, its impacts and prospects," *Renewable and Sustainable Energy Reviews*, vol. 49, pp. 365–385, 2015.

[5] E. Akhavan-Rezai, M. Shaaban, E. El-Saadany, and A. Zidan, "Uncoordinated charging impacts of electric vehicles on electric distribution grids: Normal and fast charging comparison," in *2012 IEEE Power and Energy Society General Meeting*, San Diego, CA, USA, July 2012, pp. 1–7.

[6] P. Papadopoulos, S. Skarvelis-Kazakos, I. Grau, L. M. Cipcigan, and N. Jenkins, "Electric vehicles' impact on british distribution networks," *IET Electrical Systems in Transportation*, vol. 2, no. 3, pp. 91–102, 2012.

[7] C. Farkas, G. Szűcs, and L. Prikler, "Grid impacts of twin ev fast charging stations placed alongside a motorway," in *2013 4th International Youth Conference on Energy (IYCE)*, Siófok, Hungary, June 2013, pp. 1–6.

[8] A. Rautiainen, A. Mutanen, S. Repo, P. Järventausta, A. Tammi, R. Ryymin, J. Helin, A. Unkuri, and M. Pekkinen, "Case studies on impacts of plug-in vehicle charging load on the planning of urban electricity distribution networks," in *2013 Eighth International Conference and Exhibition on Ecological Vehicles and Renewable Energies (EVER)*, Monte Carlo, Monaco, March 2013, pp. 1–7.

[9] R.-C. Leou, C.-L. Su, and C.-N. Lu, "Stochastic analyses of electric vehicle charging impacts on distribution network," *IEEE Transactions on Power Systems*, vol. 29, no. 3, pp. 1055–1063, 2014.

[10] J. de Hoog, T. Alpcan, M. Brazil, D. A. Thomas, and I. Mareels, "Optimal charging of electric vehicles taking distribution network constraints into account," *IEEE Transactions on Power Systems*, vol. 30, no. 1, pp. 365–375, 2015.

[11] E. Veldman and R. A. Verzijlbergh, "Distribution grid impacts of smart electric vehicle charging from different perspectives," *IEEE Transactions on Smart Grid*, vol. 6, no. 1, pp. 333–342, 2015.

[12] H. Wang, Q. Song, L. Zhang, F. Wen, and J. Huang, "Load characteristics of electric vehicles in charging and discharging states and impacts on distribution systems," in *International Conference on Sustainable Power Generation and Supply (SUPERGEN 2012)*, Hangzhou, China, September 2012, pp. 1–7.

[13] H.-l. Li, X.-m. Bai, and W. Tan, "Impacts of plug-in hybrid electric vehicles charging on distribution grid and smart charging," in *2012 IEEE International Conference on Power System Technology (POWERCON)*, Auckland, New Zealand, January 2012, pp. 1–5.

[14] P. Richardson, D. Flynn, and A. Keane, "Impact assessment of varying penetrations of electric vehicles on low voltage distribution systems," in *IEEE PES General Meeting*, Providence, RI, USA, September 2010, pp. 1–6.

[15] N. Leemput, F. Geth, J. Van Roy, A. Delnooz, J. Büscher, and J. Driesen, "Impact of electric vehicle on-board single-phase charging strategies on a flemish residential grid," *IEEE Transactions on Smart Grid*, vol. 5, no. 4, pp. 1815–1822, 2014.

[16] M. Neaimeh, R. Wardle, A. M. Jenkins, J. Yi, G. Hill, P. F. Lyons, Y. Hübner, P. T. Blythe, and P. C. Taylor, "A probabilistic approach to combining smart meter and electric vehicle charging data to investigate distribution network impacts," *Applied Energy*, vol. 157, pp. 688–698, 2015.

[17] M. K. Gray and W. G. Morsi, "Power quality assessment in distribution systems embedded with plug-in hybrid and battery electric vehicles," *IEEE Transactions on Power Systems*, vol. 30, no. 2, pp. 663–671, 2015.

[18] C. Dharmakeerthi, N. Mithulananthan, and T. Saha, "Impact of electric vehicle fast charging on power system voltage stability," *International Journal of Electrical Power & Energy Systems*, vol. 57, pp. 241–249, 2014.

[19] "Installation guide for electric vehicle supply equipment. massachusetts division of energy resources," pp. 1–26, 2014.

[20] [Online]. Available: https://afdc.energy.gov/data/

[21] W. Price, H. Chiang, H. Clark, C. Concordia, D. Lee, J. Hsu, S. Ihara, C. King, C. Lin, Y. Mansour *et al.*, "Load representation for dynamic performance analysis," *IEEE Transactions on Power Systems*, vol. 8, no. 2, pp. 472–482, 1993.

[22] W. Price, C. Taylor, and G. Rogers, "Standard load models for power flow and dynamic performance simulation," *IEEE Transactions on Power Systems*, vol. 10, no. 3, pp. 1302–1313, 1995.

[23] L. M. Hajagos and B. Danai, "Laboratory measurements and models of modern loads and their effect on voltage stability studies," *IEEE Transactions on Power Systems*, vol. 13, no. 2, pp. 584–592, 1998.

[24] H. Renmu, M. Jin, and D. J. Hill, "Composite load modeling via measurement approach," *IEEE Transactions on Power Systems*, vol. 21, no. 2, pp. 663–672, 2006.

[25] T. Das and D. C. Aliprantis, "Small-signal stability analysis of power system integrated with phevs," in *2008 IEEE Energy 2030 Conference*, Atlanta, GA, USA, November 2008, pp. 1–4.

[26] R. Garcia-Valle and J. G. Vlachogiannis, "Letter to the editor: Electric vehicle demand model for load flow studies," *Electric Power Components and Systems*, vol. 37, no. 5, pp. 577–582, 2009.

[27] B. Boribun, P. Paolaor, and T. Kulworawanichpong, "Impact of electric bus charging in power distribution systems," in *2013 World Congress on Advances in Nano, Biomechanics, Robotics, and Energy Research (ANBRE13)*, Seoul, South Korea, August 2013, pp. 1–8.

[28] D. P. Montoya and A. E. Díez, "Power flow steady-state model analysis of grid-connected plug-in electric vehicle charging stations," in *2015 12th International Conference on Electrical Engineering, Computing Science and Automatic Control (CCE)*, Mexico City, Mexico, October 2015, pp. 1–6.

[29] M. Etezadi-Amoli, K. Choma, and J. Stefani, "Rapid-charge electric-vehicle stations," *IEEE Transactions on Power Delivery*, vol. 25, no. 3, pp. 1883–1887, 2010.

[30] O. C. Onar and A. Khaligh, "Grid interactions and stability analysis of distribution power network with high penetration of plug-in hybrid electric vehicles," in *2010 Twenty-Fifth Annual IEEE Applied Power Electronics Conference and Exposition (APEC)*, Palm Springs, CA, USA, March 2010, pp. 1755–1762.

[31] R. Shi, X. Zhang, D. Kong, N. Deng, and P. Wang, "Dynamic impacts of fast-charging stations for electric vehicles on active distribution networks," in *IEEE PES Innovative Smart Grid Technologies*, Tianjin, China, May 2012, pp. 1–6.

[32] C. Dharmakeerthi, N. Mithulananthan, and T. Saha, "Modeling and planning of ev fast charging station in power grid," in *2012 IEEE Power and Energy Society General Meeting*, San Diego, CA, USA, July 2012, pp. 1–6.

[33] C. Dharmakeerthi, N. Mithulananthan, and T. Saha, "A comprehensive planning framework for electric vehicle charging infrastructure deployment in the power grid with enhanced voltage stability," *International Transactions on Electrical Energy Systems*, vol. 25, no. 6, pp. 1022–1040, 2015.

[34] C. Dharmakeerthi and N. Mithulananthan, "Pev load and its impact on static voltage stability," in *Plug In Electric Vehicles in Smart Grids*, ser. Power Systems, R. Sumedha, S. Farhad, and G. Arindam, Eds. Springer, Singapore, 2015, pp. 221–248.

[35] K. P. Schneider, J. C. Fuller, and D. P. Chassin, "Multi-state load models for distribution system analysis," *IEEE Transactions on Power Systems*, vol. 26, no. 4, pp. 2425–2433, 2011.

[36] A. M. Haidar, K. M. Muttaqi, and M. H. Haque, "Multistage time-variant electric vehicle load modelling for capturing accurate electric vehicle behaviour and electric vehicle impact on electricity distribution grids," *IET Generation, Transmission & Distribution*, vol. 9, no. 16, pp. 2705–2716, 2015.

[37] A. M. Haidar and K. M. Muttaqi, "Behavioral characterization of electric vehicle charging loads in a distribution power grid through modeling of battery chargers," *IEEE Transactions on Industry Application*, vol. 52, no. 1, pp. 483–492, 2016.

[38] E. Sortomme, A. Negash, S. Venkata, and D. Kirschen, "Voltage dependent load models of charging electric vehicles," in *2013 IEEE Power and Energy Society General Meeting*, Vancouver, BC, Canada, July 2013, pp. 1–6.

[39] Z. Darabi and M. Ferdowsi, "Aggregated impact of plug-in hybrid electric vehicles on electricity demand profile," *IEEE Transactions on Sustainable Energy*, vol. 2, no. 4, pp. 501–508, 2011.

[40] S. Shafiee, M. Fotuhi-Firuzabad, and M. Rastegar, "Investigating the impacts of plug-in hybrid electric vehicles on power distribution systems," *IEEE Transactions on Smart Grid*, vol. 4, no. 3, pp. 1351–1360, 2013.

[41] J. Xiong, K. Zhang, Y. Guo, and W. Su, "Investigate the impacts of pev charging facilities on integrated electric distribution system and electrified transportation system," *IEEE Trans. Transp. Electrific*, vol. 1, no. 2, pp. 178–187, 2015.

[42] M. F. Shaaban, Y. M. Atwa, and E. F. El-Saadany, "Pevs modeling and impacts mitigation in distribution networks," *IEEE Transactions on Power Systems*, vol. 28, no. 2, pp. 1122–1131, 2013.

[43] G. Li and X.-P. Zhang, "Modeling of plug-in hybrid electric vehicle charging demand in probabilistic power flow calculations," *IEEE Transactions on Smart Grid*, vol. 3, no. 1, pp. 492–499, 2012.

[44] C. Jiang, R. Torquato, D. Salles, and W. Xu, "Method to assess the power-quality impact of plug-in electric vehicles," *IEEE Transactions on Power Delivery*, vol. 29, no. 2, pp. 958–965, 2014.

[45] N. Zhou, X. Xiong, and Q. Wang, "Probability model and simulation method of electric vehicle charging load on distribution network," *Electric Power Components and Systems*, vol. 42, no. 9, pp. 879–888, 2014.

[46] R.-C. Leou, J.-H. Teng, and C.-L. Su, "Modelling and verifying the load behaviour of electric vehicle charging stations based on field measurements," *IET Generation, Transmission & Distribution*, vol. 9, no. 11, pp. 1112–1119, 2015.

[47] N. H. Tehrani and P. Wang, "Probabilistic estimation of plug-in electric vehicles charging load profile," *Electric Power Systems Research*, vol. 9124, pp. 133–143, 2015.

[48] S. F. Abdelsamad, W. G. Morsi, and T. S. Sidhu, "Impact of wind-based distributed generation on electric energy in distribution systems embedded with electric vehicles," *IEEE Transactions on Sustainable Energy*, vol. 6, no. 1, pp. 79–87, 2015.

[49] I. Karakitsios, E. Karfopoulos, and N. Hatziargyriou, "Impact of dynamic and static fast inductive charging of electric vehicles on the distribution network," *Electric Power Systems Research*, vol. 140, pp. 107–115, 2016.

[50] T. Shun, L. Kunyu, X. Xiangning, W. Jianfeng, Y. Yang, and Z. Jian, "Charging demand for electric vehicle based on stochastic analysis of trip chain," *IET Generation, Transmission & Distribution*, vol. 10, no. 11, pp. 2689–2698, 2016.

[51] K. Qian, C. Zhou, M. Allan, and Y. Yuan, "Modeling of load demand due to ev battery charging in distribution systems," *IEEE Transactions on Power Systems*, vol. 26, no. 2, pp. 802–810, 2011.

[52] P. Zhang, K. Qian, C. Zhou, B. G. Stewart, and D. M. Hepburn, "A methodology for optimization of power systems demand due to electric vehicle charging load," *IEEE Transactions on Power Systems*, vol. 27, no. 3, pp. 1628–1636, 2012.

[53] S. Rezaee, E. Farjah, and B. Khorramdel, "Probabilistic analysis of plug-in electric vehicles impact on electrical grid through homes and parking lots," *IEEE Transactions on Sustainable Energy*, vol. 4, no. 4, pp. 1024–1033, 2013.

[54] A. Lojowska, D. Kurowicka, G. Papaefthymiou, L. van der Sluis *et al.*, "Stochastic modeling of power demand due to evs using copula," *IEEE Transactions on Power Systems*, vol. 27, no. 4, pp. 1960–1968, 2012.

[55] O. Hafez and K. Bhattacharya, "Queuing analysis based pev load modeling considering battery charging behavior and their impact on distribution system operation," *IEEE Transactions on Smart Grid*, vol. 9, no. 1, pp. 261–273, 2018.

[56] A. Santos, N. McGuckin, H. Y. Nakamoto, D. Gray, and S. Liss, "Summary of travel trends: 2009 national household travel survey," Tech. Rep., June 2011. [Online]. Available: https://nhts.ornl.gov/2009/pub/stt.pdf

[57] The 2011 transportation survey. [Online]. Available: http://dmg.utoronto.ca/transportation-tomorrow-survey/tts-reports

[58] A. Ahmad, M. S. Alam, and R. Chabaan, "A comprehensive review of wireless charging technologies for electric vehicles," *IEEE Transactions on Transportation Electrification*, vol. 4, no. 1, pp. 38–63, 2018.

[59] M. Yilmaz and P. T. Krein, "Review of battery charger topologies, charging power levels, and infrastructure for plug-in electric and hybrid vehicles," *IEEE Transactions on Power Electronics*, vol. 28, no. 5, pp. 2151–2169, 2013.

[60] A. Y. Lam, Y.-W. Leung, and X. Chu, "Electric vehicle charging station placement: Formulation, complexity, and solutions," *IEEE Transactions on Smart Grid*, vol. 5, no. 6, pp. 2846–2856, 2014.

[61] F. Xu, G.-q. YU, L.-f. GU, and H. Zhang, "Tentative analysis of layout of electrical vehicle charging station," *East China Electric Power*, vol. 37, no. 10, pp. 1678–168, 2009.

[62] J. Jamian, M. Mustafa, H. Mokhlis, and M. Baharudin, "Minimization of power losses in distribution system via sequential placement of distributed generation and charging station," *Arabian Journal for Science and Engineering*, vol. 39, no. 4, pp. 3023–3031, 2014.

[63] C. Wang, R. Dunn, F. Robinson, B. Lian, W. Yuan, and M. Redfern, "Active–reactive power approaches for optimal placement of charge stations in power systems," *International Journal of Electrical Power & Energy Systems*, vol. 84, pp. 87–98, 2017.

[64] T. Lan, Q. Kang, J. An, W. Yan, and L. Wang, "Sitting and sizing of aggregator controlled park for plug-in hybrid electric vehicle based on particle swarm optimization," *Neural Computing and Applications*, vol. 22, no. 2, pp. 249–257, 2013.

[65] E. Pashajavid and M. Golkar, "Optimal placement and sizing of plug in electric vehicles charging stations within distribution networks with high penetration of photovoltaic panels," *Journal of Renewable and Sustainable Energy*, vol. 5, no. 5, p. 053126, 2013.

[66] M. H. Moradi, M. Abedini, S. R. Tousi, and S. M. Hosseinian, "Optimal siting and sizing of renewable energy sources and charging stations simultaneously based on differential evolution algorithm," *International Journal of Electrical Power & Energy Systems*, vol. 73, pp. 1015–1024, 2015.

[67] K. Khalkhali, S. Abapour, S. M. Moghaddas-Tafreshi, and M. Abapour, "Application of data envelopment analysis theorem in plug-in hybrid electric vehicle charging station planning," *IET Generation, Transmission & Distribution*, vol. 9, no. 7, pp. 666–676, 2015.

[68] P. Phonrattanasak and N. Leeprechanon, "Optimal location of fast charging station on residential distribution grid," *International Journal of Innovation, Management and Technology*, vol. 3, no. 6, pp. 675–681, 2012.

[69] Z. Liu, F. Wen, and G. Ledwich, "Optimal planning of electric-vehicle charging stations in distribution systems," *IEEE Transactions on Power Delivery*, vol. 28, no. 1, pp. 102–110, 2013.

[70] A. Awasthi, K. Venkitusamy, S. Padmanaban, R. Selvamuthukumaran, F. Blaabjerg, and A. K. Singh, "Optimal planning of electric vehicle charging station at the distribution system using hybrid optimization algorithm," *Energy*, vol. 133, pp. 70–78, 2017.

[71] Y. Zheng, Z. Y. Dong, Y. Xu, K. Meng, J. H. Zhao, and J. Qiu, "Electric vehicle battery charging/swap stations in distribution systems: comparison study and optimal planning," *IEEE Transactions on Power Systems*, vol. 29, no. 1, pp. 221–229, 2014.

[72] J. Liu, "Electric vehicle charging infrastructure assignment and power grid impacts assessment in beijing," *Energy Policy*, vol. 51, pp. 544–557, 2012.

[73] H. Xu, S. Miao, C. Zhang, and D. Shi, "Optimal placement of charging infrastructures for large-scale integration of pure electric vehicles into grid," *International Journal of Electrical Power & Energy Systems*, vol. 53, pp. 159–165, 2013.

[74] L. Song, J. Wang, and D. Yang, "Optimal placement of electric vehicle charging stations based on voronoi diagram," in *2015 IEEE International Conference on Information and Automation*, Lijiang, China, August 2015, pp. 2807–2812.

[75] J. Cavadas, G. H. de Almeida Correia, and J. Gouveia, "A mip model for locating slow-charging stations for electric vehicles in urban areas accounting for driver tours," *Transportation Research Part E: Logistics and Transportation Review*, vol. 75, pp. 188–201, 2015.

[76] H. Zhang, Z. Hu, Z. Xu, and Y. Song, "An integrated planning framework for different types of pev charging facilities in urban area," *IEEE Transactions on Smart Grid*, vol. 7, no. 5, pp. 2273–2284, 2016.

[77] X. Dong, Y. Mu, H. Jia, J. Wu, and X. Yu, "Planning of fast ev charging stations on a round freeway," *IEEE Transactions on sustainable Energy*, vol. 7, no. 4, pp. 1452–1461, 2016.

[78] H. Cai, X. Jia, A. S. Chiu, X. Hu, and M. Xu, "Siting public electric vehicle charging stations in beijing using big-data informed travel patterns of the taxi fleet," *Transportation Research Part D: Transport and Environment*, vol. 33, pp. 39–46, 2014.

[79] N. Shahraki, H. Cai, M. Turkay, and M. Xu, "Optimal locations of electric public charging stations using real world vehicle travel patterns," *Transportation Research Part D: Transport and Environment*, vol. 41, pp. 165–176, 2015.

[80] C. J. Sheppard, A. Harris, and A. R. Gopal, "Cost-effective siting of electric vehicle charging infrastructure with agent-based modeling," *IEEE Transactions on Transportation Electrification*, vol. 2, no. 2, pp. 174–189, 2016.

[81] Z.-f. Liu, W. Zhang, X. Ji, and K. Li, "Optimal planning of charging station for electric vehicle based on particle swarm optimization," in *IEEE PES Innovative Smart Grid Technologies*, Tianjin, China, September 2012, pp. 1–5.

[82] H.-Y. Mak, Y. Rong, and Z.-J. M. Shen, "Infrastructure planning for electric vehicles with battery swapping," *Management Science*, vol. 59, no. 7, pp. 1557–1575, 2013.

[83] A. Y. Lam, Y.-W. Leung, and X. Chu, "Electric vehicle charging station placement," in *2013 IEEE International Conference on Smart Grid Communications (SmartGridComm)*, Vancouver, BC, Canada, October 2013, pp. 510–515.

[84] P.-S. You and Y.-C. Hsieh, "A hybrid heuristic approach to the problem of the location of vehicle charging stations," *Computers & Industrial Engineering*, vol. 70, pp. 195–204, 2014.

[85] S. H. Chung and C. Kwon, "Multi-period planning for electric car charging station locations: A case of korean expressways," *European Journal of Operational Research*, vol. 242, no. 2, pp. 677–687, 2015.

[86] R. Riemann, D. Z. Wang, and F. Busch, "Optimal location of wireless charging facilities for electric vehicles: flow-capturing location model with stochastic user equilibrium," *Transportation Research Part C: Emerging Technologies*, vol. 58, pp. 1–12, 2015.

[87] X. Wang, C. Yuen, N. U. Hassan, N. An, and W. Wu, "Electric vehicle charging station placement for urban public bus systems," *IEEE Transactions on Intelligent Transportation Systems*, vol. 18, no. 1, pp. 128–139, 2017.

[88] F. Pan, R. Bent, A. Berscheid, and D. Izraelevitz, "Locating phev exchange stations in v2g," in *2010 First IEEE International Conference on Smart Grid Communications*, Gaithersburg, MD, USA, October 2010, pp. 173–178.

[89] G. Wang, Z. Xu, F. Wen, and K. P. Wong, "Traffic-constrained multiobjective planning of electric-vehicle charging stations," *IEEE Transactions on Power Delivery*, vol. 28, no. 4, pp. 2363–2372, 2013.

[90] W. Yao, J. Zhao, F. Wen, Z. Dong, Y. Xue, Y. Xu, and K. Meng, "A multi-objective collaborative planning strategy for integrated power distribution and electric vehicle charging systems," *IEEE Transactions on Power Systems*, vol. 29, no. 4, pp. 1811–1821, 2014.

[91] P. Sadeghi-Barzani, A. Rajabi-Ghahnavieh, and H. Kazemi-Karegar, "Optimal fast charging station placing and sizing," *Applied Energy*, vol. 125, pp. 289–299, 2014.

[92] A. Rajabi-Ghahnavieh and P. Sadeghi-Barzani, "Optimal zonal fast-charging station placement considering urban traffic circulation," *IEEE Transactions on Vehicular Technology*, vol. 66, no. 1, pp. 45–56, 2017.

[93] C. Luo, Y.-F. Huang, and V. Gupta, "Placement of ev charging stations—balancing benefits among multiple entities," *IEEE Transactions on Smart Grid*, vol. 8, no. 2, pp. 759–768, 2017.

[94] Y. A. Alhazmi and M. M. Salama, "Economical staging plan for implementing electric vehicle charging stations," *Sustainable Energy, Grids and Networks*, vol. 10, pp. 12–25, 2017.

[95] H. Zhang, S. J. Moura, Z. Hu, and Y. Song, "Pev fast-charging station siting and sizing on coupled transportation and power networks," *IEEE Transactions on Smart Grid*, vol. 9, no. 4, pp. 2595–2605, 2018.

[96] H. Zhang, S. J. Moura, Z. Hu, W. Qi, and Y. Song, "A second-order cone programming model for planning pev fast-charging stations," *IEEE Transactions on Power Systems*, vol. 33, no. 3, pp. 2763–2777, 2018.

[97] S. M. Kandil, H. E. Farag, M. F. Shaaban, and M. Z. El-Sharafy, "A combined resource allocation framework for pevs charging stations, renewable energy resources and distributed energy storage systems," *Energy*, vol. 143, no. 3, pp. 961–972, 2018.

[98] K. S. Chaudhari, N. K. Kandasamy, A. Krishnan, A. Ukil, and H. B. Gooi, "Agent based aggregated behavior modelling for electric vehicle charging load," *IEEE Transactions on Industrial Informatics*, vol. 15, no. 2, pp. 856 – 868, 2019.

[99] Z. Tang, C. Guo, P. Hou, and Y. Fan, "Optimal siting of electric vehicle charging stations based on voronoi diagram and fahp method," *Energy and power Engineering*, vol. 5, no. 4, pp. 1404–1409, 2013.

[100] W. Meng, L. Kai, and Z. Songhui, "Evaluation of electric vehicle charging station sitting based on fuzzy analytic hierarchy process," in *2013 Fourth International Conference on Digital Manufacturing & Automation*, Qingdao, China, September 2013, pp. 568–571.

[101] S. Guo and H. Zhao, "Optimal site selection of electric vehicle charging station by using fuzzy topsis based on sustainability perspective," *Applied Energy*, vol. 158, pp. 390–402, 2015.

[102] H. Zhao and N. Li, "Optimal siting of charging stations for electric vehicles based on fuzzy delphi and hybrid multi-criteria decision making approaches from an extended sustainability perspective," *Energies*, vol. 9, no. 4, p. 270, 2016.

[103] S. Rajakaruna, F. Shahnia, and A. Ghosh, *Plug in electric vehicles in smart grids*. Springer, 2016.

[104] N. Hartmann and E. Özdemir, "Impact of different utilization scenarios of electric vehicles on the german grid in 2030," *Journal of power sources*, vol. 196, no. 4, pp. 2311–2318, 2011.

[105] C. Weiller, "Plug-in hybrid electric vehicle impacts on hourly electricity demand in the united states," *Energy Policy*, vol. 39, no. 6, pp. 3766–3778, 2011.

[106] J. Mullan, D. Harries, T. Bräunl, and S. Whitely, "Modelling the impacts of electric vehicle recharging on the western australian electricity supply system," *Energy policy*, vol. 39, no. 7, pp. 4349–4359, 2011.

[107] I. Drovtar, A. Rosin, M. Landsberg, and J. Kilter, "Large scale electric vehicle integration and its impact on the estonian power system," in *2013 IEEE Grenoble Conference*, Grenoble, France, November 2013, pp. 1–6.

[108] W.-J. Park, K.-B. Song, and J.-W. Park, "Impact of electric vehicle penetration-based charging demand on load profile," *Journal of Electrical Engineering and Technology*, vol. 8, no. 2, pp. 244–251, 2013.

[109] Y. Mu, J. Wu, N. Jenkins, H. Jia, and C. Wang, "A spatial–temporal model for grid impact analysis of plug-in electric vehicles," *Applied Energy*, vol. 114, pp. 456–465, 2014.

[110] R. Gonçalves, J. T. Saraiva, J. C. Sousa, and V. Mendes, "Impact of electric vehicles on the electricity prices and on the load curves of the iberian electricity market," in *2013 10th International Conference on the European Energy Market (EEM)*, Stockholm, Sweden, September 2013, pp. 1–8.

[111] Z. Darabi and M. Ferdowsi, "Examining power grid's capacity to meet transportation electrification demand," in *2012 IEEE Power and Energy Society General Meeting*, San Diego, CA, USA, July 2012, pp. 1–7.

[112] R. Villafafila-Robles, F. Girbau-Llistuella, P. Olivella-Rosell, A. Sudria-Andreu, and J. Bergas-Jane, "Assessment of impact of charging infrastructure for electric vehicles on distribution networks," in *2013 15th European Conference on Power Electronics and Applications (EPE)*, Lille, France, October 2013, pp. 1–10.

[113] K. Clement-Nyns, E. Haesen, and J. Driesen, "The impact of charging plug-in hybrid electric vehicles on a residential distribution grid," *IEEE Transactions on power systems*, vol. 25, no. 1, pp. 371–380, 2010.

[114] R. Liu, L. Dow, and E. Liu, "A survey of pev impacts on electric utilities," in *ISGT 2011*, Anaheim, CA, USA, April 2011, pp. 1–8.

[115] A. Jiménez and N. García, "Voltage unbalance analysis of distribution systems using a three-phase power flow ans a genetic algorithm for pev fleets scheduling," in *2012 IEEE Power and Energy Society General Meeting*, San Diego, CA, USA, July 2012, pp. 1–8.

[116] J. R. Pillai and B. Bak-Jensen, "Impacts of electric vehicle loads on power distribution systems," in *2010 IEEE Vehicle Power and Propulsion Conference*, Lille, France, March 2010, pp. 1–6.

[117] L. P. Fernandez, T. G. San Román, R. Cossent, C. M. Domingo, and P. Frias, "Assessment of the impact of plug-in electric vehicles on distribution networks," *IEEE Transactions on power systems*, vol. 26, no. 1, pp. 206–213, 2011.

[118] G. Resch, A. Held, T. Faber, C. Panzer, F. Toro, and R. Haas, "Potentials and prospects for renewable energies at global scale," *Energy policy*, vol. 36, no. 11, pp. 4048–4056, 2008.

[119] S. Gao, K. Chau, C. Liu, D. Wu, and C. C. Chan, "Integrated energy management of plug-in electric vehicles in power grid with renewables," *IEEE Transactions on Vehicular Technology*, vol. 63, no. 7, pp. 3019–3027, 2014.

[120] W. Wei, F. Liu, and S. Mei, "Charging strategies of ev aggregator under renewable generation and congestion: A normalized nash equilibrium approach," *IEEE Transactions on Smart Grid*, vol. 7, no. 3, pp. 1630–1641, 2016.

[121] H. N. Nguyen, C. Zhang, and J. Zhang, "Dynamic demand control of electric vehicles to support power grid with high penetration level of renewable energy," *IEEE Transactions on Transportation Electrification*, vol. 2, no. 1, pp. 66–75, 2016.

[122] L. Liu, F. Kong, X. Liu, Y. Peng, and Q. Wang, "A review on electric vehicles interacting with renewable energy in smart grid," *Renewable and Sustainable Energy Reviews*, vol. 51, pp. 648–661, 2015.

[123] C. K. Ekman, "On the synergy between large electric vehicle fleet and high wind penetration–an analysis of the danish case," *Renewable Energy*, vol. 36, no. 2, pp. 546–553, 2011.

[124] T. Jiang, G. Putrus, Z. Gao, S. McDonald, and H. Wu, "Analysis of the combined impact of small-scale wind generators and electric vehicles on future power networks," in *2012 47th International Universities Power Engineering Conference (UPEC)*, London, UK, December 2012, pp. 1–5.

[125] C. Long, M. E. Farrag, C. Zhou, and D. M. Hepburn, "Statistical quantification of voltage violations in distribution networks penetrated by small wind turbines and battery electric vehicles," *IEEE Transactions on Power Systems*, vol. 28, no. 3, pp. 2403–2411, 2013.

[126] S. F. Abdelsamad, W. G. Morsi, and T. S. Sidhu, "On the impact of transportation electrification on distribution systems in the presence of rooftop solar photovoltaic," in *2015 IEEE Electrical Power and Energy Conference (EPEC)*, London, ON, Canada, October 2015, pp. 26–31.

[127] N. S. Pearre and L. G. Swan, "Electric vehicle charging to support renewable energy integration in a capacity constrained electricity grid," *Energy conversion and management*, vol. 109, no. 3, pp. 130–139, 2016.

[128] J. Hernández, F. Ruiz-Rodriguez, and F. Jurado, "Modelling and assessment of the combined technical impact of electric vehicles and photovoltaic generation in radial distribution systems," *Energy*, vol. 141, pp. 316–332, 2017.

[129] F. J. Ruiz-Rodriguez, J. C. Hernández, and F. Jurado, "Voltage behaviour in radial distribution systems under the uncertainties of photovoltaic systems and electric vehicle charging loads," *International Transactions on Electrical Energy Systems*, vol. 28, no. 2, p. e2490, 2018.

[130] M. Moradijoz, M. P. Moghaddam, M. Haghifam, and E. Alishahi, "A multi-objective optimization problem for allocating parking lots in a distribution network," *International Journal of Electrical Power & Energy Systems*, vol. 46, pp. 115–122, 2013.

[131] A. Dubey, S. Santoso, and M. P. Cloud, "Average-value model of electric vehicle chargers," *IEEE Transactions on Smart Grid*, vol. 4, no. 3, pp. 1549–1557, 2013.

[132] A. Arancibia, K. Strunz, and F. Mancilla-David, "A unified single-and three-phase control for grid connected electric vehicles," *IEEE Transactions on Smart Grid*, vol. 4, no. 4, pp. 1780–1790, 2013.

[133] R. Wu, S. B. Dewan, and G. R. Slemon, "A pwm ac-to-dc converter with fixed switching frequency," *IEEE Transactions on Industry Applications*, vol. 26, no. 5, pp. 880–885, 1990.

[134] O. Tremblay and L.-A. Dessaint, "Experimental validation of a battery dynamic model for ev applications," *World electric vehicle journal*, vol. 3, no. 2, pp. 289–298, 2009.

[135] D. H. Doughty, "Vehicle battery safety roadmap guidance," National Renewable Energy Lab.(NREL), Golden, CO (United States), Tech. Rep., 2012.

[136] W. H. Kersting, *Distribution system modeling and analysis*, 3rd ed. Washington D.C.: CRC press, 2012.

[137] A. S. Fotheringham and M. E. O'Kelly, *Spatial interaction models: formulations and applications*. Kluwer academic publishers Dordrecht, 1989, vol. 1.

[138] U. N. Bhat, *An introduction to queueing theory: modeling and analysis in applications*. Birkhäuser, 2015.

[139] (2016, Jun.) Ieee pes distribution test feeders, 123-bus feeder. [Online]. Available: http://ewh.ieee.org/soc/pes/dsacom/testfeeders/index.html

[140] "The math works, inc., matlab programming, 2015."

[141] (2016, Jun.) Opendss software. [Online]. Available: http://www.sourceforge.net/projects/electricdss/

[142] N. Neyestani, M. Y. Damavandi, M. Shafie-Khah, J. Contreras, and J. P. Catalão, "Allocation of plug-in vehicles' parking lots in distribution systems considering network-constrained objectives," *IEEE Transactions on Power Systems*, vol. 30, no. 5, pp. 2643–2656, 2015.

[143] M. J. Hodgson, "A flow-capturing location-allocation model," *Geographical Analysis*, vol. 22, no. 3, pp. 270–279, 1990.

[144] S. Mirjalili, S. Saremi, S. M. Mirjalili, and L. d. S. Coelho, "Multi-objective grey wolf optimizer: a novel algorithm for multi-criterion optimization," *Expert Systems with Applications*, vol. 47, pp. 106–119, 2016.

[145] S. Mirjalili, S. M. Mirjalili, and A. Lewis, "Grey wolf optimizer," *Advances in engineering software*, vol. 69, pp. 46–61, 2014.

[146] P. Maghouli, S. H. Hosseini, M. O. Buygi, and M. Shahidehpour, "A multi-objective framework for transmission expansion planning in deregulated environments," *IEEE Transactions on Power Systems*, vol. 24, no. 2, pp. 1051–1061, 2009.

[147] C. A. C. Coello, G. T. Pulido, and M. S. Lechuga, "Handling multiple objectives with particle swarm optimization," *IEEE Transactions on evolutionary computation*, vol. 8, no. 3, pp. 256–279, 2004.

[148] Q. Zhang and H. Li, "Moea/d: A multiobjective evolutionary algorithm based on decomposition," *IEEE Transactions on evolutionary computation*, vol. 11, no. 6, pp. 712–731, 2007.

[149] Y. M. Atwa and E. F. El-Saadany, "Probabilistic approach for optimal allocation of wind-based distributed generation in distribution systems," *IET Renewable Power Generation*, vol. 5, no. 1, pp. 79–88, 2011.

[150] A. H. Fathima and K. Palanisamy, "Optimization in microgrids with hybrid energy systems–a review," *Renewable and Sustainable Energy Reviews*, vol. 45, no. 2, pp. 431–446, 2015.

[151] M. R. Patel, *Wind and solar power systems: design, analysis, and operation.* CRC press, 2005.

[152] American national standard for electric power systems and equipment- voltage ratings (60 hz), ansi c84.1-2011. [Online]. Available: https://webstore.ansi.org/standards/nema/ansic842011

[153] (2018, March) Wind data. [Online]. Available: https://www.renewables.ninja

[154] M. R. B. Khan, R. Jidin, and J. Pasupuleti, "Multi-agent based distributed control architecture for microgrid energy management and optimization," *Energy Conversion and Management*, vol. 112, pp. 288–307, 2016.

Brief bio-data

Ms. Akanksha Shukla received her B.Tech. degree in Electrical Engineering from Harcourt Butler Technical University, Kanpur, Uttar Pradesh, India in 2013, and M.Tech. degree in Electrical Engineering (Power Systems) from Malaviya National Institute of Technology Jaipur, India in 2015. She completed her PhD in Electrical Engineering from Malaviya National Institute of Technology Jaipur, Rajasthan, India. Her research interests includes load modelling for power flow analysis, modelling of distribution system, renewable integration impact on distribution system performance and Electric Vehicle (EV) integration to the grid. She is Member of IEEE, USA and Member of IET, UK.